TECHNISCHE UNIVERSITÄT WIEN

Diploma Thesis

CYCLIC CARBONATES AS MONOMERS FOR HOT LITHOGRAPHY

ausgeführt zum Zwecke der Erlangung des akademischen Grades

eines Diplom-Ingenieurs

unter Anleitung von

Univ.Prof. Dipl.-Ing. Dr.techn. Robert Liska

Univ.Ass. Dr.techn. Katharina Ehrmann, MSc.

Am Institut für Angewandte Synthesechemie (IAS)

der Technischen Universität Wien

von

Stephan Schandl, BSc

01425329

[redacted]

Februar 2022

_____

Stephan Schandl, BSc

=:

Danksagung

Zuerst möchte ich mich bei Prof. Liska für die Möglichkeit bedanken meine Diplomarbeit in dieser Arbeitsgruppe über dieses spannende Fachgebiet schreiben zu dürfen. Danke nicht nur für die hervorragende fachliche Unterstützung, sondern auch für deine offene Art, die ein wunderbares Klima in der Arbeitsgruppe schafft, das einen jeden Tag sehr gerne ins Labor kommen lässt.

Des Weiteren möchte ich mich auch besonders bei Dr. Katharina Ehremann bedanken. Du hast mir stets mit besten Ratschlägen geholfen, auch oft bei Situationen, wo ich mit dem Rücken zur Wand stand.

Besonderer Dank gilt auch Dr. Thomas Koch für die beste Hilfe bei den vielen Messungen. Ich danke dir dafür, dass wir stets einen schnellen Termin für die Messungen gefunden haben.

Ich möchte mich auch besonders beim ganzen FBMC-Team für die wunderschöne Zeit bedanken! Allen mein Dank für einen reibungslosen und konstruktiven Laboralltag. Besonders hervorzuheben sind Ralle, Dani, Pontus und Anna als H31 Kollegen. Aber auch Lisa, Babsi, Oskar, Michi, Jakob, Anna Z., Viola, Davide, Sarah, Betti, David, Philip, Flo, Larissa, Fitzi, Carola, Klausi, Toni, Roli, und Tina haben mitgeholfen, die Stunden bei der Arbeit und auch viele gemeinsame Stunden außerhalb der Arbeitszeit mit Freude zu füllen.

Meiner Familie gilt ein ganz besonderer Dank, da ihr mich nicht nur finanziell, sondern auch seelisch unterstützt habt. Meine Eltern Beate und Johann, sowie meine Geschwister Michael und Matthias, ihr wart mir immer ein Ruheort an dem ich mich zurückziehen konnte.

Ein ganz besonderer Dank gilt auch meiner Freundin Anna. Du warst immer meine beste Zuhörerin, auch wenn ich mal in einer ganz fremden Sprache geredet habe.

DANKE!

Table of contents

Abstract

Additive manufacturing techniques are increasingly interesting for fast prototyping or the production of complex geometries. For accomplishing precise results, optimised materials and parameters are necessary. Light-based 3D-printing produces parts with high resolution and surface structure quality. A photo-polymerizable resin is scanned layer by layer to generate a 3D structure. With operating temperatures of up to 120 °C, Hot Lithography enables the processing of highly viscous formulations or resins, which show low reactivity at room temperature. Through Hot Lithography's elevated operating temperatures, a great variety of monomers of different classes were shown to be printable. Commonly used monomers for 3D printing, such as (meth)acrylates, suffer from polymerization shrinkage, causing low surface quality or cracks.

Cyclic carbonates are particularly interesting as they show volume expansion upon ring-opening polymerization. Because of their expanding nature, cyclic carbonates have already found their place as anti-shrinkage additives for some compatible resins. As cyclic carbonates undergo cationic and anionic polymerisation, copolymerisation is adjustable to other used monomers. Herein, the applicability of cyclic carbonates as monomers for Hot Lithography will be tested.

The monomers and resulting polymers' reactivity and (thermo-)mechanical properties were analysed, respectively. Reactivity of the monomer was investigated utilizing photo-DSC and -rheological measurements at different temperatures. NMR determined conversion of monofunctional monomers and molecular weight of linear polymers- and GPC-analysis, respectively. A difunctional cyclic carbonate was used as crosslinkers and characterised in analogy to the monofunctional monomers. Tensile tests and DMTA measurements tested (thermo-)mechanical properties of the obtained materials. Lastly, the applicability for the actual 3D-printing process was tested *via* light exposure tests.

Kurzfassung

Additive Fertigungstechniken finden reges Interesse wegen der Möglichkeit zur raschen Fertigung von Prototypen und Produktion komplexer Geometrien. Licht basierter 3D Druck erzeugt Werkstücke mit hoher Auflösung und Oberflächenqualität, jedoch sind optimierte Materialien und auch Fertigungsparameter notwendig um präzise Ergebnisse zu erzielen. Ein photo-polymerisierbares Harz wird Schicht für Schicht von einem Laser abgeraster, um eine 3D Struktur zu erzeugen. Mit einer Verarbeitungstemperatur von bis zu 120 °C, ermöglicht die Hot Lithography die Verarbeitung von hochviskosen oder bei Raumtemperatur zu unreaktiven Harzen. Die hohen Verarbeitungstemperaturen erschließen eine große Vielfalt an Monomeren verschiedener Funktionalität. Herkömmlich für den 3D Druck genutzte Monomere, wie (Meth)acrylate, weisen einen merklichen Polymerisationsschrumpf auf. Dadurch kann es bei Werkstücke aus diesen Monomeren zu einer geringeren Oberflächenqualität oder zur Rissbildung kommen.

Zyklische Carbonate sind von besonderem Interesse, da sie während der Ringöffnungspolymerisation an Volumen zunehmen. Aufgrund dieser Eigenschaft finden zyklische Carbonate ihren Einsatz als Anti-Schrumpf Additive in kompatiblen Harzen. Zyklische Carbonate können sowohl unter kationischen als auch unter anionischen Bedinungen ringöffnend polymerisiern und deshalb ist die Copolymerisation mit anderen Monomeren einstellbar. In dieser Arbeit wird die Anwendbarkeit von zyklischen Carbonaten als Monomere für Hot Lithography untersucht.

Die Monomere und erhaltenen Polymere wurden hinsichtlich ihrer Reaktivität beziehungsweise (thermo-)mechanischen Eigenschaften getestet. Die Reaktivität der Monomer wurde für verschiedene Temperaturen mittel photo-DSC und -Rheologie untersucht. Der Umsatz von monofunktionellen Monomeren wurde mittels NMR und das Molekulargewicht linearer Polymere mittel GPC untersucht. Ein difunktionelles zyklisches Carbonate wird als Quervernetzer verwendet und zusammen mit den monofunktionellen Monomeren analysiert. Die (thermo-)mechanischen Eigenschaften der erhaltenen Materialien werden über Zugprüfverfahren und DMTA ermittelt. Zu letzt wurden Belichtungstest als Machbarkeitsbeweis durchgeführt.

Introduction

1 Polycarbonates

Polycarbonates are widely used in various applications as engineering plastics. Polycarbonates can be divided into aromatic polycarbonates, primarily derived from bisphenol-A (BPA), and aliphatic polycarbonates (APC) derived from aliphatic diols. They differ in their properties and hence applications. Aromatic polycarbonates are known for their transparency, thermal stability and good mechanical properties.[1-3] Therefore, aromatic polycarbonates are used for optical glasses and lenses,[4] automotive and aerospace parts,[5] or coatings.[6] Aliphatic carbonates show good biocompatibility and biodegradability[7, 8] and hence find their applications in drug delivery,[9, 10] macromolecular chemotherapeutics,[11] tissue engineering,[12] or electrodes for batteries.[13, 14]

Other fields of interest for aliphatic carbonates and their monomers include synthesis of non-isocyanate polyurethanes,[15] materials for 3D printing,[16] and solid-phase electrolytes. [14]

Polycarbonates are usually produced *via* polycondensation of a diol, e.g. bisphenol-A, and phosgene or its derivatives like dimethyl carbonate (DMC) or diphenyl carbonate (DPC) (*Scheme* 1).

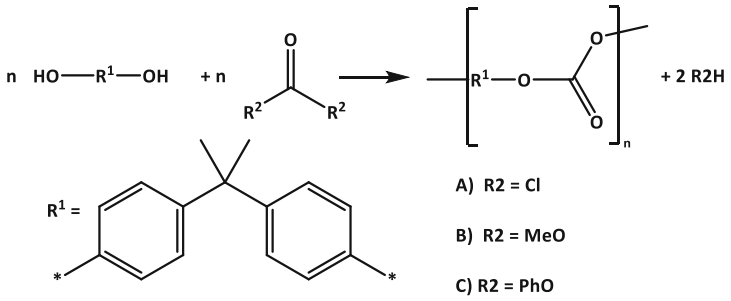

Scheme 1: General polycondensation reaction for the synthesis of Bisphenol-A Polycarbonate (BPA-PC) using phosgene (A), DMC (B) or DPC (C). Produced byproducts HCl (A), methanol (B), or phenol (C) are continuously distilled off from the reaction.

Many synthesis routes focus on phosgene derivatives or direct integration of CO_2 as a building block to avoid handling with toxic phosgene.[17-19] For the direct CO_2 integration, epoxides,

oxetanes or diols are used as starting materials for aliphatic polycarbonates.[20-22] Alternatively, APC can be synthesised *via* ring-opening polymerisation (ROP) of cyclic carbonates (CCs) (*Scheme 2*).[23-25]

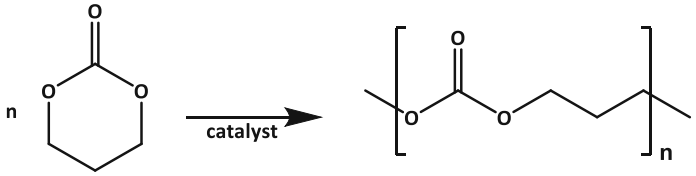

Scheme 2 Synthesis of APCs via ring-opening polymerisation. The polymerisation can be performed in bulk or in solution with varying catalyst systems.

The vast majority of polycarbonates, aromatic and aliphatic in nature, are prepared as linear polymers. Hence, PC can be dissolved, and the recycling process can be conducted in solution.[26, 27] Recycling of polycarbonates happens under acidic hydrolysis. During the hydrolysis, the diol is generated and degassing of CO_2 ensures the irreversibility of the reaction. The diol can be recovered in this process. Alternatively, transesterification with alcohols under acidic or basic conditions is possible. Both methods may retain the carbonate unit. Transesterification with methanol or ethanol in this recycling process generates the original diol and DMC or diethyl carbonate (DEC), respectively (*Scheme 3*).

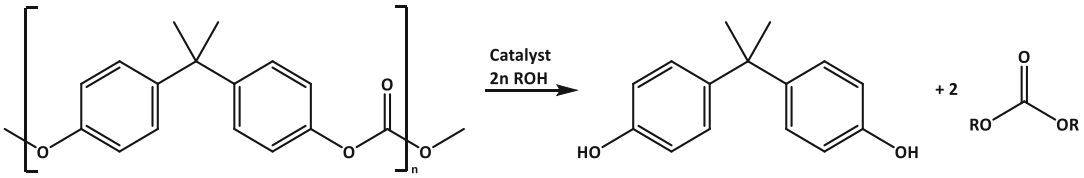

Scheme 3: Catalytic recycling of polycarbonates for the example of BPA-PC. By adding an excess of alcohol, e.g. methanol, the polymer can be decomposed to BPA and a carbonate source. The carbonate source can be purified by distillation and reused as a solvent or reactant.

All of these can be reintroduced for polycarbonate production.[26-29] Depolymerisation of aliphatic polycarbonates under basic catalysis leads to the regeneration of CCs. This ring-closing reaction occurs through the backbiting of the reactive chain end and the elimination of the cyclic carbonate. The cyclic carbonate can be recovered and recycled[30, 31] (*Scheme 4*).

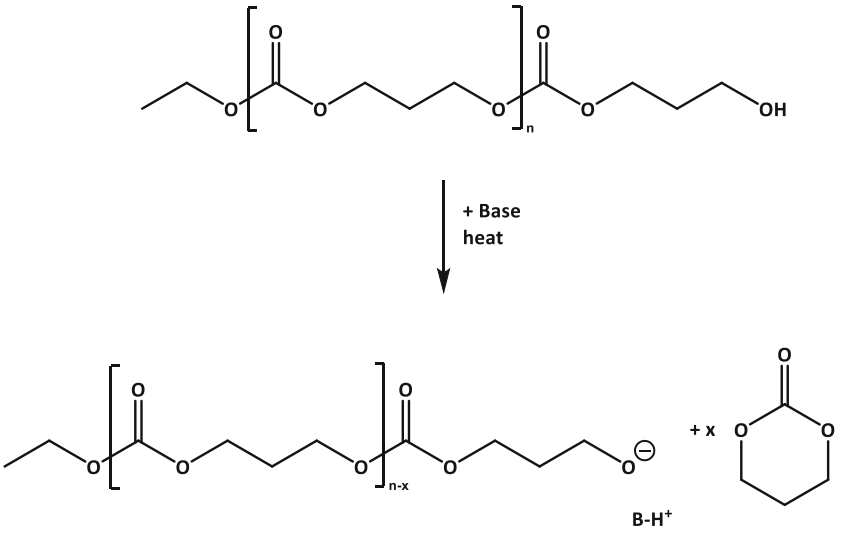

Scheme 4: Base-catalysed anionic depolymerisation of APC. The alcoholate end group of the polymer chain can react with the carbonate group in the polymer backbone and eliminate a cyclic carbonate. The cyclic carbonate is continuously distilled at high temperatures and high-vacuum to shift the equilibrium towards the CC monomer.

2 Ionic Polymerisation

Ionic polymerisation distinguishes from radical polymerisation in the active species present. The active centre of ionic polymerisation is an ion, i.e. either an anion or a cation. After generating the active centre, the monomer is added to it to form the polymer. In contrast to radical polymerisation, solvents and initiators are factors that have a strong influence on the polymerisation process.[32, 33] Contrary to radical polymerisation, the active centres in ionic polymerisation are hindered in recombination by electronic repulsion.[32] Due to the absence of termination and transfer reactions, many ionic polymerisations can be conducted in a living polymerisation fashion. The living character of ionic polymerisation enhances the control over polymer growth and, particularly, design in block copolymerisation. The ability of monomers to undergo ionic polymerisation depends on the electronic structure and the possibility to stabilise the active centre. Ionic polymerisation is more sensitive toward humidity and impurities in the form of protic substances. Most monomers used can polymerise either *via* anionic or cationic polymerisation. Some can undergo polymerisation under both mechanisms. For monomers to undergo ionic polymerisation, the monomers need an electron-withdrawing group to stabilise the formed anion and an electron-donating group to

stabilise the formed cation.[32, 34] The general reaction scheme of the ionic polymerisation can be seen in *Scheme 5* below.

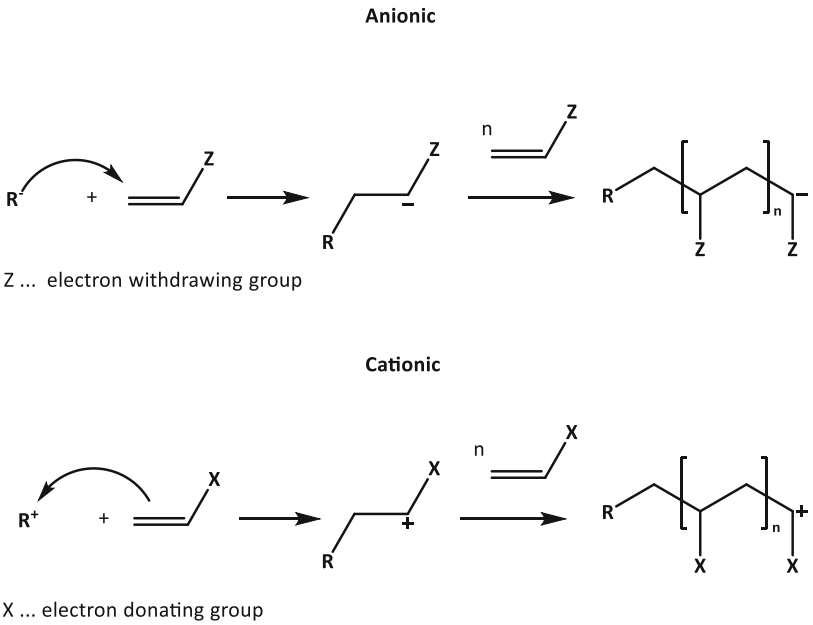

Scheme 5: Generalised mechanism of anionic and cationic polymerisation

2.1 Cationic Polymerisation

Initiated by strong Brönsted or Lewis acids, cationic polymerisation is mainly used for isobutene, vinyl ether, and cyclic monomers as these monomers can stabilise the active centre.[35, 36] Such cyclic monomers are epoxy rings, cyclic esters and ethers, oxazolines or sulfur-containing ring-structures (*Scheme 6*).[37] Big advantages of cationic polymerisation are its robustness against traces of water and dissolved oxygen in solution. In some cases, water has an activating effect on initiators for cationic polymerisation.[38] The drawbacks of cationic polymerisation are its possible ion pair recombination or β-hydrogen abstraction as termination reactions.[35] Hence, nucleophilic groups must be excluded if the propagating species is a carbocation. For these reasons, living cationic polymerisation was not achieved until the mid-1980s.[39] In cases of cyclic monomers, nucleophiles, like alcohols, can act as chain-transfer agents or initiators.[40-42]

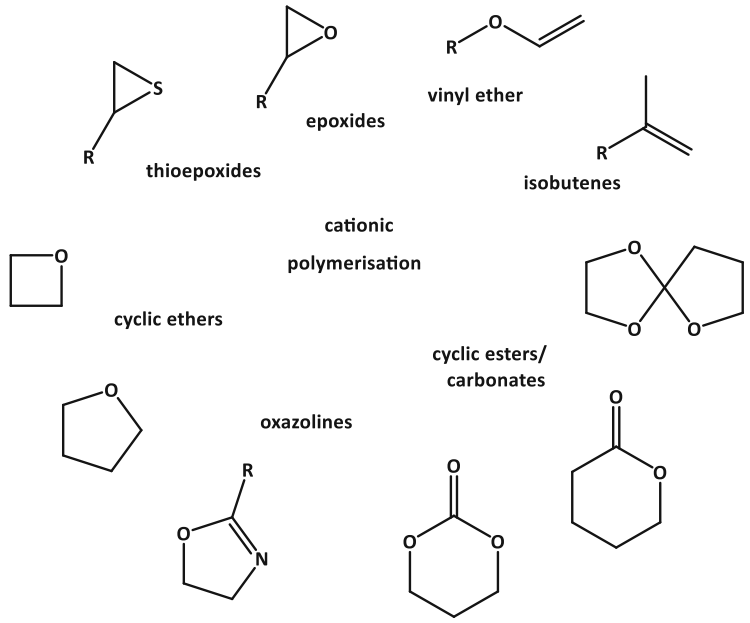

Scheme 6: Overview on cationically polymerisable monomer

2.2 Anionic Polymerisation

Anionic polymerisation with its living character allows controlled polymer structures, predictable molecular weight and narrow polydispersity. First introduced by Szwarc,[34] the term "living polymerisation" describes a polymerisation, where termination and transfer reactions are absent. For a living polymerisation to exist, it requires exceptionally high monomer purity, exclusion of water and high-vacuum techniques.[34] For monomers to undergo anionic polymerisation, the propagating negative charge must be stabilised by adjacent electron-withdrawing groups. Well researched monomers regarding anionic polymerisations are dienes, styrenes and cyclic monomers (*Scheme 7*).[43] Cyclic monomers include epoxides, lactones and lactams. Highly pure monomers and solvents are necessary to realise living polymerisation in anionic polymerisation.[43] Electrophilic groups, such as amino- and hydroxyl groups and acidic proton donating groups, must be excluded or masked during anionic polymerisation.[43] Monomers bearing ester functionalities as electron-withdrawing groups, such as (methyl)methacrylates, must be polymerised at low temperature to avoid unwanted reactions at the carbonyl carbon.[44-46]

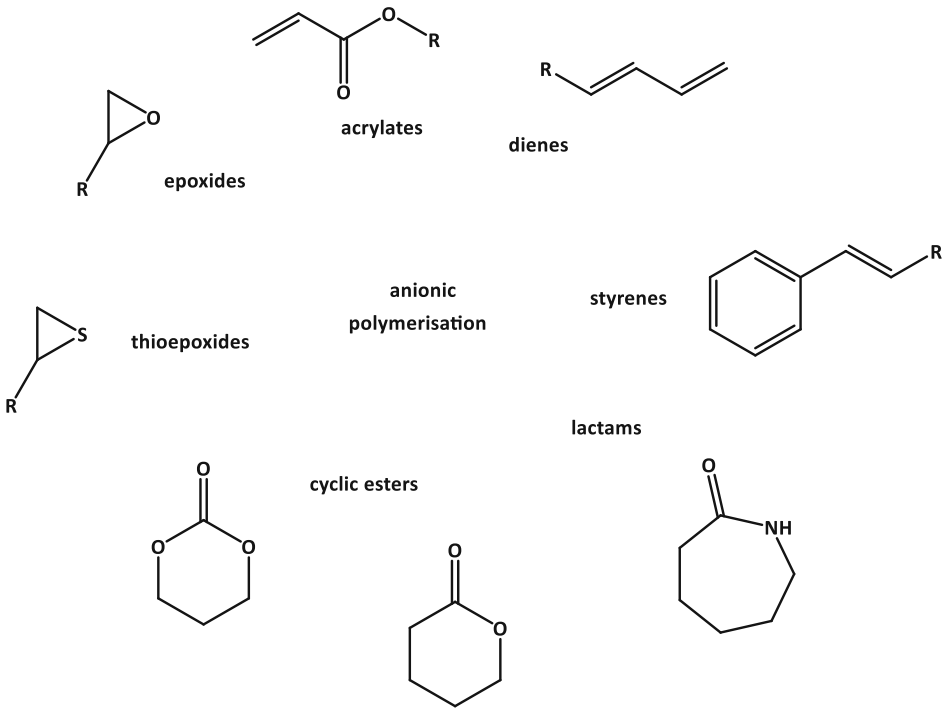

Scheme 7: Overview on anionically polymerisable monomer

3 Ring-Opening Polymerisation

Cyclic monomers with strongly polarised bonds due to heteroatoms or highly strained rings may undergo ionic polymerisation *via* a ring-opening mechanism. Monomers mostly contain one or more heteroatoms in the ring structure.[36] Ring-opening reactions can undergo various mechanisms: coordination, ionic, metathesis, radical or enzymatic. The equilibrium between the monomer and polymer should be shifted towards the polymer for ring-opening polymerisation to be favoured, as most ROPs are reversible reactions. [36]

3.1 Cationic Ring-Opening Polymerisation

Cationic ring-opening polymerisation (cROP) is a chain growth polymerisation in which the active centre is a cationic species. Cyclic structures containing at least one heteroatom can be polymerised via cROP. Two pathways for cROP are postulated, which differ in the location of the active centre. The active chain-end pathway occurs through an S_N2 or S_N1 reaction

mechanism depending on the stability of the formed cation[47] (*Scheme 8*). In this case, the cyclic monomer reacts as the nucleophile, leading to the ring-opening process.

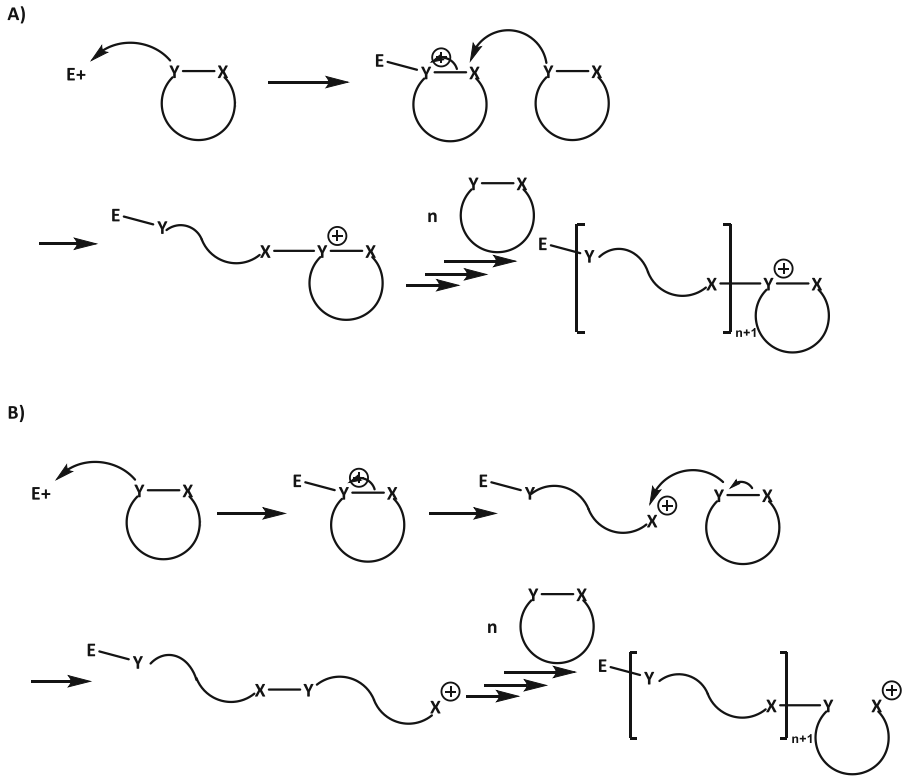

Scheme 8: Comparison of both SN-reaction mechanisms for the active chain-end pathway.[47] Depending on the stability of the formed cation, an SN2 (A) or an SN1 (B) reaction mechanism will dominate the ring-opening.

For the activated monomer mechanism, the active centre of the polymerisation is not on the growing polymer (*Scheme 9*). Here, the monomer is activated by a Lewis or Brönsted acid in the first step and forms a cation. The cation may react with a nucleophile leading to the ring-opening. The activated monomer can then be attacked by an alcohol or an amine. The resulting alcohol after ring-opening attacks the following activated monomer, which is repeated during the polymerisation.[47]

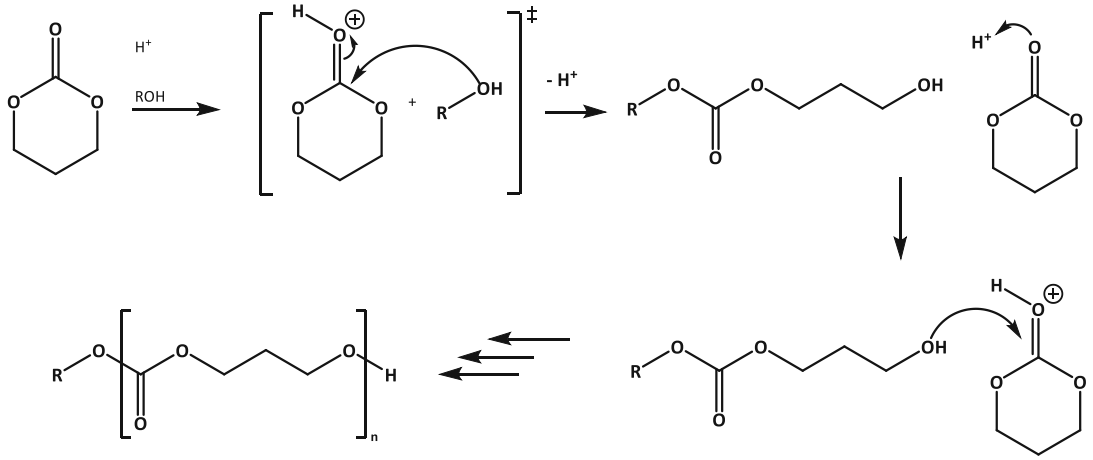

Scheme 9: Activated monomer pathway for cROP. The cyclic carbonate monomer is activated via protonation of the carbonyl oxygen. The carbonyl carbon is further attacked by an alcohol, which opens the ring generating an alcohol functionality at the end of the polymer chain. This alcohol attacks the next activated monomer.[47]

For cyclic carbonates, both pathways can co-occur if no free hydroxyl functional groups are present. In that case, the protonated – activated – monomer is attacked by the carbonyl oxygen of another monomer (*Scheme 10*). Ring-opening leads to the formation of a mono-ester of carbonic acid. After decarboxylation, it forms an alcohol functionality on one side and an activated chain end on the other side. Monomers can then be attached on both sides of the chain end.[48] Therefore, the use of alcohol might not be necessary depending on the reaction conditions.

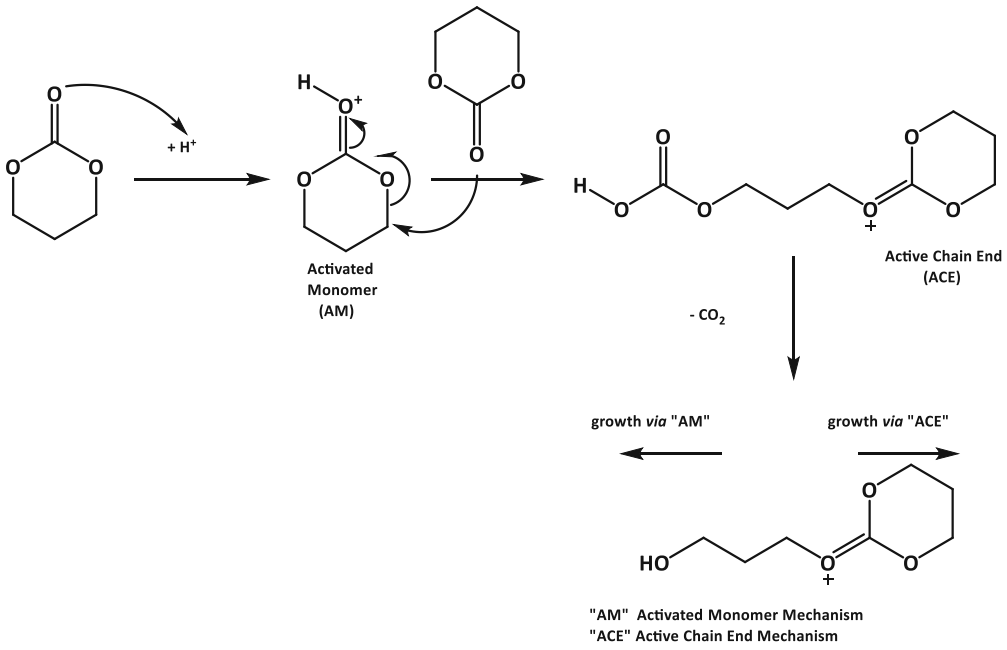

Scheme 10: cROP mechanism for CCs using acids to activate the monomer without initiating alcohol functionalities. The activated monomer is attacked by the carbonyl oxygen of another CC and forms the mono-ester of carbonic acid. After decarboxylation, an alcohol moiety is formed on one side, and the attacking CC monomer is now the active chain end. New monomers can either be attacked by the alcohol moiety or attack at the active chain end.

Cationic ring-opening polymerisation of cyclic carbonates can also be initiated *via* alkylation agents[49] or alkyl halides.[24] The latter was also reported suppressing CO_2 formation at higher temperatures when using 20 mol% of alkyl halides in bulk and solution.[24]

Due to volume expansion during polymerisation, cyclic carbonates are often used as comonomers.[25] Reported expansions of cyclic carbonates range from 1 to 7% and are independent of the polymerisation mode.[25] However, the copolymerisation behaviour is dependent on the mode of polymerisation (*Scheme 11*).[41, 50-54] Copolymerisation is possible with epoxy resins,[52, 54] lactones,[40, 55-57] and oxetanes.[58] Under cationic reaction conditions, copolymerisation with epoxides comes with several side reactions depending on the carbonate compound's ring size (*Scheme 11* and *Scheme 12*). Under these conditions, the polymerisation proceeds *via* spiroorthocarbonates. These can then undergo double ring-opening (DROP), transacetalisation, or elimination of smaller molecules.[50, 51]

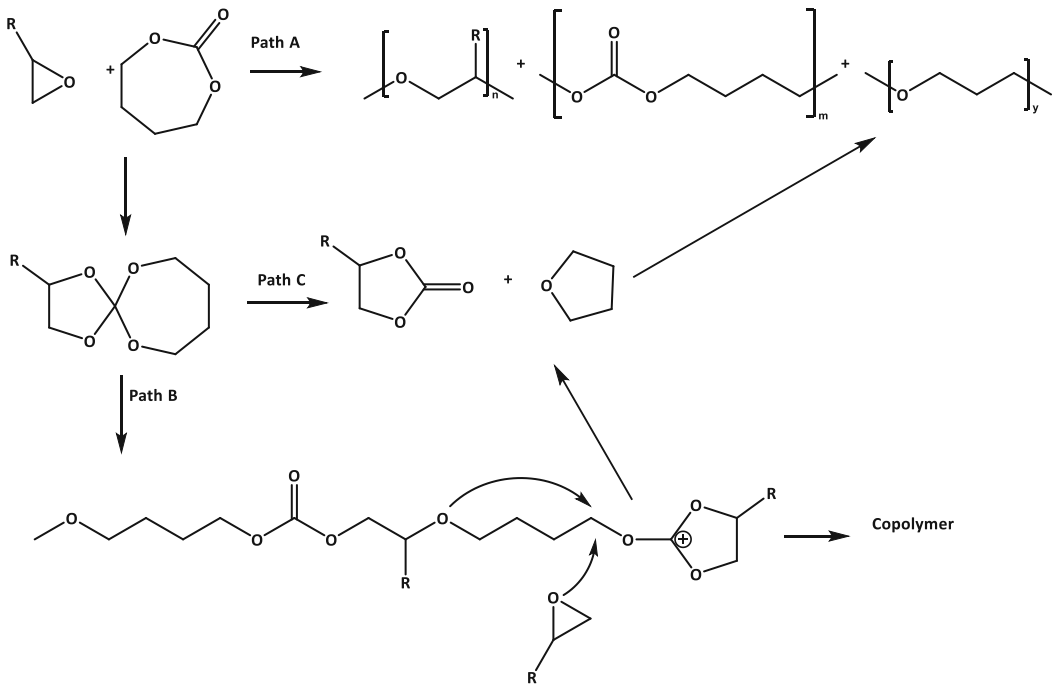

Scheme 11: Various reactions of an epoxy resin with a seven-membered cyclic carbonate under cationic conditions. The main products are homopolymers of each monomer and a poly(THF) derivate (Path A). Poly(THF) is formed via transesterification over a spiroorthocarbonate intermediate (Path C). The formed five-membered cyclic carbonate does not polymerise under cationic conditions.[50] The copolymer (Path B) is the minor product of cationic copolymerisation.

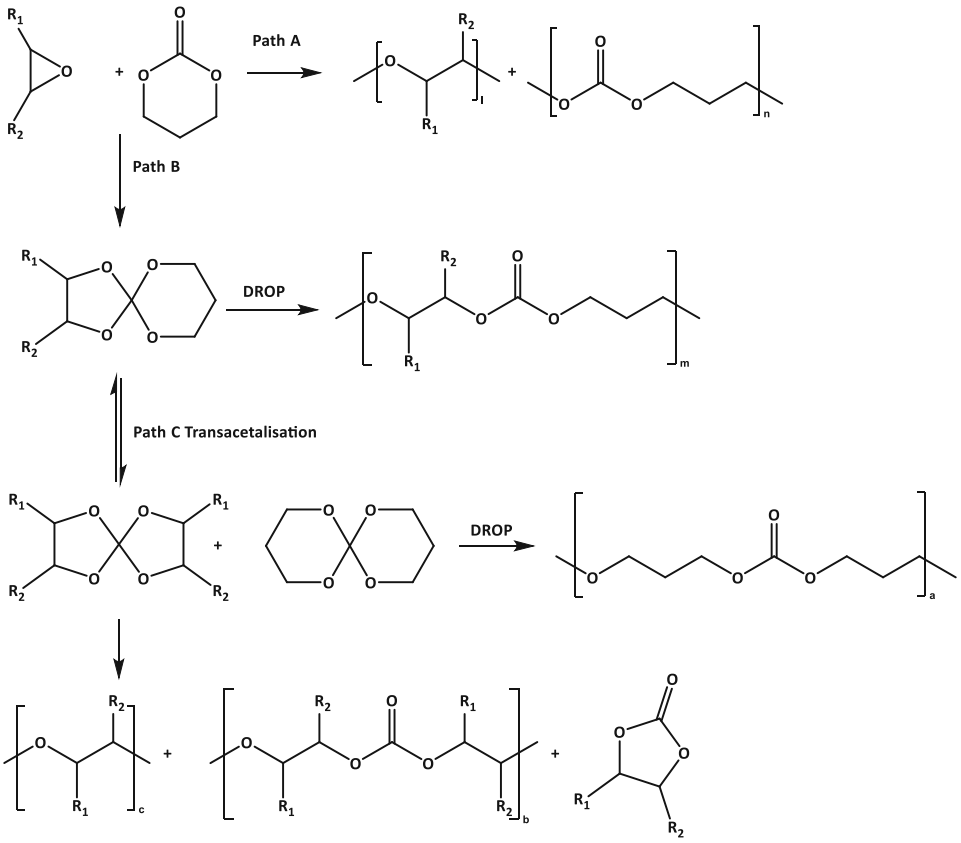

Scheme 12: Overview of the reactions of epoxides with six-membered cyclic carbonates. Both monomers can homopolymerise (Path A) or form a spiroorthocarbonate intermediate (Path B). This asymmetric intermediate may undergo DROP and is in equilibrium with two symmetric spiroorthocarbonates (Path C). The six-membered spiroorthocarbonate further undergoes DROP to a poly(ether-carbonate). The five-membered spiroorthocarbonate forms the poly(ether) and the five-membered cyclic carbonate.

Ariga *et al.* reported a one-shot method for block-copolymerisation of cyclic carbonates with oxetanes.[58] The oxetane monomer is consumed faster than the cyclic carbonate and at lower temperatures to form a poly(oxetane)-block. The second block is formed from the cyclic carbonate, generating a poly(oxetane) – *block*- poly(carbonate). Random and block copolymers can be obtained from the reactions of cyclic carbonates with lactones.[58]

3.2 Anionic Ring-Opening Polymerisation

In contrast to cationic ring-opening polymerisation, the active species in anionic ROP (aROP) is a negatively charged ion. Anionic ring-opening polymerisation of cyclic carbonates leads to high molecular weight polymers without ether units. Contrary to cationic conditions, the carbonyl group is not activated, and the active species is an alcoholate group. The initiator attacks the carbonyl carbon and sets free an alcoholate end group. This alcoholate attacks the next monomer on the carbonyl carbon.[42] During aROP, the polymer is in equilibrium with the cyclic monomer, which can be exploited for recycling purposes (*Scheme 13*).[59]

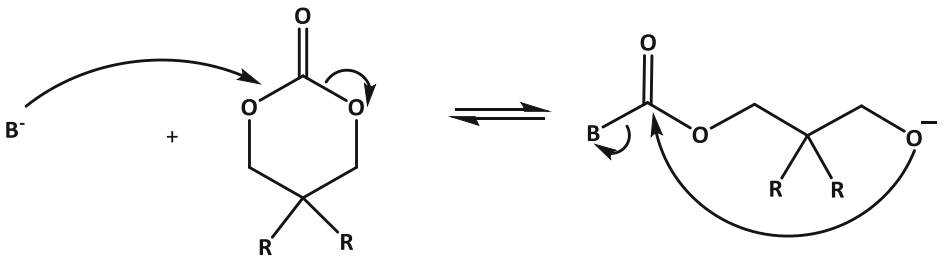

Scheme 13: Equilibrium reaction between the initiator B⁻ and the CC monomer. The alcoholate end group may react with the carbonyl group and release the base B- (backbiting).

The bulkier the substituents on the cyclic structure, the less likely the polymerisation will happen. Alcoholates, organolithium compounds and amine-based initiators are commonly used in aROP of cyclic carbonates, lactones and lactams.[12, 41, 44, 53, 56] When an amine-based initiator is used, a zwitterionic polymerisation mode can be observed (*Scheme 14*).

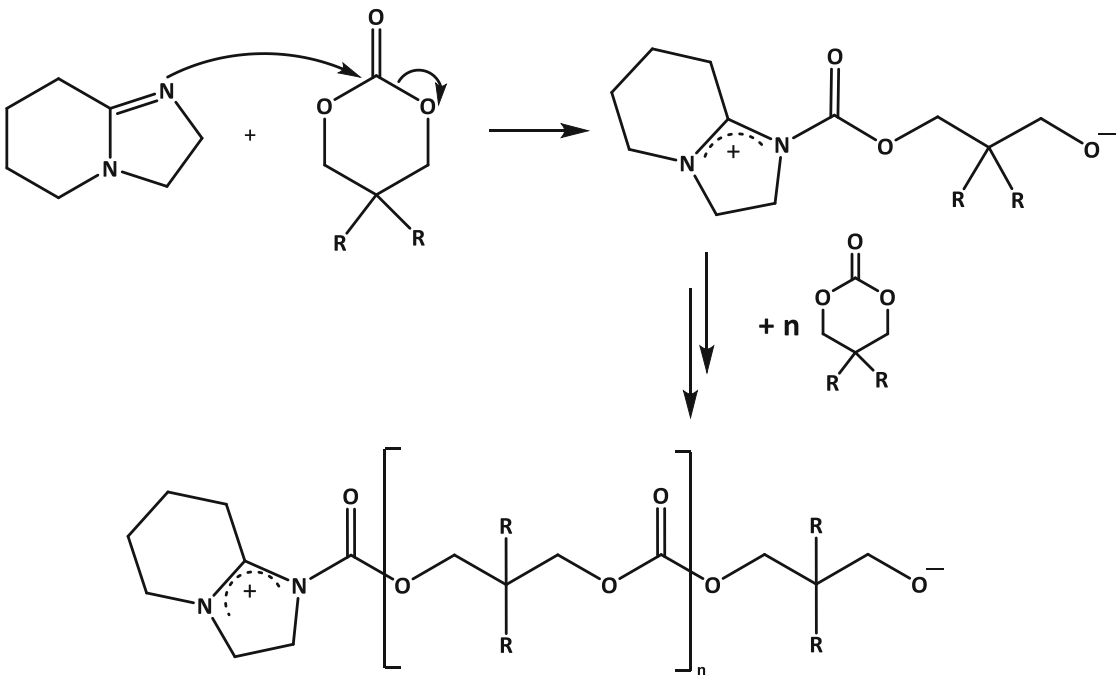

Scheme 14: aROP using an amidine base as an initiator. The base attacks the monomer, and an alcoholate is set free. This alcoholate attacks the next monomer and leads to polymerisation.

Backbiting of the alcoholate end group of the growing polymer chain may release the initiator and form a macrocyclic structure. Alcohols can be combined with organic super bases as an initiating system to improve the initiation process further.[12] Organic superbases are often bulky and may be blocked by steric hindrance due to substituents on the cyclic monomer.[41] Copolymerisation is possible with epoxy resins,[52, 54] lactones,[40, 55-57] and oxetanes.[58] Under anionic reaction conditions, the reaction speed of epoxy resins can be drastically increased with the use of cyclic carbonates as a comonomer.[54] In this polymerisation mode, the spiroorthocarbonate is not formed, and thus, no side reactions occur.

4 Ionic Photopolymerisation

Using light as an energy source to start polymerisation enables polymerisation on-demand and spatial control of the polymerisation.[60, 61] Photopolymerisation is used in a broad spectrum of applications such as lithography,[62] photoresists,[63, 64] dental applications,[65-67] coatings,[63, 68, 69] biomaterials[11, 70] or adhesives.[37, 71] Often other components such as fillers,

pigments or additives can be added.[65, 66, 71] The wavelength of the light source can range between UV and IR.[62, 72, 73]

The polymerisation process is started once the initiator absorbs light of a suitable wavelength. Then, depending on the initiating system, either a base, an acid or a radical is formed upon irradiation to start the reaction. Although radical polymerisation is the industry's most common type of polymerisation,[74] ionic photopolymerisation is heavily investigated. In the field of ionic photopolymerisation, cationic photopolymerisation is more extensively studied.[75-77]

Ionic photopolymerisation inhibits several advantages besides a broad scope of monomers. Its low sensibility towards oxygen, high conversion rates, and the living character of ionic polymerisation are often sought. Cyclic monomers often undergo cationic and anionic ROP and show low polymerisation shrinkage. Some monomers, such as spiroorthocarbonates, sprioorthoesters and cyclic carbonates, expand during polymerisation, which counteracts shrinkage stress upon curing.[24, 25, 50, 54]

4.1 Cationic Photopolymerisation

Cationic photopolymerisation equals standard cationic polymerisation initiated by light. Photoinitiators for cationic photopolymerisation release strong Brönsted or Lewis acids upon irradiation and, hence, are called photo-acid generators (PAG).[77] Such PAGs are often salts of the conjugated base to the acid they generate and a counterion acting as the chromophore. Onium-salts, especially diaryliodonium and triarylsulfonium salts, are well known in the literature for this purpose.[37, 64, 75, 77]

The cation, acting as the chromophore, is responsible for the absorption maximum, quantum yield and thermal stability of PAGs. The anion, the conjugated base to the generated acid, is responsible for acid strength and the propagation rate constant.[64] High fluorination of the anion decreases nucleophilicity and increases the acid strength.[77]

Sensitisers can be added if the used wavelength is outside the absorption spectrum of the chromophore.[78] Such sensitisers can be perylene, anthracene or phenothiazine.

Exemplary, the initiation process of iodonium salts is shown below. Homo- and heterolytic cleavage generates a superacid HX, which initiates the polymerisation (*Scheme 15*).

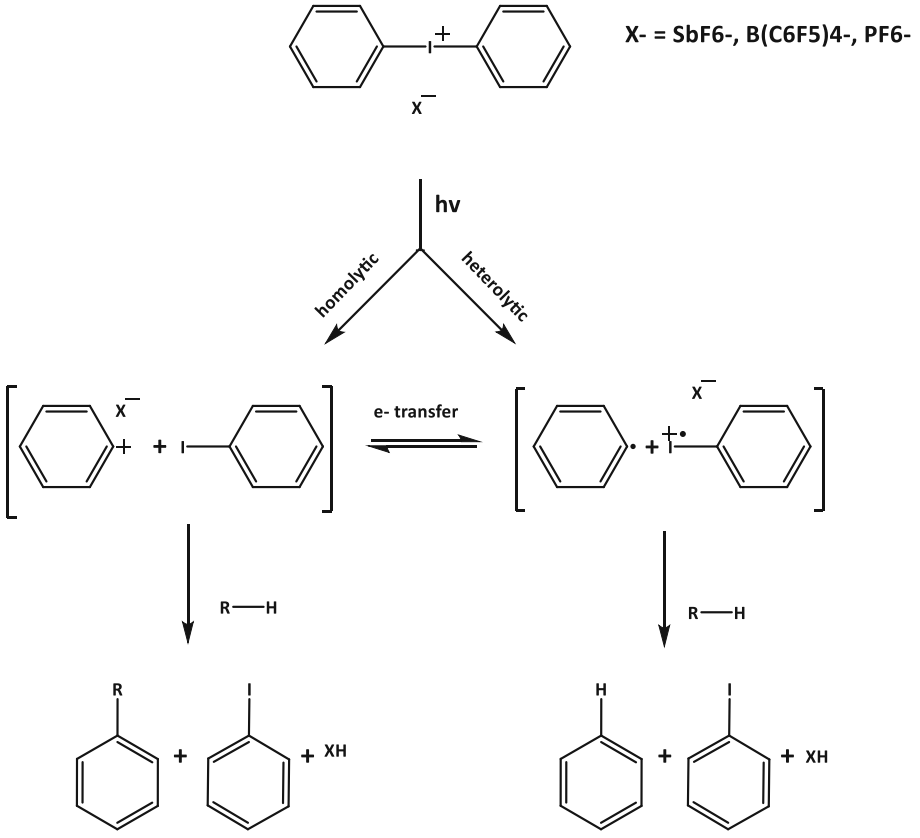

Scheme 15: Photo-induced heterolytic and homolytic cleavage of diphenyliodonium salts. The generated superacid HX initiates the cationic polymerisation.

A so-called dark reaction may proceed after turning off the light source if the polymerisation has a living character. This dark reaction happens until all monomer is integrated into the polymer.[74]

4.2 Anionic Photopolymerisation

Anionic photopolymerisation equals standard anionic polymerisation initiated by light. Photo-base generators (PBG) in anionic photopolymerisation are the counterparts to PAGs in cationic photopolymerisation and generate bases when irradiated. The development of efficient PBGs progressed slower compared to the development of various PAGs. First reported PBG released

primary or secondary amines as bases, which were not strong enough to induce anionic polymerisation.[76, 79] Therefore, the development of PBGs that release stronger bases, such as tertiary amines,[80-82] amidines[83] or phosphazenes[84] was performed.

The cleavage of an amidine derived PBG is depicted in the scheme below. After homolytic cleavage of the benzylic N-C bond, hydrogen abstraction from the bridging carbon atom forms the active organic superbase (*Scheme 16*).

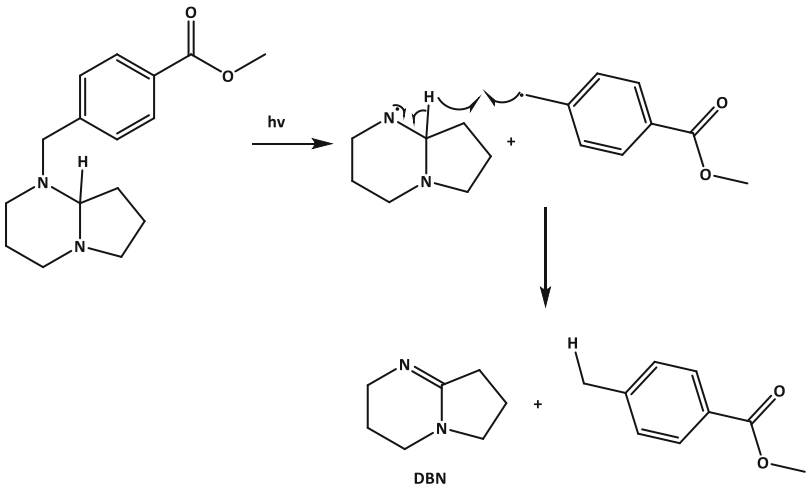

Scheme 16: Photodecomposition of the PBG based on the organic base 1,5-Diazabicyclo[4.3.0]non-5-en (DBN). After homolytic cleavage of the benzylic C-N bond, the benzylic radical abstracts the hydrogen on the bridging carbon between the nitrogen atoms. Hydrogen abstraction forms the amidine bond and hence generates the organic superbase.

5 Additive Manufacturing

3D printing or Additive Manufacturing (AM) is a well-established technique for the generation of complex structures. The spectrum of materials used in AM is continually growing and includes polymers, metals and ceramics.[65, 71] Depending on the technique, the used material can be in the liquid or solid state. In AM, a structure is built up layer by layer in z-direction onto the x-y plane. The structure is digitally sliced into these layers with the step size in the z-direction as layer thickness. The layer thickness can be reduced to increase the resolution of

the 3D printing process. Vice versa, the layer thickness can be increased to increase the printing speed. Photopolymerisation is used in various AM techniques:[71]

- Inkjet 3D printing: photo-initiated polymerisable inks are printed onto an XYZ-moveable stage[85] analogue to standard inkjet printers.

- Stereolithography: a UV-laser source rasters the surface of a photo-curable resin. A structure is polymerised onto a moveable stage, which is immersed into the resin. After one layer is polymerised, the stage is moved downwards and covered with resin, and the process starts again (Bottom-up).[72] Another approach is by irradiation from the bottom through a UV transparent window. Here, the building platform is completely immersed into the resin. After irradiation of one layer, the platform is moved upwards, and the next layer can be irradiated.

- Digital Light Processing: the principle of Digital Light Processing follows the one of stereolithography, with the main difference being simultaneous irradiation of an entire layer.[72]

The advantages of light-based AM techniques (AMT) are given through high writing speeds, high penetration depths and curing depths, and commercially available monomers. Though most light-based AMTs primarily work with radical polymerisation, some results using ionic photopolymerisation were reported in recent years.[62, 63, 86] To compensate for low reactivities or high viscosities and enhance printing resolution, a heatable material vat was developed, leading to Hot Lithography.[62, 72] The printing setup is the same as stereolithography (Figure 1).

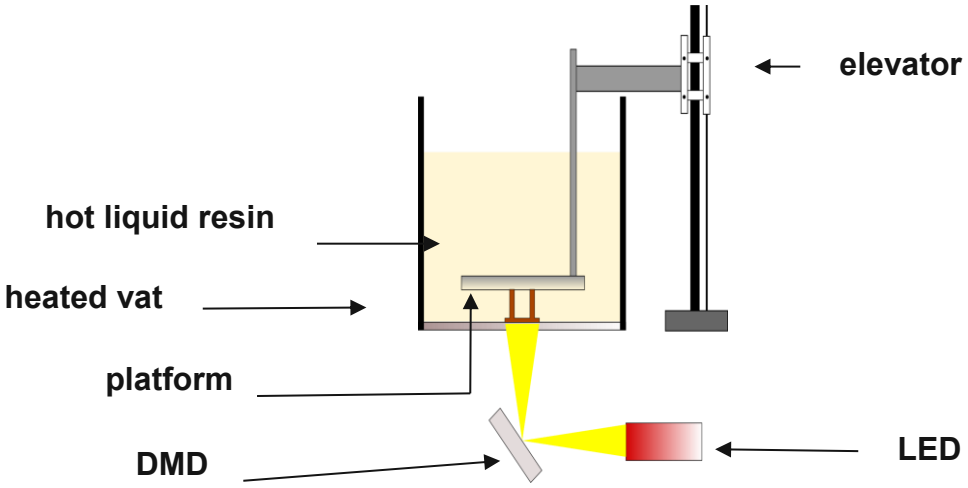

Figure 1 Schematic set up for Hot Lithography 3D printing

Objective

Commonly used monomers for AMTs, like (meth)acrylates, suffer from polymerisation shrinkage. This shrinkage can cause cracks and low surface quality. Cyclic carbonates may show volume expansion during ring-opening polymerisation (ROP). This expanding characteristic may help reduce the polymerisation stress and improve the mechanical properties of 3D printed materials. Therefore, cyclic carbonates are a promising monomer class for several reasons. The choice of substituents can widely tune the mechanical properties of aliphatic polycarbonates (APC). Due to their hydrolysable carbonate backbone, the APC network can be fully degraded and the starting material recovered.

Currently, all used monomers for photo-crosslinked polycarbonates for 3D printing devices are imitating carbonate characteristics. Used macromer precursors have a polycarbonate origin but have end groups, which can be crosslinked by radical polymerisation.

This work should focus on developing cyclic carbonates (CCs) as monomers for Hot Lithography. Ionic ROP of cyclic carbonates in bulk is mainly investigated for monofunctional monomers. The synthesis of crosslinked polycarbonates through ROP has been reported for hydrogels with up to 15 mol% crosslinkers. There are few reports on the bulk polymerisation of crosslinked polycarbonates through ROP. However, photo-induced bulk polymerisation of highly crosslinked polycarbonate systems through cationic and anionic ring-opening polymerization will be investigated.

For this, six-membered cyclic carbonates with different substituents will be synthesised and analysed regarding their reactivity for ionic ring-opening polymerization. Photo-DSC and photo-rheology will give an insight into the reactivity, whereas NMR and GPC analysis will investigate the conversion and molecular weight, respectively. Furthermore, NMR analysis can help investigate the molecular structure of the polymer. Reactivity will be analysed at various temperatures. A difunctional monomer will be used as a crosslinker based on monofunctional polymerisable cyclic carbonates. (Thermo-)Mechanical analyses will be conducted on the obtained polycarbonates. Concludingly, laser exposure tests will be performed to determine the applicability of cyclic carbonates as monomers for Hot Lithography.

State of the Art

The ring-opening polymerization (ROP) of cyclic carbonates, in bulk and solution, was investigated for various cyclic carbonates (CC) in literature, with trimethylene carbonate and 5,5-dimethyl-1,3-dioxane-2-one being the most prominent ones.[24, 49, 51, 87-90] Initiated by mono- and multifunctional alcohols, ROP of CC was mainly investigated for monofunctional CCs.[24, 25, 40, 49, 51, 59, 91] Multifunctional CCs are mostly reported for the synthesis of films,[92] coatings[5, 6, 93] or hydrogels.[94-98]

Barker and Dove previously reported photo-initiated cationic ROP for cyclic carbonates.[99] In their experiments, triarylsulfonium hexafluorophosphate salts were used as photoacid generators (PAGs), trimethylene carbonate as monomer, and benzyl alcohol as initiator. It was reported that the cROP of trimethylene carbonate proceeds in a bimodal way (Scheme 10, page 11). Some of the initially activated monomer (AM) is attacked by another monomer molecule, leading to a mono-ester of carbonic acid. Decarboxylation leads to the formation of an alcohol functionality that can attack following AMs. The bimodality of cROP was also present when using 1,4-butanediol as the initiator.[99] At first, it was found that residual water may lead to decarboxylation of the monomer, forming the original diol and hence initiating the reaction.[48] Jimenez-Pardo et al. proved that cROP of cyclic carbonates always proceeds in a bimodal way by partial decarboxylation of the monomer (Scheme 10, page 11).[100] Other monomers can then attack the present active chain-end (ACE). Decarboxylation can further occur if the endocyclic oxygen of the monomer attacks the ACE. The subsequent monomer attacks at the 4-position of the new ACE and leads to ring-opening through decarboxylation, forming an ether bridge (*Scheme 17*). This side reaction is predominant at temperatures above 80 °C during cROP.[41] To avoid these side-reactions, ROP of CCs is more often performed *via* anionic ROP, which also allows control over copolymerisation with other monomer classes.[36]

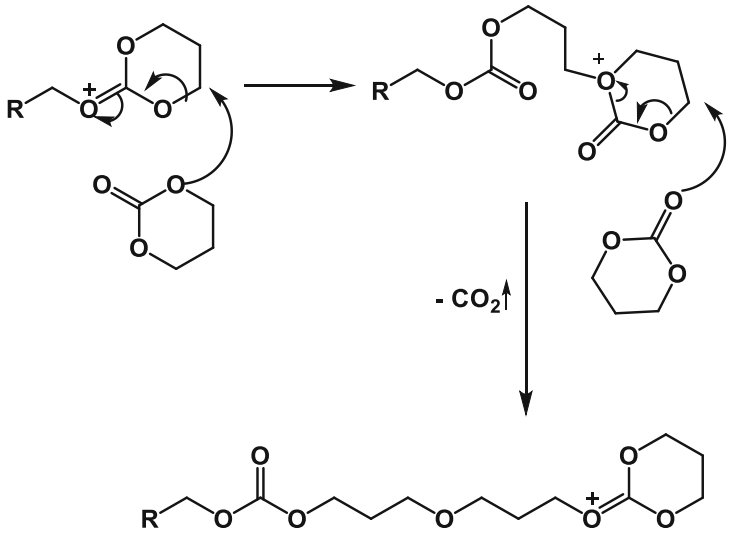

Scheme 17: Side-reaction of cROP during the ACE mechanism leading to decarboxylation and formation of ether bridged aliphatic polycarbonates (APCs). The attack of the ACE can either happen through the carbonyl or the endocyclic oxygen. If the attacks proceed through the endocyclic oxygen, the subsequent monomer attacks at the 4-position relative to the activated endocyclic oxygen and ring-opening proceeds via decarboxylation and activation of the attacking monomer. Higher temperatures lead to higher content of ether units in the polymer backbone.[41]

Crosslinking of PC structures can be achieved *via* various methods:

Physical crosslinking has previously been achieved by thermoreversible crosslinking of triblock copolymers consisting of poly(trimethylene carbonate)-block-PEG-block-poly(trimethylene carbonate) polymers to obtain hydrogels (Scheme 18, A).[94-96]

Bartolini et al. used protected carboxylic acids and protected guanidine-based side-groups to increase the non-covalent interaction between polymer chains for physical crosslinking by non-covalent interactions (Scheme 18, B).[101] Another approach was implementing two reactive side groups, which exhibit thermally induced labile crosslinks *via* (retro-)Diels-Alder reaction.[102, 103] This enables the thermal remodelling of the crosslinked polycarbonate (Scheme 18, C).[103]

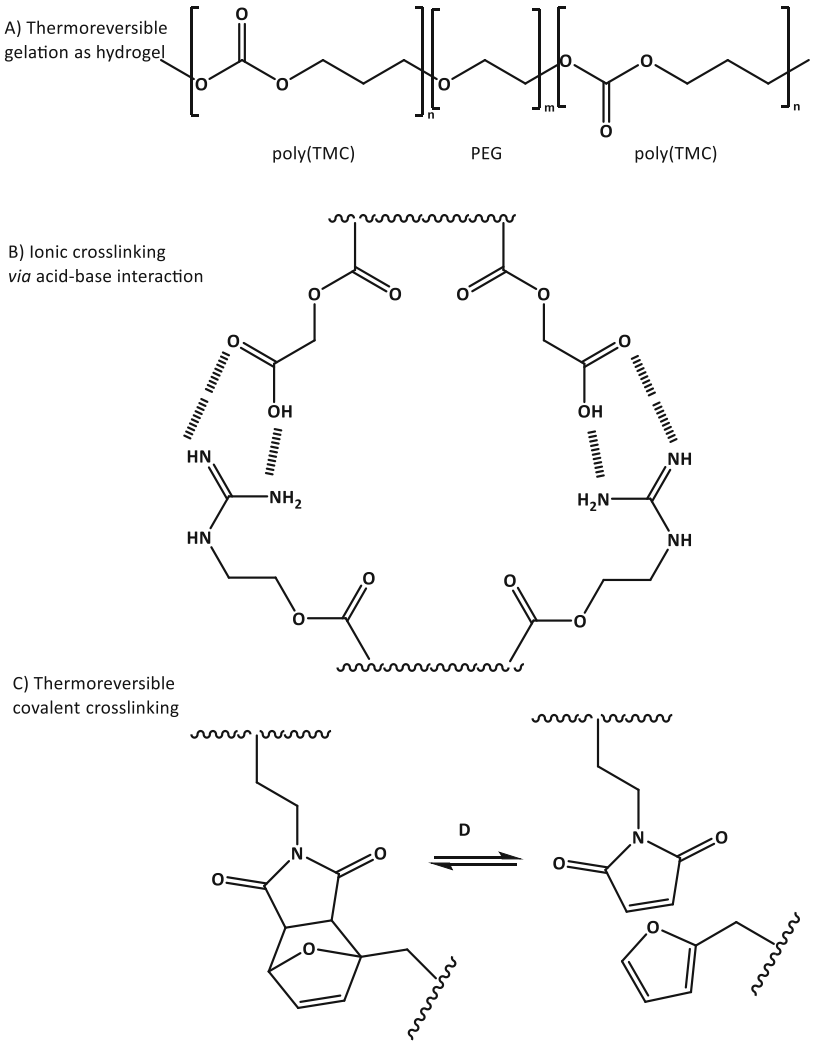

Scheme 18: Overview on non-covalent interactions used for crosslinking of aliphatic polycarbonate. A) Hydrogen bonds between the the linear poly(TMC)-block-PEG-block-poly(TMC) as thermoreversible gelation; B) Acid-base interaction between two differently modified polymer strands; C) thermoreversible covalent crosslinking via substituents, that undergo thermally induced (retro-)Diels-Alder reaction.

Covalent crosslinking can be achieved using monomers bearing multiple CC groups.[92, 101, 104, 105] Di(trimethylolpropane carbonate) (5,5'-(oxybis(methylene))bis(5-ethyl-1,3-dioxan-2-one; Di-C) was used as a crosslinker by Matsukizono and Endo (Scheme 19, D).[92] They performed aROP of 5,5-dimethyl-1,3-dioxane-2-one and DI-C in solution to cast films of carbonate networks.[92] Films with different ratios between 0 and 100% DI-C were investigated and tested in their mechanical and optical properties. The films were highly transparent in the UV and near-IR regions.[106] Tensile strengths ranged between 10.4 MPa for 10mol% DI-C and 25 MPa for 20 and 30 mol% Di-C. Di-C was homopolymerised in melt, using diols as co-initiators and various organic bases of different strengths by Wang et al.[106] The diol was implemented to achieve an organo catalysed anionic ROP. Triethylamine catalysed aROP at 130 °C to yield 53%

conversion after 30 min. At a temperature of 110 °C, 7% conversion was obtained after 90 min. The concentration of triethylamine was held constant at 2.2 mol%. 1,8-diazabicyclo[5.4.0]undec-7-en (DBU), 4-dimethlaminopryidine and 1,5,7-triazabicyclo [4.4.0] dec-5-ene led to conversions between 93 and 99% after 30 min at 130 °C.[106] DI-C was also used as an efficient crosslinking reagent for the synthesis of polyester-based elastomers.[105]

2,2-Bis(hydroxymethyl)propionic acid (bis-MPA) was used for the synthesis of crosslinkers for PCs by esterification of bis-MPA with multifunctional alcohols.[91, 101, 107] By the introduction of α,ω-hydroxyl-PEG this difunctional crosslinker is used for the synthesis of hydrogels.[101, 104]

Photo-induced crosslinking of APCs was achieved by introducing photo-polymerisable end- or side groups.[69, 70, 108] Polymerisabe double bonds can be introduced and crosslinked *via* photo-initiated thiol-ene click chemistry.[70] This allows fast and precise photo-induced crosslinking using multifunctional thiols. Weems et al. reported a method for 3D printing scaffolds comprising a polycarbonate backbone bearing vinyl moieties, a urethane-based reactive diluent and tetrafunctional pentaerythritol tetrakis(3-mercaptoprionate) as crosslinker.[70] Photopolymerization of pure polycarbonate networks has not been shown so far.

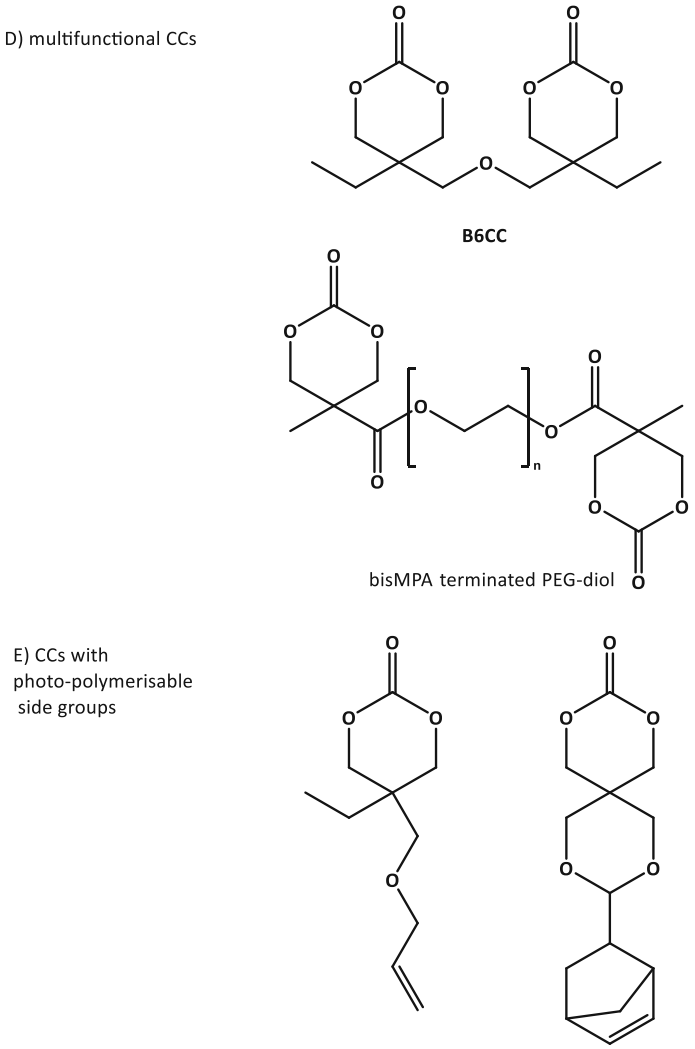

Scheme 19: Overview of multifunctional CCs for covalent crosslinking. D: multifunctional CC monomer such as DI-C and bisMPA terminated alpha,omega PEG diol; E) CC monomer bearing photo-polmerisable side groups, such as double bonds.

Results and Discussion

1 Monomer Synthesis

New monomers need to be synthesised to investigate cyclic carbonate's (CC) applicability as monomer class for Hot Lithography. Six-membered CCs were chosen due to their polymerisation behaviour. In contrast to five-membered ring systems, six-membered CCs polymerise under cationic and anionic conditions.[41] Five-membered CCs do not polymerise under cationic conditions and, therefore, were excluded. Ring-opening polymerisation of seven-membered CCs can be thermally induced, leading to the formation of polymers and hence reduced storage stability.[41] This behaviour of seven-membered CCs would lead to undesired polymerisation within the heated material vat during the Hot Lithography printing process. For these reasons, six-membered CCs with different substituents were targeted to be synthesised to investigate their processability for Hot Lithography (Scheme 20). For this thesis, monomers based on 2,2-diethylpropane-1,3-diol (Et-C),[59] diethyl bis(hydroxymethyl)malonate (Mal-C), dihydroxyacetone (DHA-C),[109] 2-phenylpropane-1,3-diol (Ar-C),[109] di(trimethylolpropane) (Di-C)[92] and pentaerythritol[109] (Di-C-S) were selected.

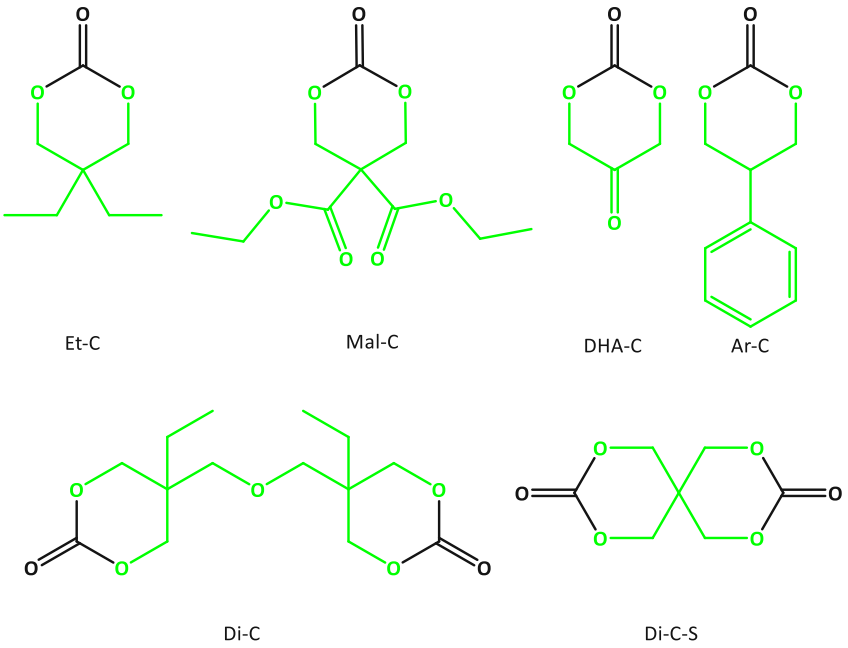

Scheme 20: Targeted CC monomers based on 1,3-diols with different substituents. In green the underlying alcohols: 2,2-diethylpropane-1,3-diol (Et-C), diethyl bis(hydroxymethyl)malonate (Mal-C), dihydroxyacetone (DHA-C), 2 phenylpropane 1,3-diol (Ar-C), di(trimethylolpropane) (Di-C) and pentaerythritol (Di-C-S).

The corresponding polycarbonate always accompanies the synthesis of CCs as the most commonly used catalysts catalyse the reaction between the diol and carbonyl source and the ring-opening polymerisation. The catalyst load and temperature can be adjusted to shift the reaction towards the CC. Many routes were developed over time to target the CC as the main product of the reaction. Most synthetical routes, excluding the usage of phosgene, utilise reagents such as di(m)ethyl carbonate[41, 59] or diphenyl carbonate (DPC)[92], gaseous CO_2[22] or 1,1'-carbonyldiimidazole (CDI)[91] as carbonyl source (Scheme 21).

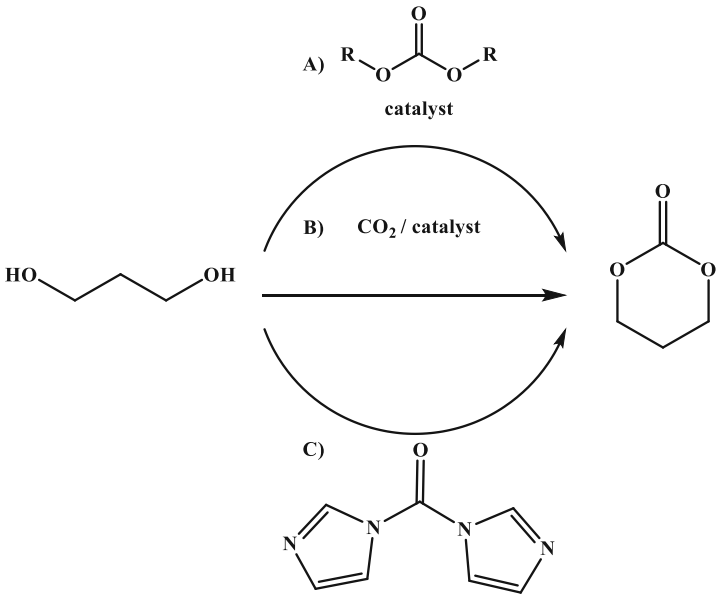

Scheme 21: Different synthesis pathways for cyclic carbonates: A: transesterification using symmetrical organic carbonates as carbonyl source, B: utilisation of gaseous CO_2 as carbonyl source and C: synthesis using CDI as carbonyl source.

The carbonyl source can significantly affect the reaction conditions and time. For this thesis, three synthetical pathways were compared with each other.

1.1 Transesterification with Diethyl Carbonate

The first approach was the transesterification of diethyl carbonate with the diol towards the cyclic carbonate monomer (Scheme 21, A). This approach can be performed in a polymerisation-depolymerisation set up to distillate the cyclic carbonate as the elimination product from the backbiting reaction.[59] Batch production with purification of the monomer by distillation is also possible and was performed in this thesis (Scheme 22).[59, 110] In general the synthesis procedure was as following. 1 eq. of the precursor were dissolved in 1.4 eq of diethyl carbonate. After 5 minutes of stirring at room temperature, 0.1 eq of base were added and the temperature increased to 70 °C. Formed ethanol was distilled off and excess diethyl carbonate was distilled off *in vacuo*. The CC was purified *via* distillation. Due to the need for high temperatures and high vacuum, purification was only possible *via* Kugelrohr distillation. Due to the limitation of small sample sizes, this synthesis pathway was disregarded later in the thesis, as the batch production did not work in the lab scale.

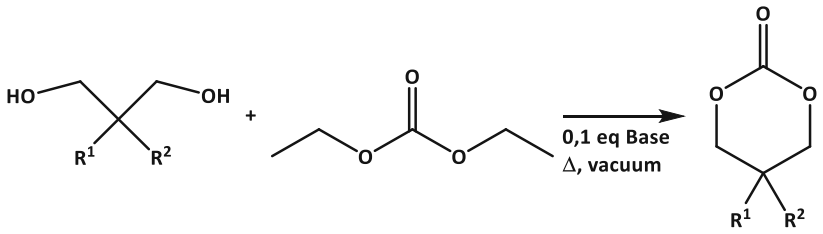

Scheme 22: Generalised reaction scheme of base-catalysed transesterification of diethyl carbonate with a diol

This method made the synthesis of 5,5-diethyl-1,3-dioxane-2-one (Et-C) possible (Scheme 23). Therefore, 2,2-Diethylpropane-1,3-diol (1 eq.) was dissolved in diethyl carbonate (1.4 eq.) and stirred at room temperature. 0.1 eq. of sodium hydride was added, and the reaction was heated to 70 °C to distil off formed ethanol. Excess diethyl carbonate was distilled under reduced pressure. Afterwards, the crude reaction mixture was transferred into a Kugelrohr distillation apparatus. The product was purified by Kugelrohr distillation in a high vacuum at 180 – 200 °C. A yield of 71.9% was obtained on a 2 g scale.

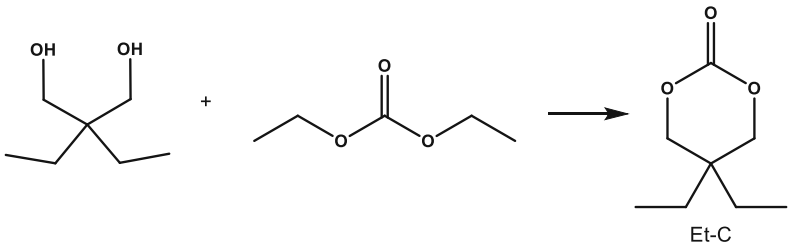

Scheme 23: Synthesis of the monomer Et-C via *transesterification using diethyl carbonate*

Furthermore, diethyl bis(hydroxymethyl)malonate was tested as a different potential precursor for diethyl 2-oxo-1,3-dioxane-5,5-dicarboxylate (Mal-C). For this synthesis, 1 eq. of the diol was dissolved in 1.4 eq. diethyl carbonate. 0.1 eq. of sodium hiydride was added and the reaction mixture was heated up to 70 °C. Formed ethanol was distilled off. However, a crosslinked gel was formed during the transesterification reaction as the transesterification did not solely occur between diethyl carbonate and the precursor (Scheme 24). The base catalysed transesterification also occurred between diethyl bis(hydroxymethyl)malonate molecules leading to a crosslinked polyester. Increasing the equivalents of diethyl carbonate from 1.4 eq to 3 eq resulted in a crosslinked gel. Sodium methanolate was then chosen as the catalyst, leading to the same results.

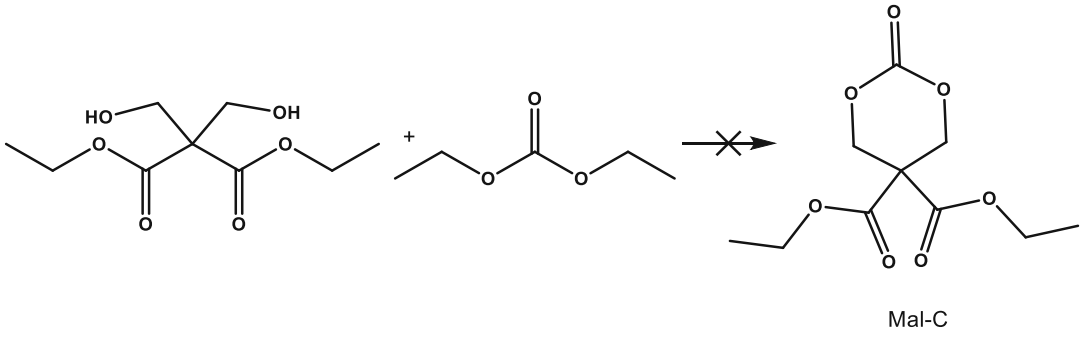

Scheme 24: Attempted synthesis of Mal-C based on diethyl bis(hydroxymethyl)malonate resulting not in the formation of the cyclic carbonate but a crosslinked gel.

The synthesis method was tested for the derivatisation of dihydroxyacetone to obtain 1,3-dioxane-2,5-dione (DHA-C). Therefore, 1 eq. of dihydroxyacetone was suspended in 1.4 eq. diethyl carbonate. After stirring at room temperature for 5 minutes, 0.1 eq. sodium methanolate was added, and the reaction mixture was heated to 70 °C. However, ethanol formation was not observed as no ethanol could be distilled. Applying reduced pressure to remove excess diethyl carbonate gave a dark brown viscous oil with a caramel-like smell (Scheme 25).

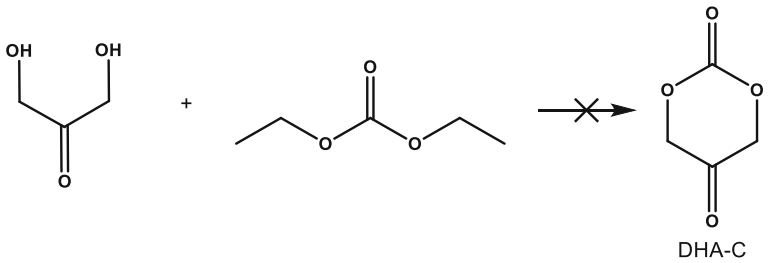

Scheme 25: Attempted synthesis of DHA-C. The targeted product was not obtained through this synthesis. Instead, a dark brown viscous oil with a caramel-like smell was formed.

The cyclic carbonate 5-phenyl-1,3-dioxane-2-one (Ar-C) was selected as next target anymore. The diol was dissolved in 1.4 eq. diethyl carbonate and stirred at room temperature for 5 minutes. After adding 0.1 eq. sodium hydride, the temperature was increased to 70 °C and formed ethanol distilled off. Excess diethyl carbonate was distilled off under reduced pressure, and the reaction flask was transferred into a Kugelrohr distillation apparatus. The reaction mixture was heated up to 220 °C in a high vacuum. However, the cyclic monomer Ar-C could not be obtained from the reaction mixture due to the thermal stability of the resulting polycarbonate. As NMR and STA analyses suggest, the linear polycarbonate might be the more prominent product of this reaction (Scheme 26). STA measurements of the reaction product suggest thermal stability up to 200 °C at ambient pressure (Figure 2). This implies that the final product of this reaction was the linear polymer and not the desired cyclic monomer

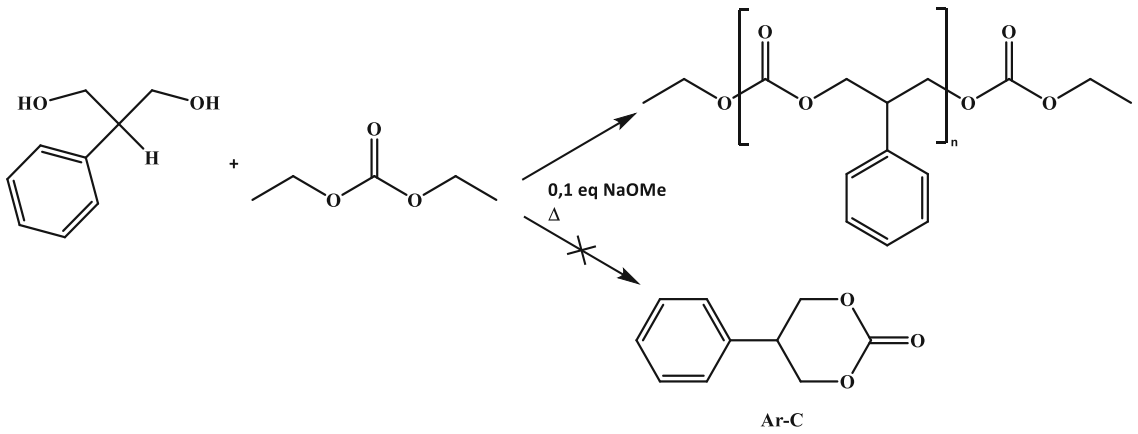

Scheme 26: Synthesis approach towards Ar-C. The linear polycarbonate was the reaction's main product, and the cyclic carbonate could not be isolated from this reaction.

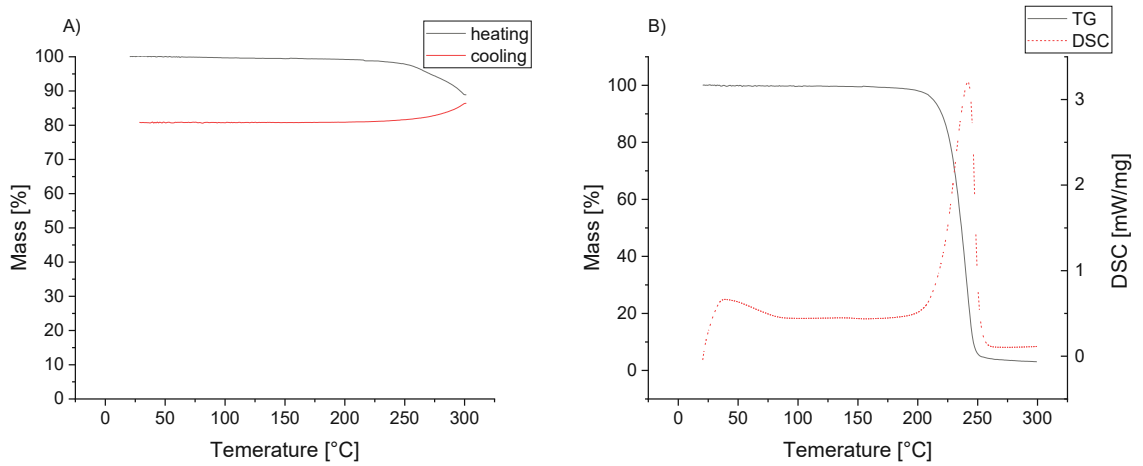

Figure 2: STA measurements of poly(Ar-C) (A) and the corresponding monomer Ar-C, obtained later (B). The STA measurement implies a high boiling point of the cyclic monomer Ar-C and high thermal stability until 300 °C poly(Ar-C)

The synthesis of the crosslinker 5,5'-(oxybis(methylene))bis(5-ethyl-1,3-dioxane-2-one) (Di-C) was the next target through this approach (Scheme 27). Therefore, 1 eq. di(trimethylolpropane) was dissolved in 3 eq. diethyl carbonate. 0.1 eq. of sodium hydride were added and the reaction flask was equipped with a distillation apparatus. The reaction mixture was heated to 70 °C and formed ethanol was distilled off. Excess diethyl carbonate was removed under reduced pressure. The product formed was a 3D crosslinked network and thermal depolymerisation to the difunctional cyclic carbonate was not achieved even at 230 °C oil bath temperature.

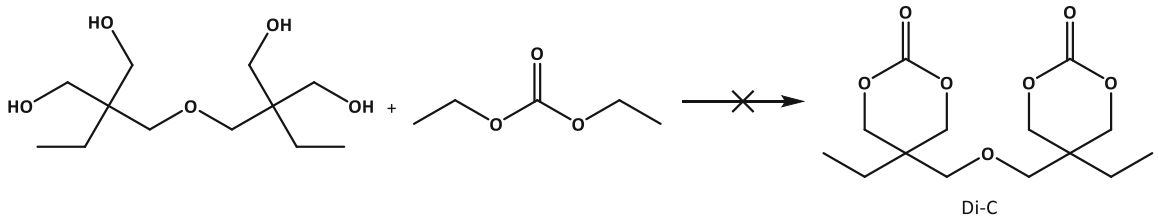

Scheme 27: Synthesis approach towards the crosslinker Di-C via base-catalysed transesterification of di(trimethylolpropane) and diethyl carbonate. The final product was a fully crosslinked polymer.

A different result was observed when pentaerythritol was used as a precursor to form the difunctional crosslinker 2,4,8,10-tetraoxaspiro[5.5]undecane-3.9-dione (Di-C-S). Therefore, 1 eq. pentaerythritol was suspended in 3 eq. of diethyl carbonate and stirred at room temperature for

5 minutes. Afterwards, sodium methanolate was added as catalyst for the reaction. The reaction mixture was heated up to 70 °C and stirred for 30 minutes. However, no ethanol formation was observed. Hence, it was concluded that there was no reaction between pentaerythritol and diethyl carbonate using sodium methanolate as catalyst (Scheme 28). Increasing the amount of diethyl carbonate and using sodium hydride as the catalyst did not alter the outcome of the synthesis.

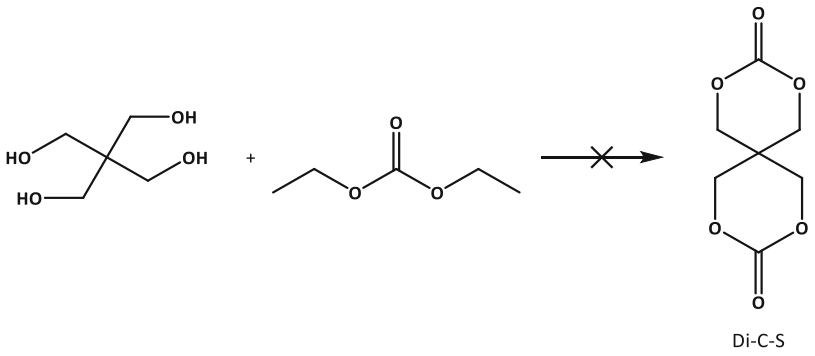

Di-C-S

Scheme 28: Attempted synthesis for the monomer Di-C-S. No ethanol formation was observed during the reaction. Hence, no reaction between the reagents was concluded.

1.2 Transesterification using Diphenyl Carbonate

The second synthetical pathway was transesterification with diphenyl carbonate (DPC). This synthesis does not need any catalyst, as the stability of the phenolate leaving group is the driving force of this reaction. The second bulky phenyl group sterically hinders the attachment of a second unit on the free OH-group.[92] The general reaction procedure was adopted from literature.[92] Here, DPC is heated to 140 °C and used as a reagent and reaction solvent. At 140 °C, the alcohol is added to the DPC melt, and the reaction mixture is stirred for 48 h. The reaction control was performed by TLC analysis. The crude products were purified *via* column chromatography.

For Et-C (Scheme 29) and Di-C (Scheme 30), 78.6% and 84% yields were obtained.

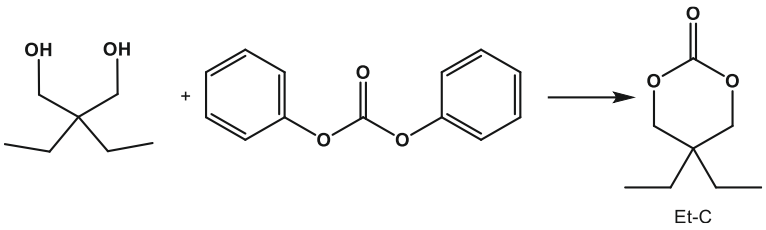

Scheme 29: Synthesis of Et-C via transesterification using DPC. The product was purified by column chromatography

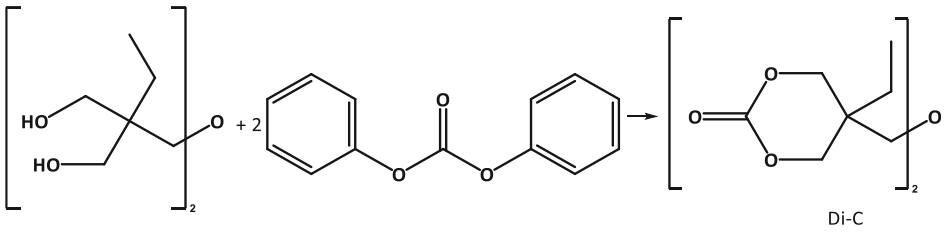

Scheme 30: Synthesis of Di-C via transesterification using DPC. The product was purified by column chromatography.

Long reaction times of 48 h and purification *via* column chromatography are drawbacks of this synthesis approach. The reaction mixture's 6x excess of diphenyl carbonate cannot be reused as the generated phenol cannot be separated from the leftover diphenyl carbonate by column chromatography. Despite this being an easy synthesis as it does not require any more reactants or catalysts, the disadvantages, as mentioned earlier, make upscaling difficult. For efficient purification, the target monomer should have a significantly distinct Rf-value from diphenyl carbonate or phenol in the eluent.

The other targeted CC monomers were not obtainable through this synthesis:
Phenol formation was observed using diethyl bis(hydroxymethyl)malonate as a reagent. However, it was not possible to perform column chromatography of the reaction solution. When applying the reaction solution on silica gel, the flow of the eluent was instantly stopped, leading to clogging of the column. It might be possible that a crosslinked system was formed during the reaction. Although not catalysed, the high reaction temperature of 140 °C might have led to the separation of ethanol, and hence, the diethyl bis(hydoxymethyl)malonate formed a crosslinked polyester network.

In the case of dihydroxyacetone, again, a dark brown viscous oil was observed within the reaction solution. This oil was not soluble in the elution solvent used for column chromatography and had a caramel-like smell. Furthermore, no phenol formation was observed by TLC analysis.

For Ar-C, this synthesis was the case, as indicated by TLC analysis. However, the isolation through column chromatography did not yield any pure product as the excess of the reactants overloaded the column. Complete separation of the reactant from the product was hence not possible.

For the synthesis of Di-C-S, Pentaerythritol was not soluble in DPC at 140 °C. According to TLC analysis, no reaction was observed after 120 h.

1.3 Cyclisation using 1,1'-Carbonyldiimidazole

The last method investigated was the use of 1,1'-carbonyldiimidazole (CDI) as a carbonyl source (Scheme 21, C, page 29). Literature reported this method for fast synthesising cyclic carbonates based on 2,2-bis(hydroxymethyl)propionic acid (bis-MPA) and several esters derived from bis-MPA. This route should be feasible for synthesising all kinds of cyclic carbonates.[91] The advantages of this synthesis are its green reactants and solvents, relatively low reaction temperature and fast reaction times. In general, the precursor was dissolved in ethyl acetate, and 1.5 eq. of CDI was added in two batches with 5 minutes of stirring at room temperature. Reaction control was performed by ^{1}H-NMR analysis. After full conversion of the diols was observed, 16 eq. of acetic acid were added, and the reaction flask was equipped with a reflux condenser. The reaction mixture was heated to 70 °C and held for three hours. After cooling, the reaction mixture was diluted with ethyl acetate and washed with water. The organic phase dried over sodium sulphate. After evaporation of two thirds of the solvent, toluene was added to remove acetic acid *via* azeotropic distillation. The purification of Et-C and Di-C was performed by precipitation from ethyl acetate (EA) with petroleum ether (PE) to obtain the monomers as white solids. Ar-C was purified by column chromatography with ethyl acetate and petroleum ether as eluent to obtain the cyclic carbonate monomer as a colourless oil. The purities of the monomers were checked *via* NMR and TLC and melting point analysis. Yields of 89%, 74%, and 86% were obtained for Et-C, Ar-C and Di-C, respectively (Scheme 31).

Although the reaction led to high yields for Et-C, Ar-C and Di-C, the other precursors, dihydrxyacetone, diethyl bis(hydroxymethyl)malonate and pentaerythritol, did not show any conversion in the ^{1}H-NMR under the reaction conditions. Strong degassing of the reaction solution containing these alcohols was observed during the addition of acetic acid. This degassing would indicate the decomposition of CDI and therefore no reaction from CDI with the alcohols. Hence, the targeted monomers Mal-C, DHA-C and Di-C-S were not investigated further later in this thesis.

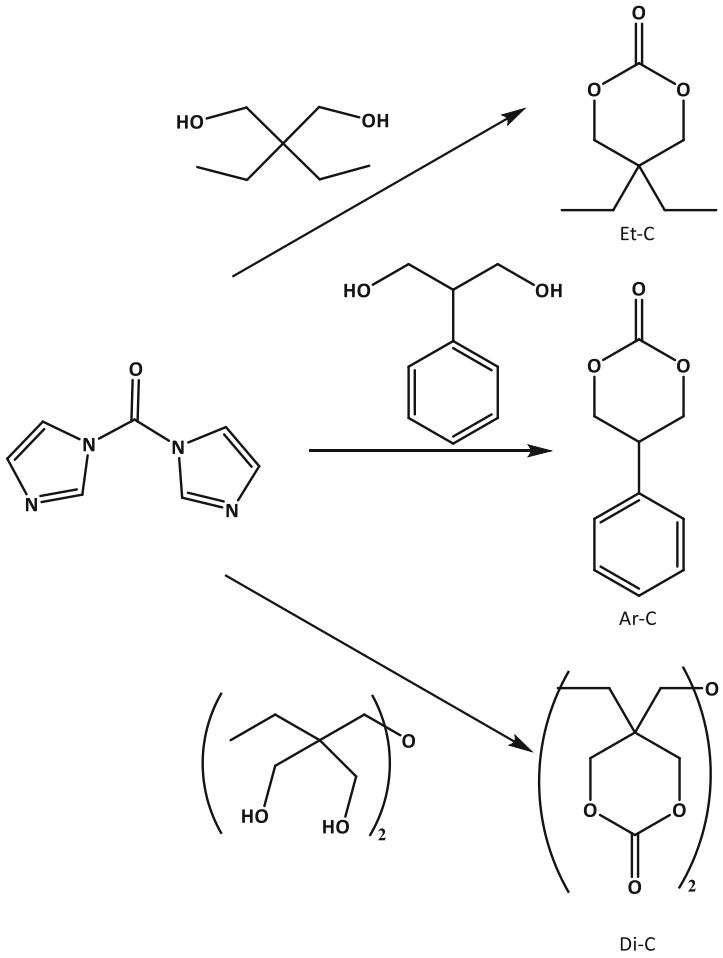

Scheme 31: Reaction scheme of the CC precursors with CDI to the successfully obtained cyclic carbonate monomers.

2 Cationic Ring-Opening Polymerisation

2.1 Photo-DSC Analysis

Photo-DSC measurements were performed to analyse the calorimetric behavior of the monomers. For this, the samples with 1 mol% photoacid generator (PAG) (triarylsulfonium hexafluoroantimonate S-Sb, 50% w/w in propylene carbonate, Figure 3) were irradiated twice for 300 s (320 – 500 nm, 50 mW cm^{-2}). The samples from the photo-DSC measurements were also used to investigate the polymerisation behaviour of the monomers further. ^{1}H-NMR analysis gave the yield of the polymerisation and the possibility to observe the presence of formed ether bridges in the polymer after decarboxylation. GPC measurements gave additional information about the formed polymers' molecular weight and polydispersity (PDI). The reactivity of the monomers was screened between 70 and 120 °C. As decarboxylation can occur as a side reaction in cROP, all samples were weighed before and after irradiation.

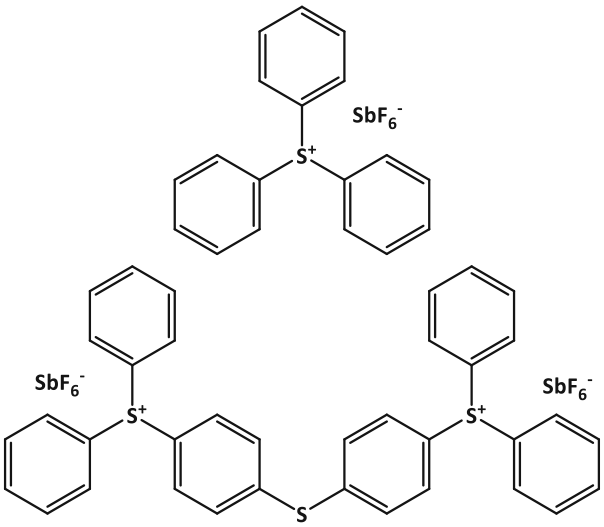

S-Sb

Figure 3: Structure of the PAG triarylsulfonium hexafluoroantimonate (S-Sb)

2.1.1 5,5-Diethyl-1,3-dioxan-2-one (Et-C)

Photo-DSC analyses were performed as described in Materials and Methods using 1 mol% S-Sb as PAG (Scheme 32).

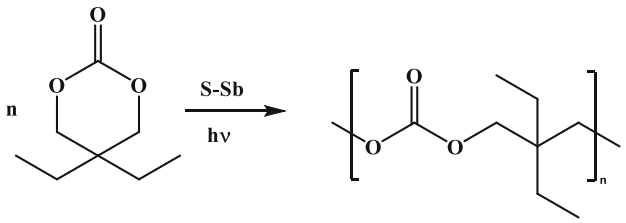

Scheme 32: Photopolymerisation in the photo-DSC measurements of Et-C

Due to very low ring-strain, no exothermic behaviour was recorded during the photo-DSC measurements, and hence no calorimetric data for the cROP was obtained. The polymerisation can occur *via* various mechanisms, resulting in different backbone structures. Therefore, the molecular weight could not be estimated *via* NMR spectroscopy. However, the polymerisation yield could be estimated by the ratio of the integrals of the signals of the methylene group next to the carbonate unit of the cyclic monomer to the linear polymer. This signal slightly shifts to lower chemical shifts when the ring opens, as shown exemplarily for Et-C in Figure 4.

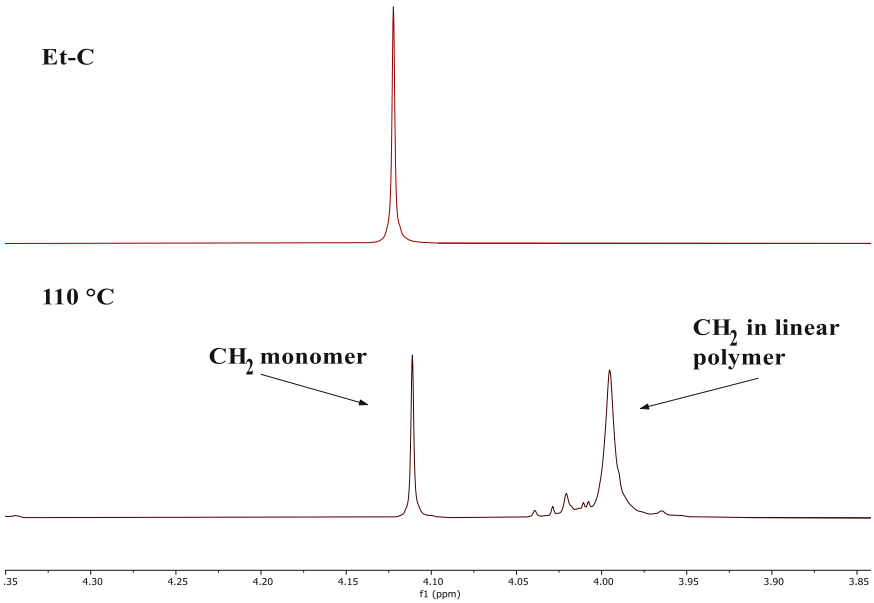

Figure 4: Exemplary ^{1}H-NMR comparison of Et-C with its linear polymer resulting from the photo-DSC measurement at 110 °C

Table 1 summarises the results from the GPC and ^{1}H-NMR analyses. Weighing the samples before and after the photo-DSC measurements showed no mass loss during the photo-DSC measurement. Therefore, decarboxylation after the initiation step can be excluded. As the temperature increases, the reactivity of the cyclic carbonate increases and leads to higher molecular weights. The lower molecular weight of the sample at 120 °C compared to the samples cured at 100 °C could be explained by more transesterification and chain transfer reactions. As the initiator sets free three equivalents of acid per PAG, the targeted degree of polymerisation was 33, resulting in a theoretical molecular weight of 5200 Da, which was not obtained for the monomer Et-C. However, the lower molecular weights indicate that a lower degree of polymerisation was achieved in the observed period of time, and the reaction was not complete. While this is an indicator for the degree of polymerization compared to the targeted value, it must be kept in mind that the obtained GPC data was calibrated with external polystyrene standards and therefore does not describe absolute values. Because there was no clear end group on the polymer due to the addition of monomer on two sides of the growing chain, calculating the degree of polymerisation was not possible from ^{1}H-NMR data. ^{1}H-NMR also indicates that no decarboxylation was taking place at the investigated temperatures as no signal indicated the presence of ether linkages. The system's reactivity increases with increasing temperature, and the PDI remains relatively low at all temperatures.

Table 1: Summary of the results from the photo-DSC samples in regards to their molecular weight and yield. Higher conversions and molecular weights were obtained. The molecular weights are increasing with increasing temperature.

T (°C)	Conversion (%)	M_n (Da)	DP	PDI
70	43.5	2 300	15	1.19
100	70	3 100	20	1.32
120	62.5	2 800	18	1.35

2.1.2 5-Phenyl-1,3-dioxan-2-one (Ar-C)

The polymerisation of Ar-C was performed as described in Materials and Methods (Scheme 33).

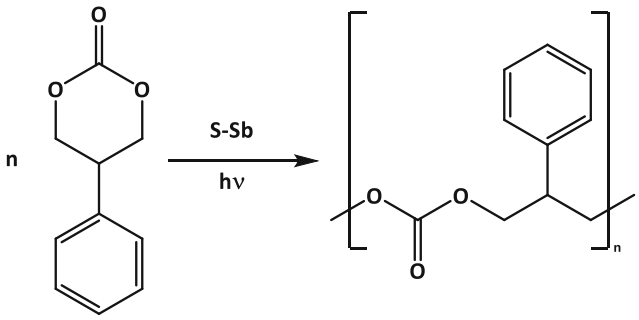

Scheme 33: Photopolymerisation of Ar-C

Again, no exothermic behaviour was recorded during the photopolymerisation. The results from the analyses of the cured samples are shown in Table 2.

Table 2: Summarised results from the photopolymerisation of Ar-C with 1 mol% S-Sb. Overall, increasing reactivity was observed with increasing temperature. Almost full conversion and high molecular weights were obtained for all tested temperatures.

T (°C)	Conversion (%)	M_n (Da)	DP	PDI
70	95	6 100	34	1.34
100	>99	6 300	36	2.27
120	>99	5 300	30	1.51

Ar-C showed a higher reactivity for ROP and high molecular weights compared to Et-C. The high PDI of the sample cured at 100 °C could be caused by the attack of the OH-functionality on one side of polymer chain B at the active chain end (ACE) of chain A (Scheme 34), drastically increasing the molecular weight.

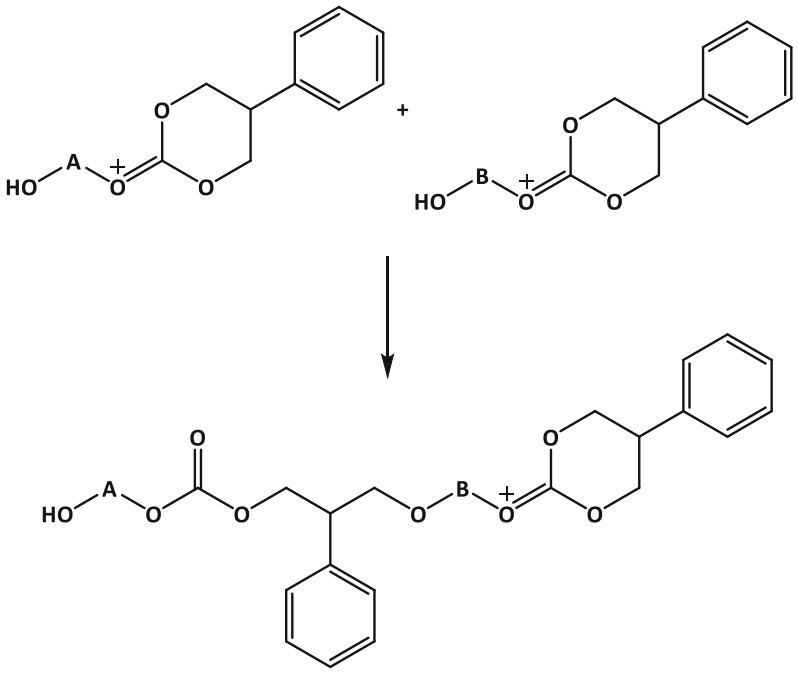

Scheme 34: Possible way of chain-chain interaction. The growing chain has two sites where monomers can be attached. The OH-end group of chain B may attack at the ACE of chain A. This attack could lead to a sudden increase of the molecular weight and broadening the molecular weight distribution of the obtained polymer.

Decarboxylation could be excluded, as weighing the samples before and after the photo-DSC measurements showed no mass loss upon irradiation. Additionally, no signal in the ^{1}H-NMR spectrum indicated the presence of ether linkages. The higher reactivity of Ar-C in comparison to Et-C may come from less steric hindrance of Ar-C compared to the diethyl substituent on Et-C. Additionally, higher ring strain caused by the phenyl substituent on the CC may result in

higher reactivity. Another cause for high reactivity is the drastic change in rotational freedom of the CH_2 group next to the carbonate group, which can be seen in the ^{1}H-NMR spectra (Figure 5). The signal changes from a multiplet signal (4.66-4.46 ppm) to a duplet signal (4.31 ppm). The different chemical environments cause the multiplet signal for the protons on the CH_2 group in the cyclic monomer. One proton faces the neighbouring proton, and the other interacts with the substituent's phenyl group. Both protons face the same chemical environment in the polymer backbone and are chemically equal upon ring-opening.

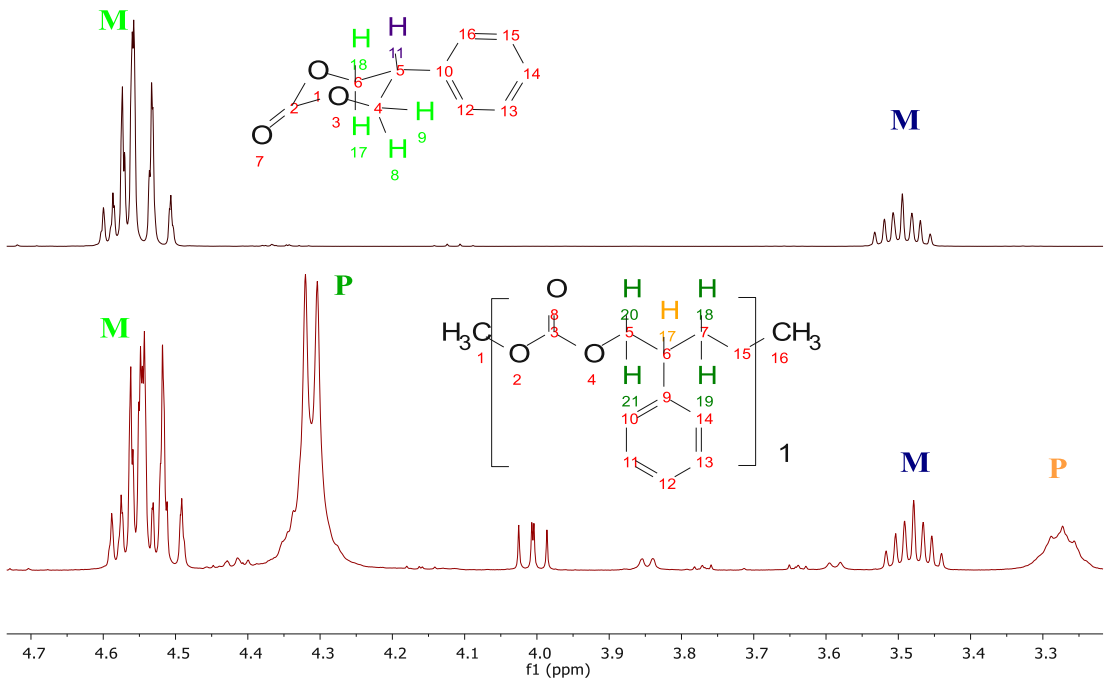

Figure 5: Exemplary ^{1}H-NMR comparison of Ar-C (M) and the linear polymer (P) from the photo-DSC sample. The methylene groups in the cyclic carbonate gain freedom of rotation during the ring-opening. Hence, the signal changed from a multiplet to a duplet as now both protons experience the same chemical environment. M: signal of the H from the monomer; P: signals deriving from the polymeric structure.

2.1.3 5-Ethyl-5-(((5-ethyl-2-oxo-1,3-dioxan-5-yl)methoxy)methyl-)1,3-dioxan-2-one (Di-C)

The photopolymerisation of Di-C was performed as described in Materials and Methods (Scheme 35). Due to the high melting point of Di-C (104 °C), only measurements at 120 °C were performed.

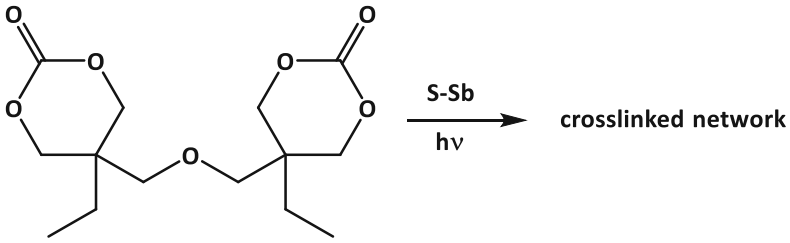

Scheme 35: Photopolymerisation of the crosslinker Di-C using S-Sb as PAG

Again, the absence of exothermic behaviour was observed. As expected, the samples were fully cured into solids, which were neither soluble in chloroform nor in THF for NMR or GPC measurements, respectively. This experiment delivered the proof of concept that the difunctional monomer, Di-C, was indeed leading to a crosslinked system.

2.2 Bulk Curing Method Analysis

As the photo-DSC analysis showed no sign of decarboxylation during photopolymerisation, bulk curing tests were performed. To define the best curing conditions, several formulations consisting of monofunctional CC reactive diluent, a bis-CC crosslinker, and a photoinitiator were tested. All curing tests were performed in a Uvitron UV 1080 Flood Curing-oven (320 – 500 nm) in ambient atmosphere. Table 3 shows the composition of the formulations. The structures of the used materials are depicted in Figure 6.

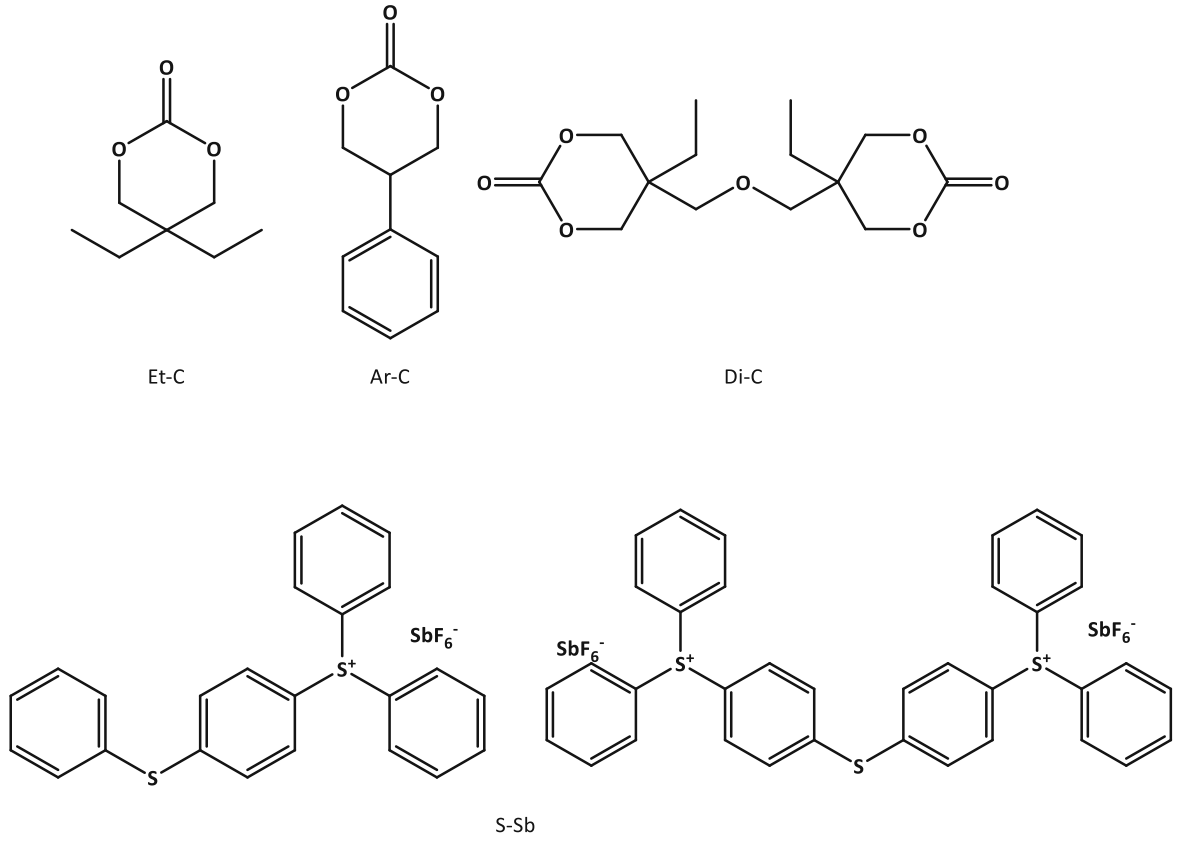

Figure 6: Chemical structures of the formulations' components

All formulations were tested under different conditions. The monomers and the photoinitiator were weighed into a 10 mL vial and mixed at 60 °C. The formulations were filled into a silicone mould and irradiated. After irradiation, a post-curing step (1 h up to overnight) was performed in a drying oven at 50, 60, or 120 °C

Table 3: Summary of the first formulations for bulk curing analysis. The initiator PAG was held constant at 1 mol%

reactive diluent	Di-C (mol%)
Et-C	10
	20
Ar-C	10
	25

Although the photo-DSC measurements showed no decarboxylation beyond the initiation step, the bulk curing tests led to highly porous materials upon irradiation for 300 s at 65 mW cm^{-2} intensity due to bubble formation. Several factors could cause the different polymerisation behaviour. One possible explanation could be the depth of penetration from the used wavelength. For the photo-DSC samples, the entire formulation can be penetrated from the light to initiate the reaction, which cannot be achieved in the bulk curing tests. This might cause the polymerisation of the surface before deep curing occurs. Another possibility for the different behaviour might be the higher light intensity from the Uvitron device. Therefore, more energy is introduced into the system, which could cause higher tendencies for side-reactions. For Et-C, a very soft, sponge-like material was obtained. A stiffer, foam-like material was obtained with Ar-C (Figure 7), which already shows a drastic difference in mechanical properties depending on monomer substituents.

Figure 7: Bulk cured sample from Ar-C under cROP conditions, using 1 mol% S-Sb as initiator and 25 mol% DI-C. The samples showed clear signs of decarboxylation, which causes highly porous structures.

Several parameters were varied to reduce the CO_2 development during the curing process. Increasing the content of Di-C led to more rigid but still highly porous structures. A heated mold and a heating plate were used to achieve higher reactivity within the formulation. The

temperature was held at 100 °C, as the photo-DSC showed the best results at this temperature. Subsequently, the light intensity was varied between 65 mW cm^{-2} and 110 mW cm^{-2} to investigate the polymerisation behaviour at different irradiation intensities. Higher intensities from 90 mW cm^{-2} on led to severely darkened materials with higher porosity (Figure 8).

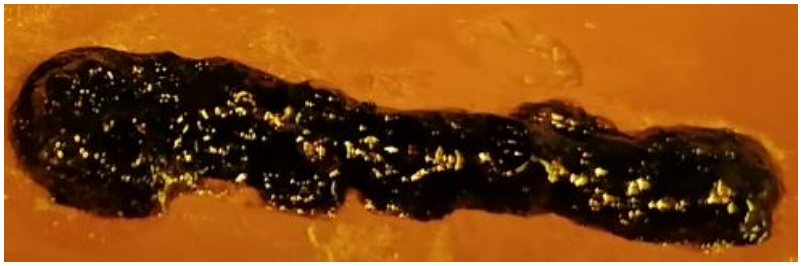

Figure 8: Bulk curing test with Et-C at 100 mW cm^{-2} light intensity. Due to the high light intensity, the formulation is strongly darkened and porous through a decarboxylation side reaction.

Reducing the irradiation time from 300 to 150 s, with light intensities ranging from 65 mW cm^{-2} to 120 mW cm^{-2}, did not alter the tendency for bubble formation. Additionally, no form-stable material was obtained after photopolymerization at 65 mW cm^{-2}. However, during the post-curing step, all formulations showed strong signs of bubble formation due to decarboxylation. This was observed even at the lowest post-curing temperature of 50 °C. Bubble formation during the post-curing process took place within 5 min (120 °C), 40 min (60 °C) or 60 min (50 °C) (Figure 9). As the initiator does not decompose instantly but over time,[99] it could also cause degradation of the polymer and hence decarboxylation, especially during the post-curing process.[111]

Figure 9: Comparison of the formulation after irradiation and before post-curing (A, low bubble formation) and after 60 min post-curing at 50 °C (B, strong bubble formation)

As these formulations have been proven not to be polymerisable without bubble formation, alcohols were added to initiate the polymerisation reaction. The alcohol should shift the reaction from the two-fold chain growth (AM and ACE mechanism, Scheme 36) towards the AM mechanism as the dominant pathway (Scheme 37). Since both mechanisms are always present, there is always an active chain end during cROP. The active chain end may react with a free monomer irreversible, whereby CO_2 is formed.[100] Restricted diffusion of the monomer through the network may increase the chance of the endocyclic oxygen from the monomer (Scheme 17, page 23).

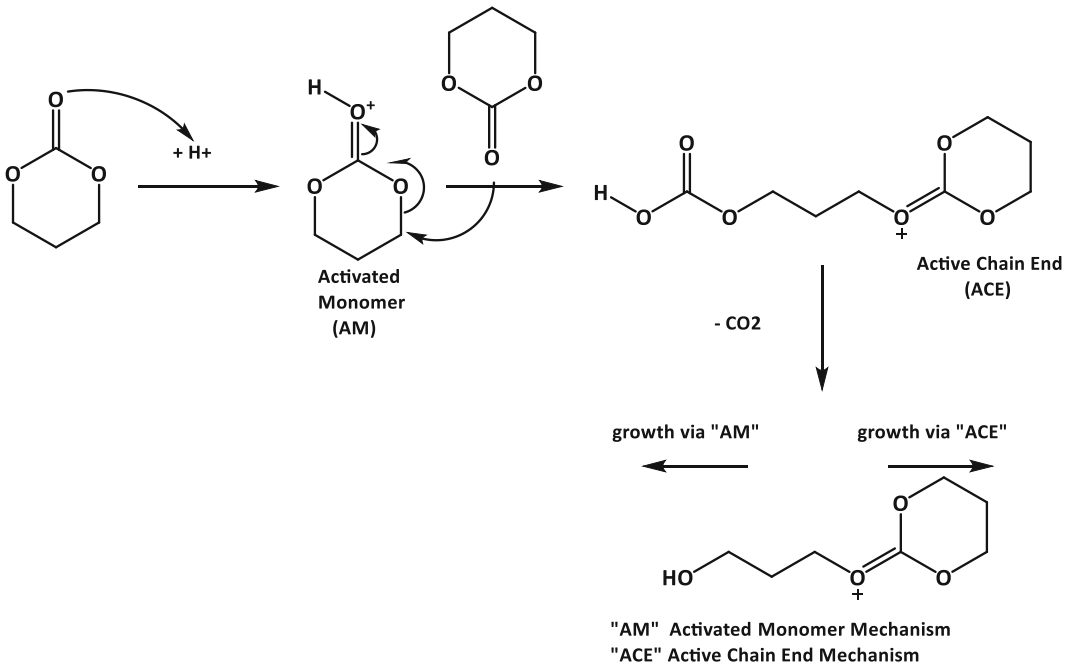

Scheme 36: cROP mechanism for CCs using acids to activate the monomer without initiating alcohol functionalities. The activated monomer is attacked by the carbonyl oxygen of another CC and forms the mono-ester of carbonic. This mono-ester decarboxylates and forms an alcohol functional group. The chain can subsequently grow via *attack of the OH-group on the activated monomer and attack of monomers on the ACE.*

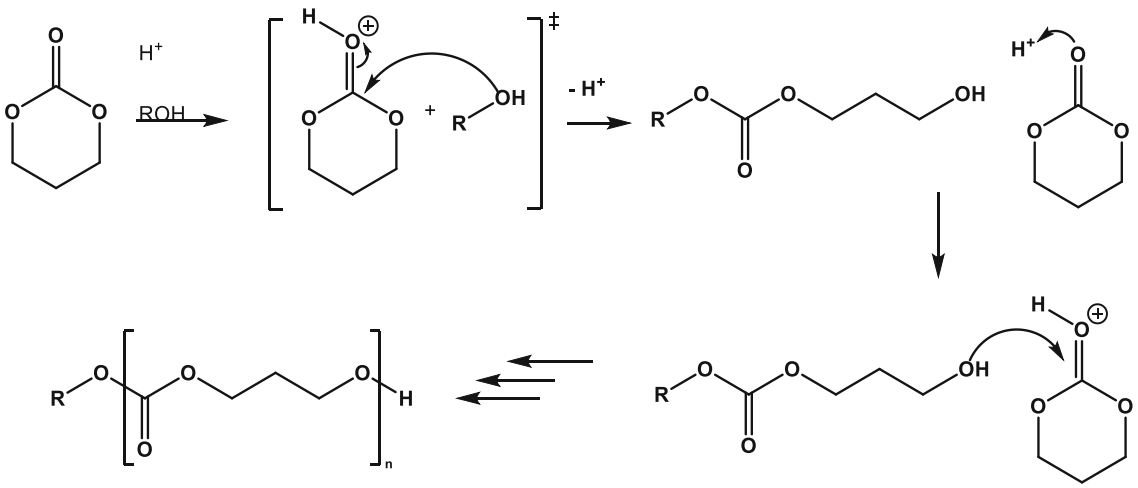

Scheme 37: Activated Monomer mechanism in the presence of a nucleophile alcohol functional group

For this approach, 3-phenylpropanol was introduced as initiating alcohol. Although the addition of alcohol cannot suppress the AM/ACE mechanism entirely, a reduction to 31% was reported from Jimenez-Pardo et al.[100] The ratio between generated acid equivalents and alcohol was varied between 0.75 and 1.5. Light intensity was set to 65 mW cm^{-2}, and irradiation time was varied between 150 s and 300 s. Post-curing temperatures were again set to 50, 60, and 120 °C, respectively. However, similar results were observed compared to the

tests without alcohol addition. The bubble formation proceeded more slowly but could not be eliminated from the polymerisation process.

Lowering the S-Sb concentration to 0.33 mol%, resulting in 1 mol% of acid, reduced the initial bubble formation. However, during post-curing excessive bubble formation was observed again.

As the acid strength of the initiating super acid influences the initiation of cROP and the decomposition of PCs, other PAGs were tested. An iodonium (tBuI-Al) and a different sulfonium (IC 290) based salts were tested (Figure 10). The formulations with the other PAGs were in analogy to the tests mentioned in Table 3.

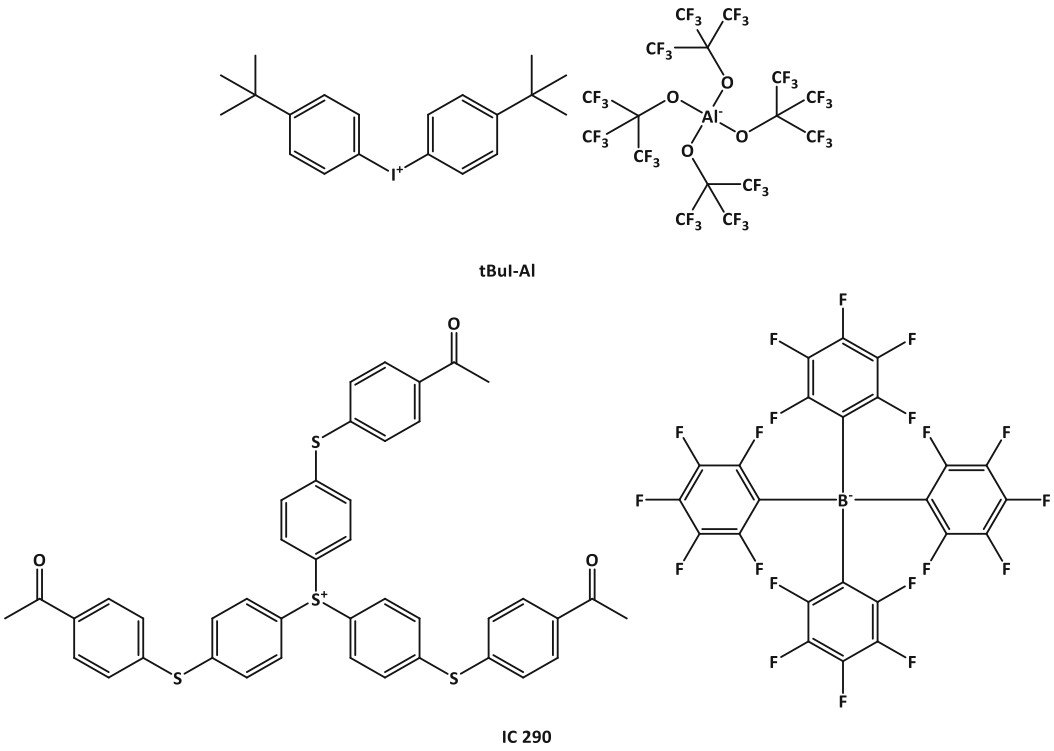

Figure 10: PAGs tBuI-Al and IC 290 tested in bulk curing analyses

Both alternative PAGs investigated showed very different results. The PAG tBuI-Al showed no visible change in the ^{1}H-NMR after 300 s of irradiation and even after 12 h of post-curing at 120 °C. Using IC 290 resulted in solubility issues within the formulation. The formulation with IC 290 showed miscibility issues after irradiation. Dark spots within a colourless in a still liquid formulation were visible, depicting a phase separation between the dissolved PAG and the monomer, as shown in Figure 11.

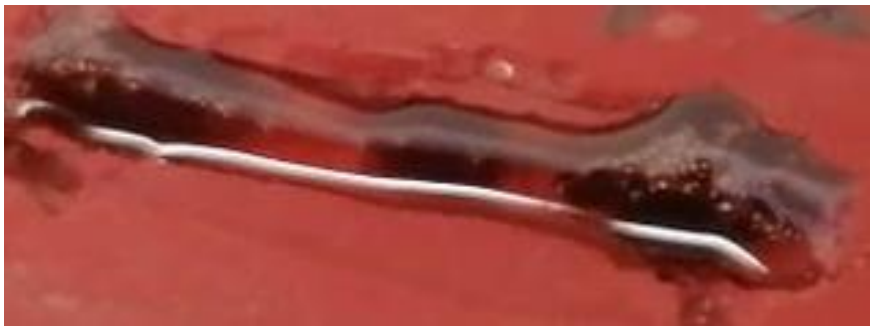

Figure 11: Inhomogeneities of the formulation using IC 290 observable as dark spots within the formulation after irradiation

A deeper analysis of the monofunctional reactive diluents *via* ^{1}H-NMR of bulk cured samples showed the presence of two different bridging units, the desired carbonate and the corresponding ether. These can be seen as either a singlet for Et-C (Figure 12, 3.38 ppm) or an additional multiplet for Ar-C (Figure 13, 3.15 ppm). Those side reactions occur during the post-curing process as the corresponding signals are not present in the photo-DSC samples. Additionally, there might not be any influence of the PAG on the occurrence of these side reactions, as they can be seen in both cases, using S-Sb and IC 290. From these NMR studies, it is estimated that roughly 30% of all linkages are ether linkages, as can be estimated by the integrals of the signals of the CH_2 groups. It can also be seen that the reaction proceeds during the post-curing process. The signal of the methylene groups of the monomer decreases over time. Furthermore, it can be assumed that the reaction primarily proceeds by decarboxylation as the ratio of the CH_2 signal from the linear aliphatic polycarbonates (APCs) to the signal from the ether linkages decreased upon post-curing.

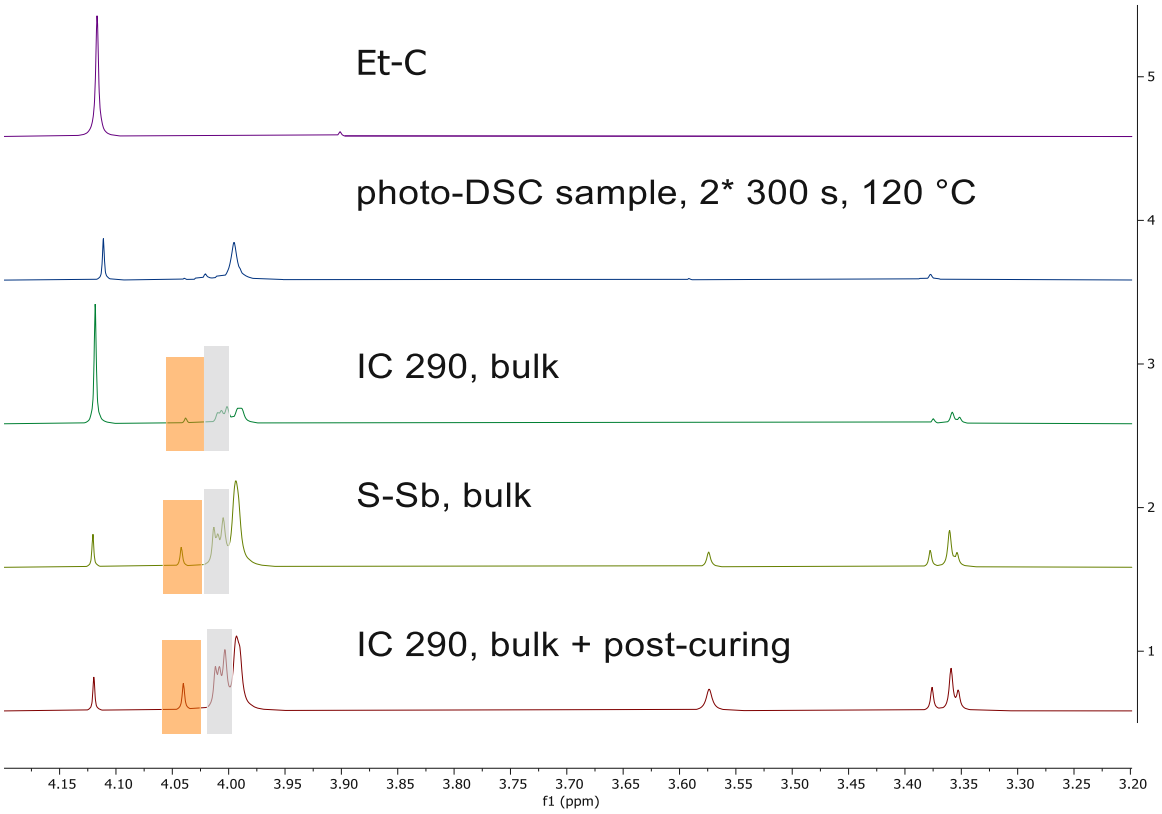

Figure 12: Comparison of the ^{1}H-NMR of Et-C in its initial form, after photo-DSC curing, and after bulk curing tests. Additional signals appear in between both methylene signals of the CC and the linear PC, indicating the presence of different substituents in the polymer backbone (orange and grey boxes). Furthermore, a singlet signal at 3.57 ppm indicates the presence of ether linkages. The signals ranging from 3.38 to 3.35 ppm may represent the other side of asymmetrically substituted units. The reactions seem to occur during the post-curing process as the corresponding observed signals are not as intense as in the photo-DSC sample.

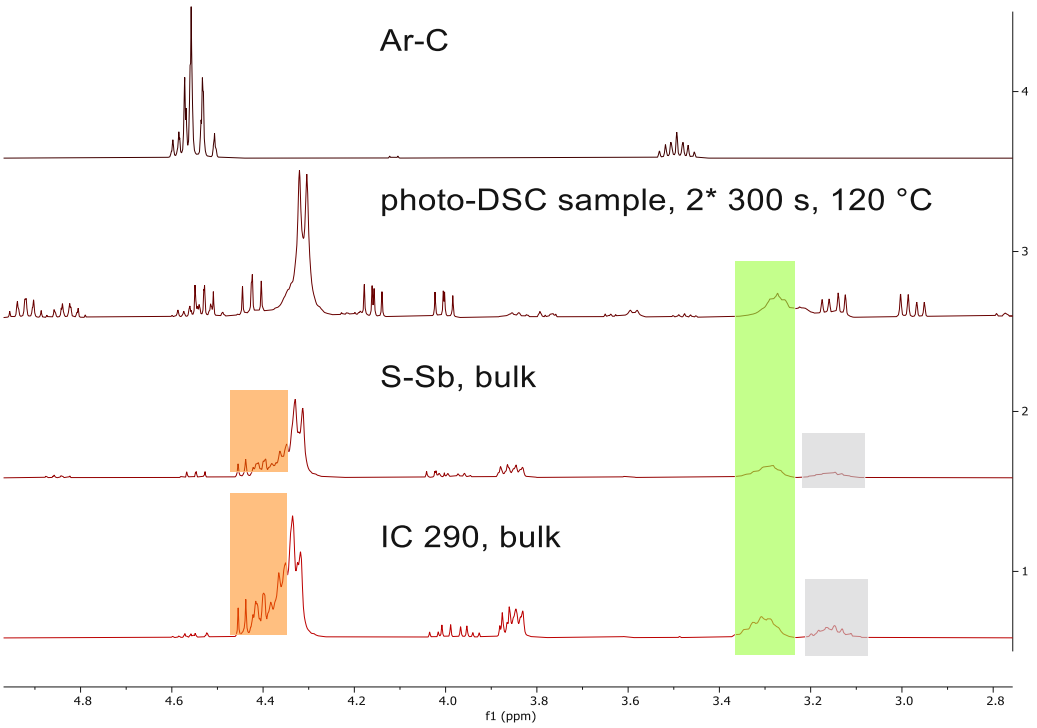

Figure 13: Comparison of ^{1}H-NMR spectra of Ar-C in its initial form, cured during photo-DSC and during bulk curing tests with different initiators (top to bottom). As seen in the photo-DSC sample, duplet from the homopolymer cannot be seen clearly in bulk cured samples. Additionally, the benzylic H can be seen with two distinct shifts, indicating the presence of different substituted linkages. Integration of both signals for the benzylic proton showed that roughly 33% might be linked via ether linkages.

These results proved that the bulk curing of CC could not be performed *via* cationic polymerisation, as the side reactions and decarboxylation dominate the cROP reaction. Though porous materials can be generated *via* light-induced cROP using PAGs, no control over pore size or distribution could be observed.

3 Anionic Ring-Opening Polymerisation

As cROP is an inadequate polymerisation method to gain a polycarbonate network, another approach was necessary. Contrary to cROP, anionic ring-opening polymerisation (aROP) does not require the activation of the carbonyl group. The ring-opening is caused by the attack of a strong nucleophile, in this case, a base. This leads to the preservation of the carbonate group and therefore, no decarboxylation is happening (Scheme 38).[36]

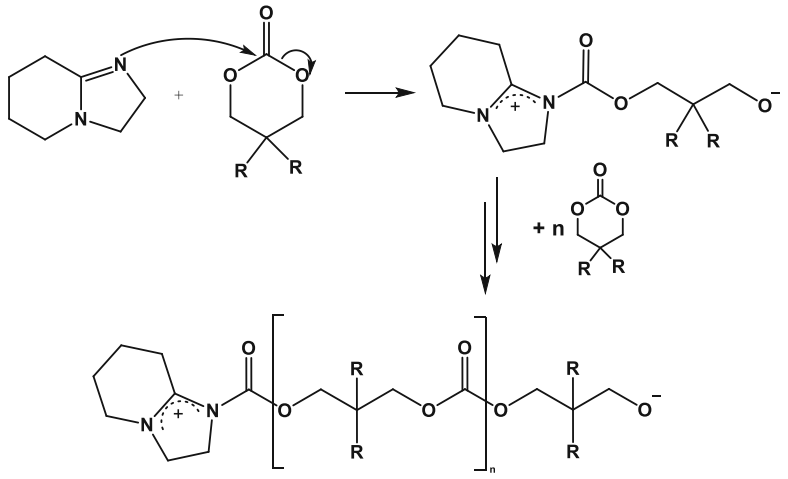

Scheme 38: aROP using DBN as an initiator. The base attacks the monomer, and an alcoholate is set free. This alcoholate attacks the next monomer and leads to polymerization. The direct attack of the base on the carbonyl carbon makes activation of said group unnecessary. Hence, decarboxylation is not happening.

Photo-base generators (PBGs) were necessary to achieve a photo-induced reaction. A benzylated derivative of 1,5-diazabicyclo[4.3.0]non-5-en (DBN) was used as PBG, as it has a reported melting point above 100 °C, indicating its thermal stability at elevated temperatures.[112] The synthesis of the PBG follows a two-step synthesis. Firstly, the amidine base needs to be reduced to a diamine (reduced DBN, RDBN). Secondly, the reduced base is alkylated with a benzylhalogenide derivative (Scheme 39).

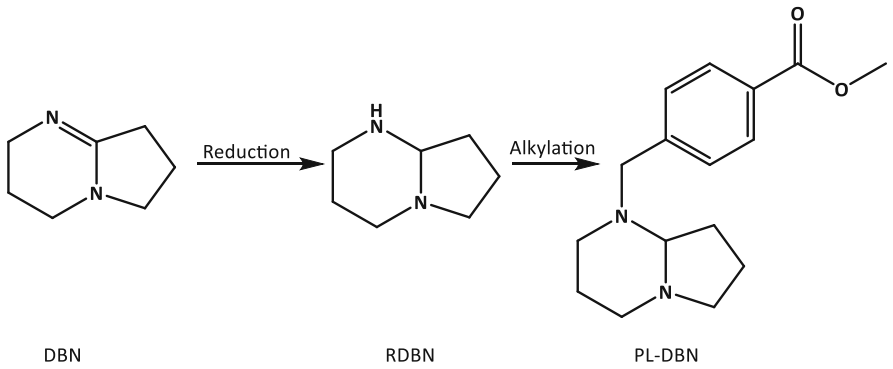

Scheme 39: Synthesis route to the photobase PL-DBN. The precursor DBN is first reduced to RDBN, which is alkylated to the final product

3.1 Synthesis of the Photo-Base Generator

3.1.1 Synthesis of Reduced 1,5-Diazabicyclo[4.3.0]non-5-en

The reduction of DBN can either be performed in dry THF or methyl tert.-butyl ether as solvent using $LiAlH_4$ as a reducing agent (Scheme 40).[112] THF was chosen as the solvent in this thesis due to its higher boiling point, allowing the reaction to be performed at higher temperatures. Evaporation of the solvent led to the product in quantitative yield.

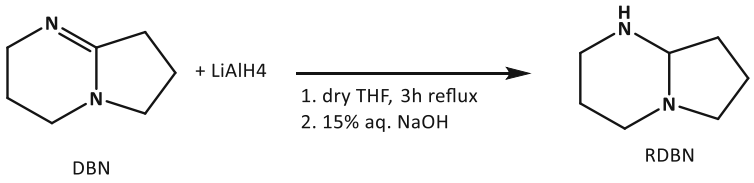

Scheme 40: Reduction of DBN to RDBN

Purity of the product was confirmed by ^{1}H- and ^{13}C-NMR. This method of reaction control is also commonly used in literature to check conversion.[112]

3.1.2 Alkylation of Reduced 1,5-Diazabicyclo[4.3.0]non-5-en

The alkylation of RDBN follows a standard Hoffman alkylation procedure of amines (Scheme 41).

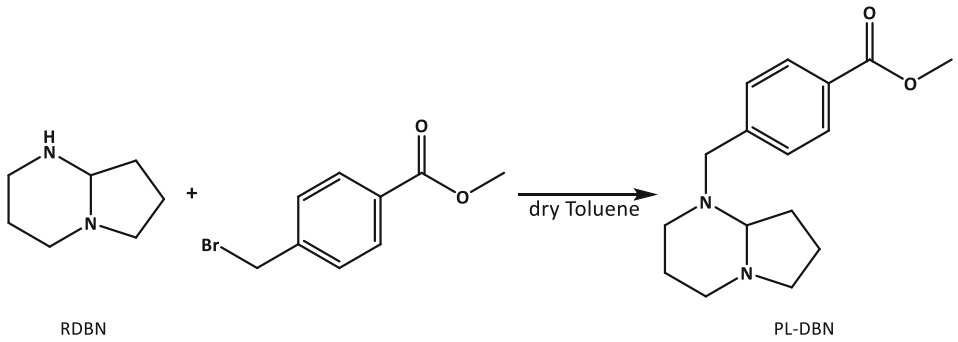

Scheme 41: Alkylation of RDBN to PL-DBN

There are two reported methods of performing this reaction. Studer et al. performed the reaction as depicted in Scheme 41.[113] Another method was reported by Li using one equivalent of aq. NaOH solution.[112] The aq. NaOH deprotonates the secondary amine to direct the reaction towards the desired product, minimising the amount of formed ammonium salt intermediate.[112]

It was decided to perform the reaction according to Studer.[113] Therefore, 1 eq. of methyl 4-(bromomethyl)-benzoate were dissolved in toluene. 2 eq. of RDBN were added and the reaction stirred at room temperature for 48 h. After full conversion, according to TLC analysis, the formed ammonium salt was filtered off. The filtrate was distilled off *in vacuo,* and PL-DBN is gained as a white solid without further purification. Yields up to 65% were obtained. The product was characterised *via* ^{1}H- and ^{13}C-NMR and melting point analysis. The thermal stability up to 150 °C was investigated by STA measurements. For this, two heating cycles were performed with a cooling phase in between.

3.2 Thermal Stability

Using PL-DBN as PBG may significantly impact the storage stability of formulations. PL-DBN itself contains two tertiary amines, which exhibit basic character. Upon irradiation and cleavage, a stronger base is set free. This stronger base may catalyse reactions that are not catalysed by the tertiary amines, e.g., initiation of aROP without co-initiators. However, the tertiary amines are also capable of catalysing some reactions, especially at elevated temperatures. Therefore, each monomer's formulation was tested for thermal stability to see if longer 3D printing processes were possible. For this, the formulations were heated to 120 °C and samples were taken at fixed points in time. Conversion and molecular weights were analysed *via* ^{1}H-NMR and GPC, respectively. Figure 14 shows the results of the thermal stability tests.

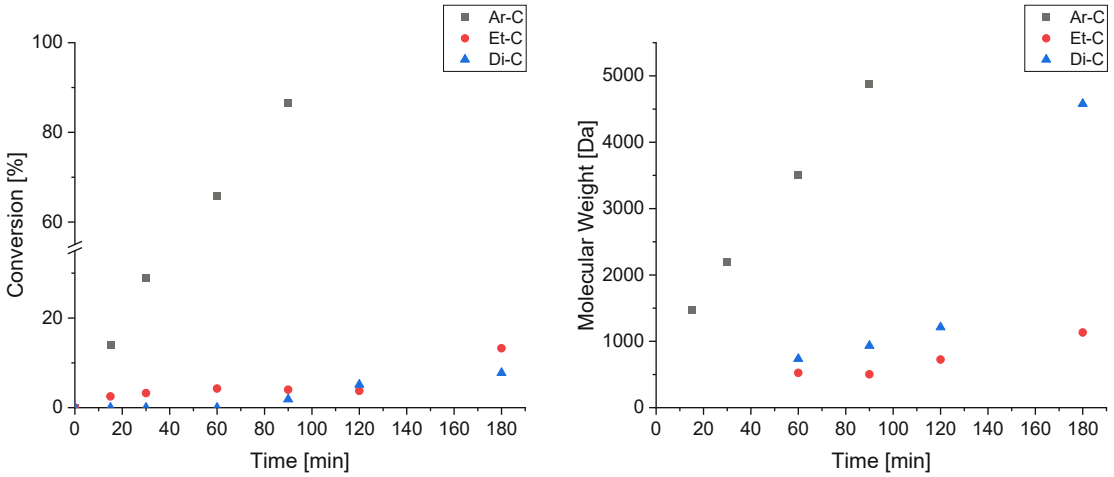

Figure 14: Thermal stability tests of the different monomers. Left: monomer conversion over time. Right: change of the molecular weight over time.

The higher reactivity of Ar-C is depicted in its fast conversion despite the lack of photo-initiation. This could have electronic reasons. With the ester moiety, the aromatic ring of PL-DBN possesses an electron-withdrawing group. Electronic interactions between the aromatic ring of Ar-C and PL-DBN could lead to the interaction that might increase the probability of an attack of the tertiary amine. Therefore, the thermal instability renders formulations containing Ar-C unsuitable for the printing process as it will polymerise in the

entire heated vat within 120 min or less. The obtained data would indicate a linear growth behaviour over time.

It can also be noted that some conversion takes place for the other two monomers, Et-C and Di-C. However, both monomers remained liquid for at least 180 min. It was no longer possible to draw samples of Di-C after 240 min, as it is reacting with PL-DBN at high temperatures over time. The molecular weight for Di-C drastically increases between 120 min and 180 min, indicating that linear oligomers are forming prior to crosslinking, as the samples were still soluble in the NMR solvent. Although low conversions were observed, high molecular weights were measured. Until 180 min, the NMR samples were dissolved completely, as no residue was visible in the NMR tube. For Et-C, a similar conclusion could be drawn.

Small oligomers are formed first, which are in equilibrium with the monomer *via* backbiting reactions. After the chain's length has reached a certain threshold, the active centre primarily attacks fresh monomer. This could explain the relatively stable conversion but increasing molecular weight until 120 min and then increasing conversion and molecular weight afterwards. Although Et-C and Di-C have bulky substituents, PL-DBN can attack the carbonate group and initiate the aROP reaction without irradiation.

3.3 Photo-Reactivity Analysis

3.3.1 Photo-DSC Analysis

The photo-DSC analysis was performed in analogy to the procedure described at Materials and Methods. As PL-DBN does not show absorption behaviour in the range of 320 – 500 nm, a sensitizer was necessary. Isopropylthioxanthone (ITX, Figure 15) is widely used as a sensitiser for PL-DBN and used during this experiment.[113] The initiating system consisted of PL-DBN and ITX in a ratio of 2:1 by weight. Each formulation contained 5 mol% PL-DBN as PBG. Again, the temperature was set to 70, 100, or 120 °C. The samples were irradiated 2x 300 s with an intensity of 50 mW cm^{-2}. Conversion and molecular weight were determined by ^{1}H-NMR and GPC, respectively.

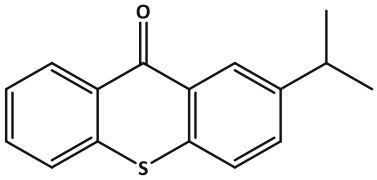

Figure 15: Structure of the Sensitizer ITX

3.3.1.1 Et-C

Photo-DSC analyses were performed as described in Materials and Methods using PL-DBN (Scheme 42).

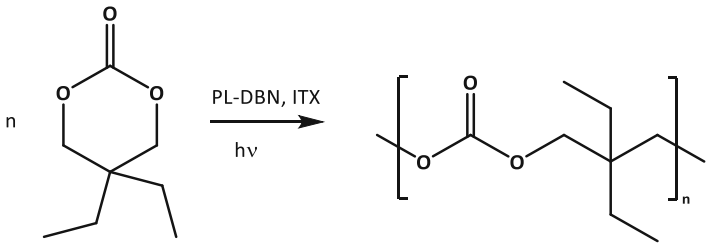

Scheme 42: Photopolymerisation of Et-C through aROP using PL-DBN as photo-base generator (PBG) and ITX as sensitizer.

As in chapter 2.1.1, no exothermic behaviour was recorded in this case, either. Table 4 summarises the GPC and ^{1}H-NMR analysis results of the photo-DSC samples. Again, the samples were weighed before and after the experiment to monitor side reactions counteracting polymerisation, and no mass loss was observed.

Table 4: Summarised results of the photo-polymerisation of Et-C. It was observed that the molecular weight is increasing, and the PDI is decreasing with increasing temperature. This could indicate a more homogenous distribution in the reaction equilibrium during the aROP of Et-C.

T (°C)	Conversion (%)	M_n (Da)	DP	PDI
70	30	1 400	9	1.20
100	41	1 900	12	1,18
120	30	1 900	12	1.16

Characteristically for anionic polymerisation, the obtained PDI was small for each tested temperature and decreased with increasing temperature. With 5 mol% PL-DBN, a targeted degree of polymerisation of 19 would result in molecular weights of about 3000 Da. Interestingly, the sample at 120 °C showed similar molecular weight as the sample at 100 °C despite having lower conversion. This could be due to a more homogeneous distribution between the polymer and the cyclic monomer, which the slightly lower PDI could also indicate. The lower conversion could also be explained due to the nature of this mode of polymerisation. Under anionic conditions, the polymerisation is reversible, showing an equilibrium between the linear aliphatic polycarbonate (APC) and the cyclic carbonate (CC). It can also be noted that signals beside the CH_2 signal of the linear polymer can be seen in the ^{1}H-NMR (Figure 16, purple box). Those signals could result from the addition of the base on the monomer, building the starting point of the growing chain. This addition results in an asymmetric starting point of the growing chain (Scheme 43). After neutralising the reaction with acid, an alcohol is formed on the other end of the polymer. The symmetry of the end-group is hence not given, as one CH_2 group faces the carbonate unit and the other CH_2 group faces the alcohol end group.

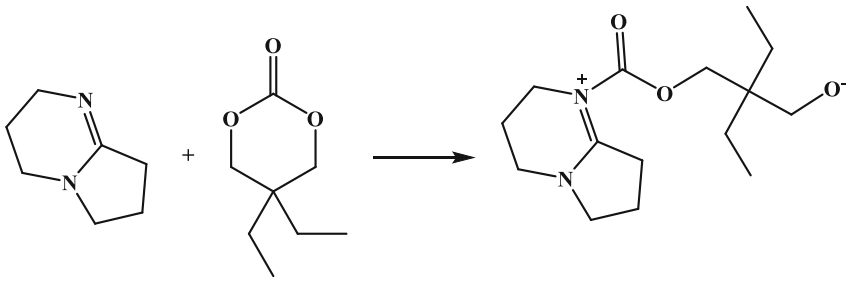

Scheme 43: Initiation step of the aROP reaction. The amidine base reacts with the carbonate unit of the cyclic monomer. For this unit as for the end group, the symmetry is not given, and hence the CH_2 groups of the starting and end units show different chemical shifts in the ^{1}H-NMR.

The starting unit (Figure 16, both singulet signals in the purple box) is more visible for low degrees of polymerisation than for high degrees of polymerisation. The ratio of the starting unit to the polymer signal decreases with higher conversion. Therefore, this signal is more visible for the sample cured at 70 °C than those cured at higher temperatures. This also correlates with the conversion, as the ratio between the starting unit and the APC's CH_2 integral is lowest at the highest observed conversion.

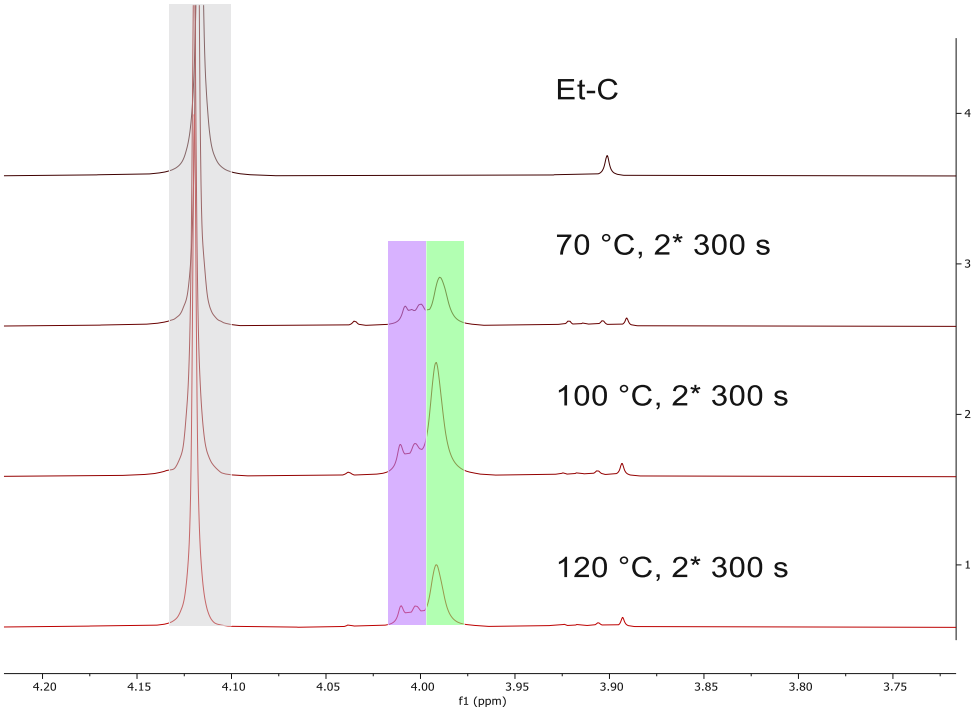

Figure 16: Comparison of the ^{1}H-NMR of the cyclic monomer, Et-C, and the photo-DSC samples. The monomer signal (grey box) is predominant as the conversions are relatively low. The polymeric signal is divided into the starting units CH_2 groups (purple box) and the symmetric CH_2 units of the growing polymer (green box).

Compared to the cationic system, lower conversions were obtained despite higher initiator concentration within the same irradiation time. As the cROP proceeds in two directions, a chain could also grow faster than it can with growth in one direction during aROP. The cROP mechanism, therefore, resulted in higher molecular weights. However, aROP shows smaller PDIs for all tested temperatures.

Furthermore, the initiation step of aROP might be the rate-determining step as the bulky base needs to attack the carbonate unit. The two ethyl groups in the 5-position of the monomer may sterically hinder the initiation and cause lower molecular weights of the photo-DSC samples. Furthermore, DBN might not diffuse as quickly through the monomer melt compared to the small proton released from the PAG in cROP. It can also be assumed that the energy transfer between the sensitizer and the PL-DBN slows down the initiation process.

3.3.1.2 Ar-C

The photo-polymerisation of Ar-C (Scheme 44) was performed as described in Materials and Methods.

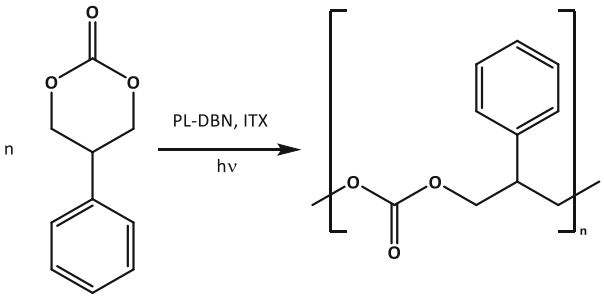

Scheme 44: Photopolymerisation of Ar-C with PL-DBN as the initiator for aROP

Again, no exothermic behaviour was observed during the measurements. Table 5 summarises GPC and ^{1}H-NMR analysis results from the photo-DSC samples. No weight loss was observed after the measurements. Interestingly, the sample irradiated at 120 °C showed higher conversion at similar molecular weights than at 100 °C. The obtained PDIs were slightly increased compared to the measured PDIs of the photo-DSC analysis of Et-C, which could be caused by premature polymerisation. Oligomers could have been formed during the heating

phase. Ar-C showed increasing reactivity with increasing temperatures. The monosubstituted Ar-C showed higher reactivity and molecular weights for all tested temperatures compared to Et-C. However, lower molecular weights were obtained again compared to the cROP tests.

Table 5: Summary of the photo-DSC results for Ar-C with 5 mol% PL-DBN. The formulation showed increasing reactivity with increasing temperature. Almost full conversion was observed at the sample cured at 120 °C

T (°C)	Conversion (%)	M_n (Da)	DP	PDI
70	37	3 050	17	1.20
100	75	4 400	25	1.27
120	93	4 200	24	1.37

The ^{1}H-NMR spectra of the photo-DSC samples of Ar-C are depicted in Figure 17. A triplet signal (4.40 ppm) can be seen next to the rising duplet signal of the CH_2 group (green box) from the growing polymer chain. This triplet signal does not increase for higher conversion, which could lead to its interpretation as the starting unit for aROP. However, the multiplicity does not correspond to the structural environment of such a group. Calculating the molecular weight indicated by the starting unit was not possible.

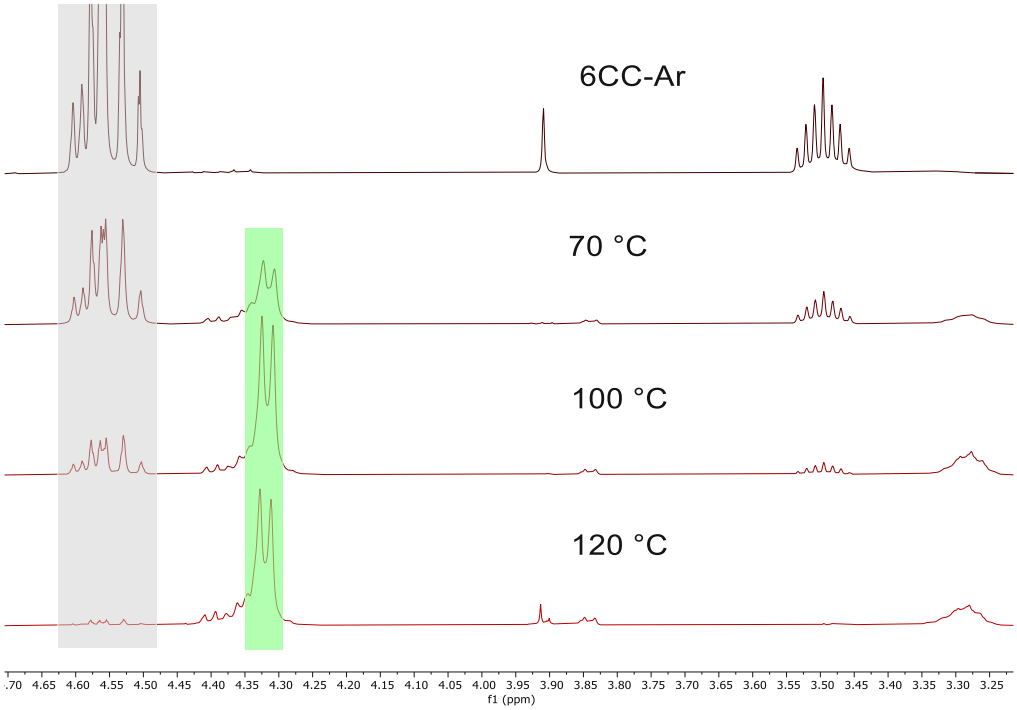

Figure 17: Comparison of the different ^{1}H-NMR spectra of Ar-C in its original form and after photo-DSC. The multiplet of the CH_2 group of the monomer (grey box) changes to a duplet (green box) due to more freedom of rotation of the linear polymer in solution. The multiplet of the benzylic position also exhibits a different chemical shift (3.33 – 3.24 ppm) compared to the CC monomer (3.50 ppm)

3.3.1.3 Di-C

The photopolymerization of Di-C was performed analogue to the procedure as described in Materials and Methods (Scheme 45). Due to the high melting point of Di-C, only measurements at 120 °C were performed.

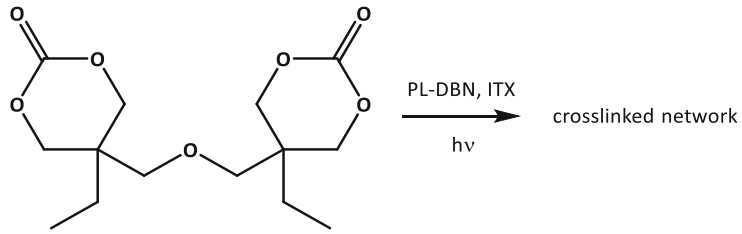

Scheme 45: Photopolymerisation of the DI-C using Pl-DBN

The results of the aROP approach mirror the results of the cROP tests. No exothermic behaviour was observed. The samples were also cured into solid and were neither soluble in THF nor in $CDCl_3$

3.3.2 Photo-Rheology

The photo-rheological measurements were performed with a light intensity of 50 mW cm^{-2} (320-500 nm) on the sample surface and an irradiation time of 15 min. The same initiator concentration used during photo-DSC experiments (5 mol%) was chosen. For the photo-rheological experiments, the glass surface, protected with a heatproof PE tape, was first heated to 110 °C, and 130 µL of the samples were added. The temperature was chosen based on higher conversions observed during the photo-DSC experiments. For the experiments, formulations with different contents of crosslinker (35 - 95 mol%) were tested to investigate its influence on the gelation behaviour as a function of crosslinker content. Figure 18 shows the obtained curves for the formulations of Et-C with different concentrations of the crosslinker Di-C (35, 50, 65, 80 mol%) and the pure crosslinker with 5 mol% PL-DBN each. The decrease in the storage modulus G' after the maximum could be caused by delamination of either the sample from the protective PE tape or the PE tape from the glass plate.

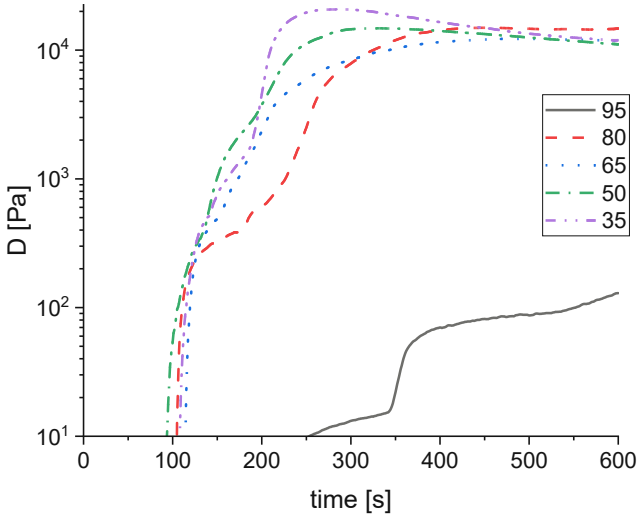

Figure 18: Photo-rheology analysis of Et-C, 35 (purple), 50 (green), 65 (blue), 80 (red), 95 (black) mol% Di-C and 5 mol% PL-DBN using an irradiation intensity of 50 mW cm^{-2}

The time until the gel point was reached was defined as the time until curves of storage modulus G' and loss modulus G'' intersected. A more detailed summary of the results is shown in Figure 19. The introduction of Et-C as reactive diluent showed significant improvement

compared to the pure Di-C formulation as the time until the gel point was reduced by up to 45%. However, the amount of reactive diluent did not cause any observable trend regarding the time until the gel point is reached within the investigated concentration range (35 – 95% Di-C). In summary, the reaction is relatively slow, with up to 230 s, until the gel point is reached. The slow reactivity might lead to extensively prolonged printing times, which could be fatal for spatial resolution. Several reasons might cause the reduced reactivity of the crosslinker Di-C with 5 mol% PL-DBN. The solubility of PL-DBN might be one reason. As the melting points of PL-DBN and Di-C are 115 °C and 104 °C, respectively, PL-DBN could be less soluble in the Di-C melt than the melt, which includes the reactive diluent Et-C, which has a melting point of 45 °C. At 110 °C, Et-C might be the better solvent for PL-DBN than Di-C and, hence, cause higher reactivity when the reactive diluent is added.

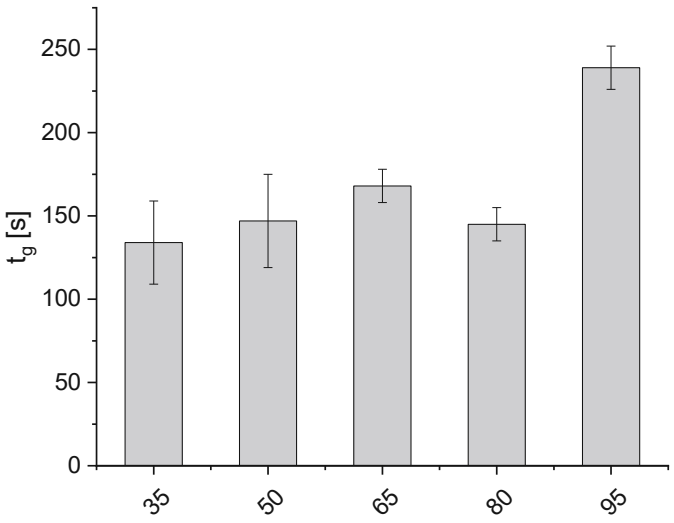

Figure 19: Summarised results of the photo-rheology analysis for Et-C, 35, 50, 65, 80, 95 mol% Di-C and 5 mol% PL-DBN. The time until the gel point is reached is decreased by the addition of the reactive diluent. However, no clear trend was observed within the formulations with reactive diluent.

It was also observed that the normal force was rising during the measurement (Figure 20). This indicated that the sample pressed against the stamp of the rheometer, which could be interpreted as a result of the characteristic volume expansion of cyclic carbonates during ROP. It was observed that the increasing normal force is decreasing with increasing content of Di-C. This trend could be explained by the formation of a tighter network, leaving less possibility for

increasing the volume of the sample. It can also be noted that the increase of the normal force is shifted towards longer times with increasing content of Di-C.

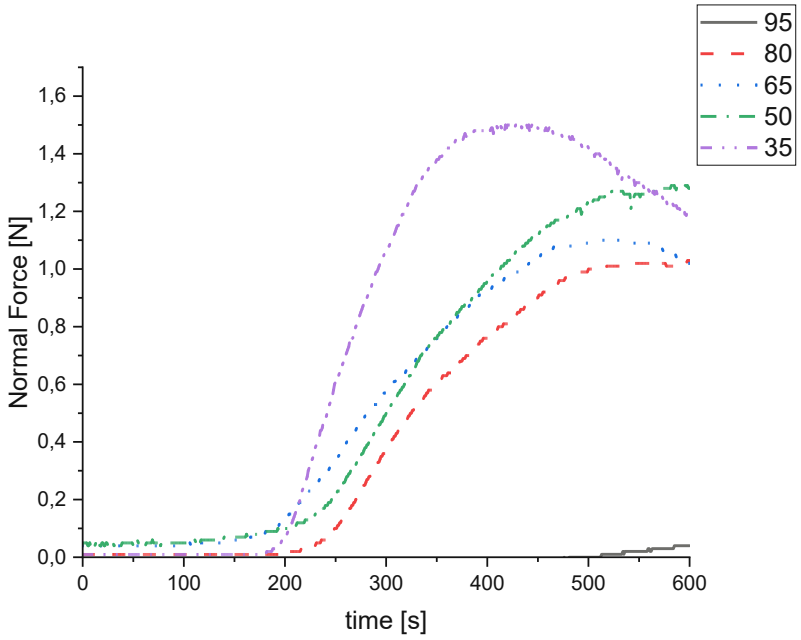

Figure 20: Normal force as a function of time of the photo-rheology tests of the formulation containing Et-C, 35 (purple), 50 (green), 65 (blue), 80 (red), 95 (black) mol% Di-C and 5 mol% PL-DBN. During the polymerisation of the samples, the normal force is increasing over time. The maximum of the normal force is decreasing with increasing content of Di-C indicating more restrict and hindered volume expansion during the reaction. It can also be seen that the reactivity of the formulation is decreasing with increasing content of Di-C in a shift to longer times for the onset of increasing normal force.

Photo-rheology experiments were also performed with Ar-C as the reactive diluent. These, however, were not reproducible, as there were drastic discrepancies within the repetitions. Ar-C showed already gel-like behaviour within a series of measurements, as the storage modulus G' was higher than the loss modulus G'' at all times. As a result, no intersection of G' with G'' was observable, and no gel point was obtained.

Furthermore, those results had enormous deviations from each other. The same formulation could show a gel point after 150 s, 65 s, or no gel point at all. The thermal instability of the formulations could cause these deviations as they were stored at elevated temperatures in between the measurements.

3.4 Thermal and (Thermo-)Mechanical Analysis

Different methods were chosen to investigate the obtained polymers' thermal and (thermo-)mechanical properties. Differential scanning calorimetry (DSC) was performed to determine the glass transition temperature (T_g) of the linear homopolymers of both reactive diluents, Et-C and Ar-C. The T_g is visible as a shift in the baseline of the DSC signal. To investigate (thermo-)mechanical properties, bulk curing tests were performed to determine the optimal curing method to obtain test specimens. Dynamic mechanical thermal analysis (DMTA) was performed on the crosslinked systems for determining the T_g. The T_g was evaluated as the temperature at the peak maximum of the tan δ (loss factor) curve. Tensile tests were performed to investigate stress and strain at break and tensile toughness of the obtained materials. Thermogravimetric analysis was performed for all polymers to investigate the thermal stability.

3.4.1 Bulk Curing Method Analysis

The bulk curing method analysis was performed in analogy to chapter 2.2. The same conditions were chosen to test the bulk curing behaviour. Contrary to the cROP approach results, the aROP approach led to acceptable test specimens (Figure 21).

Figure 21: Comparison of a formulation containing 50 mol% DI-C cured via cROP (left) and aROP conditions (right). Both specimens show colouration due to relatively long exposure times (600 s) and high post-curing temperatures (120 °C). The cROP specimen is highly porous due to decarboxylation reaction, while the aROP specimen does not show porosity.

Although good specimens were obtained during aROP of Et-C and the pure Di-C system, Ar-C showed bubble formation and expansion upon irradiation. A heating plate and a pre-heated silicone mould were used to test different temperatures (60 – 100 °C) during the irradiation. Bubble formation and expansion during irradiation increased with increasing temperature during irradiation and post-curing. Water might attack at the starting unit of aROP, releasing the DBN and forming a mono-ester of carbonic acid. This mono-ester could decarboxylate and cause bubble formation. To exclude water, drying overnight in high vacuum was performed. However, the exclusion of water did not solve this problem. There might be a reaction that takes place with the sensitiser ITX. ITX is known to initiate radical polymerisation through H-abstraction. The benzylic position on the monomer would be the preferred position for hydrogen abstraction (Scheme 46). Hydrogen abstraction would generate a tertiary radical, additionally stabilised by the aromatic ring. Through homolytic cleavage of the neighbouring C-O bond, an α-methyl styrene derivate would be generated. On the other side, an oxy-radical with low reactivity is formed. The oxy-radical could decompose by rearrangement or H-abstraction from the sensitizer, generating the carbonic mono-ester. This mono-ester could decarboxylate to generate the alcohol and CO_2, leading to bubble formation within the specimen.

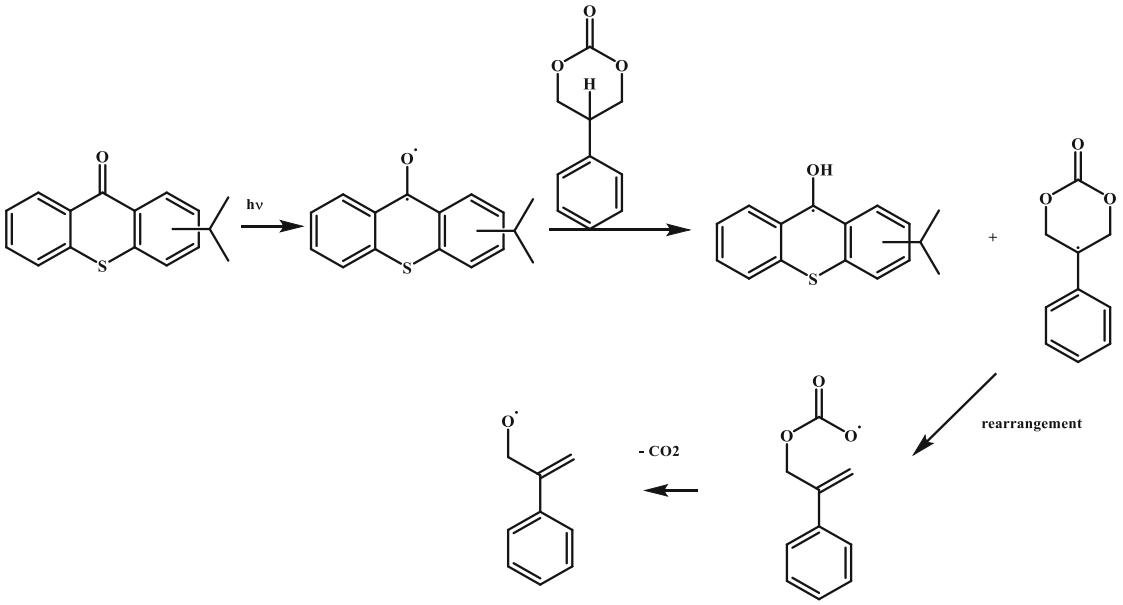

Scheme 46: Hypothesised radical initiation for Ar-C with ITX. Activated ITX molecules may abstract the hydrogen on the benzylic position of the monomer, leading to a radical pathway that could generate CO_2 as a side-product.

3.4.2 DSC of Linear Polymers

For the determination of the glass transitions of the linear polymers for Et-C and Ar-C, the samples were directly cured in the DSC pans. The samples were irradiated for 300 s with a light intensity of 60 mW cm^{-2} and post-cured for 2 h at 120 °C. For the DSC measurement, two heating cycles were performed. The first run was performed to delete the sample's thermal history and investigate whether the polymerisation was complete. The second run was used to determine the T_g. Any changes of the T_g due to thermal stress could be observed as well. The thermal behaviours of Et-C and Ar-C (Figure 22) are depicted below.

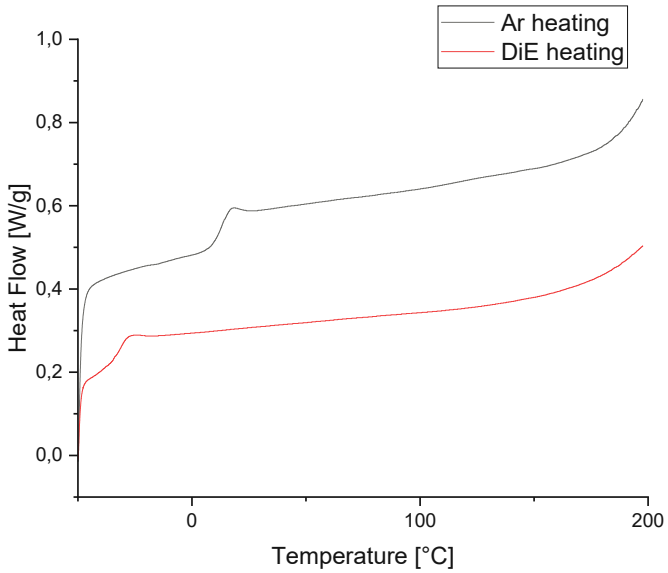

Figure 22: DSC graphs for poly(Ar-C) (black) and poly(Et-C) (red) No crystalline moieties can be observed hence amorphous structures can be assumed. The linear polymer of Et-C shows a very low T_g of -30 °C, which is characteristic of aliphatic polycarbonates. The Tg increases to about room temperature by introducing the phenyl ring as a substituent on Ar-C.

The introduction of the aromatic ring as a side group of the APC backbone drastically increases the T_g. Et-C shows the T_g at very low temperatures (-30 °C), whereas the T_g of Ar-C is at about room temperature. This can also be seen in bulk cured samples, as poly(Et-C) is a viscous liquid and poly(Ar-C) was obtained as a solid and stiff material at room temperature. The obtained T_gs for both polymers were not yet reported in the literature.

3.4.3 DMTA of Crosslinked Polymers

The test specimens for DMTA were prepared with formulations containing Et-C, the given amount of Di-C, 5 mol% PL-DBN and ITX (50 wt% relative to PL-DBN). The composition of the formulations is given in Table 6 below.

Table 6: Compositions of the investigated formulations

Formulation	mol% Et-C	mol% DI-C	mol% PL-DBN
35Di-C	60	35	5
50Di-C	45	50	
65Di-C	30	65	
80Di-C	15	80	
95Di-C	0	95	

The formulations were cured in silicone moulds (5 x 2 x 40 mm^3) in an Ivoclar Lumamat 100 at a temperature of 104 °C (400 – 580 nm) for 25 min. A post-curing step at 120 °C overnight was introduced to ensure complete conversion. ATR-IR was used to follow the changes in the molecular structure during the curing process. The DMTA measurements were conducted on an Anton Paar device in torsion mode (0.1% strain, 1 Hz). Storage and loss modulus were recorded while the test specimen was heated from -100 to 250 °C with a heating ramp of 2 °C min^{-1}. The loss factor was given as the ratio of the loss modulus to the storage modulus. The curves for storage modulus and tan δ are depicted in Figure 23 below. The T_g is slightly influenced by up to 30 mol% reactive diluent, but decreases with higher amounts. The shift towards lower temperatures is caused by the very low T_g of the reactive diluents.

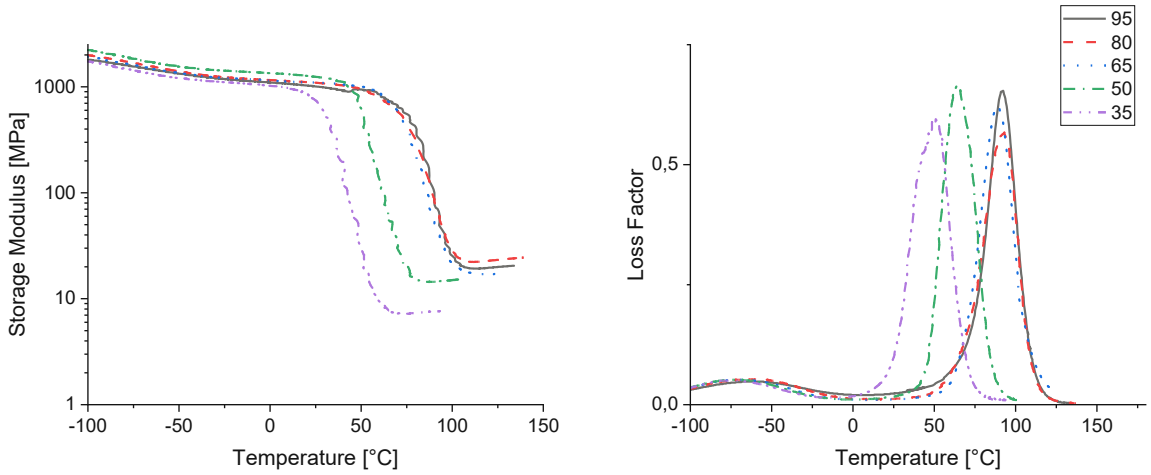

Figure 23:Graphs for the storage modulus (left) and loss factor (right) as function of temperature. With increasing amount of reactive diluent, the T_g is shifted towards lower temperatures. This can be seen as shift of the maxima of the loss factor curve to lower temperatures. The formulation containing 35 mol% of crosslinker Di--C has the lowest T_g of 47 °C.

3.4.4 Thermogravimetric Analysis

The thermal stability was investigated for all aforementioned materials. Again, the formulations containing Et-C, the given amount of Di-C, 5 mol% PL-DBN and ITX (50 wt% relative to PL-DBN) were prepared. The linear polymer poly(Et-C) was used as a reference to investigate the influence of the reactive diluent on the material's thermal stability. Obtained data is shown in Figure 24.

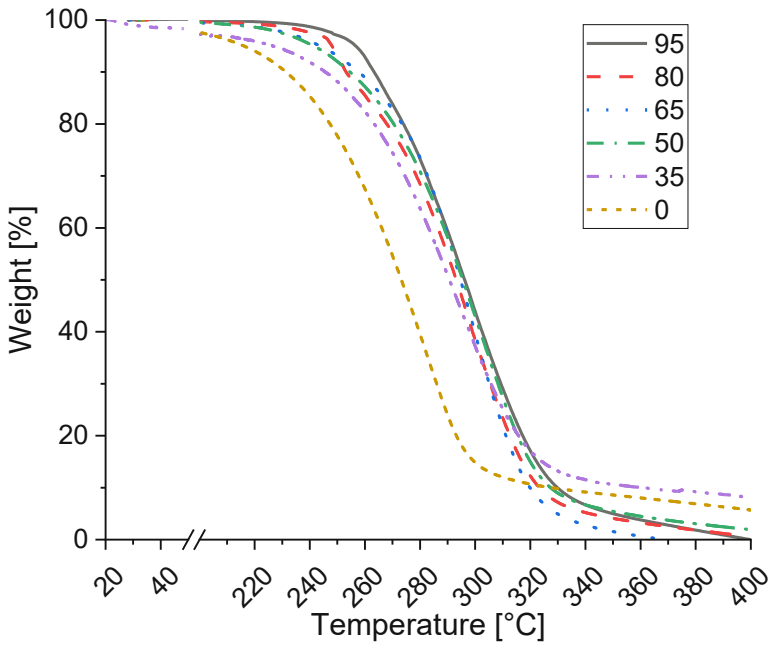

Figure 24: Thermogravimetric analysis of investigated materials. The linear polymer poly(Et-C) (yellow dotted line) as the reference material. The reactive diluent Et-C decreases the temperature of the onset of weight loss compared to the system containing pure crosslinker (95 mol% Di-C and 5 mol% PL-DBN, black line). However, the temperature, where most of the weight loss happens, did not change significantly.

Significant weight loss was observed between 220 and 290 °C. The addition of Et-C lowers the temperature for the onset of weight loss, although the main weight loss was observed for all materials between 280 and 310 °C. No 100% weight loss was observed with any mixed systems. With increasing amounts of reactive diluent, more residue was left at the final temperature of 400 °C.

3.4.5 Tensile Tests

Tensile tests were performed to determine the maximum stress and strain at break. Furthermore, the tensile toughness was obtained by integration of the stress-strain curve. The tensile test specimens were cured in analogy to the DMTA test specimen (chapter 3.4.3). The results of the tensile tests are shown in Figure 25 and Figure 26 below.

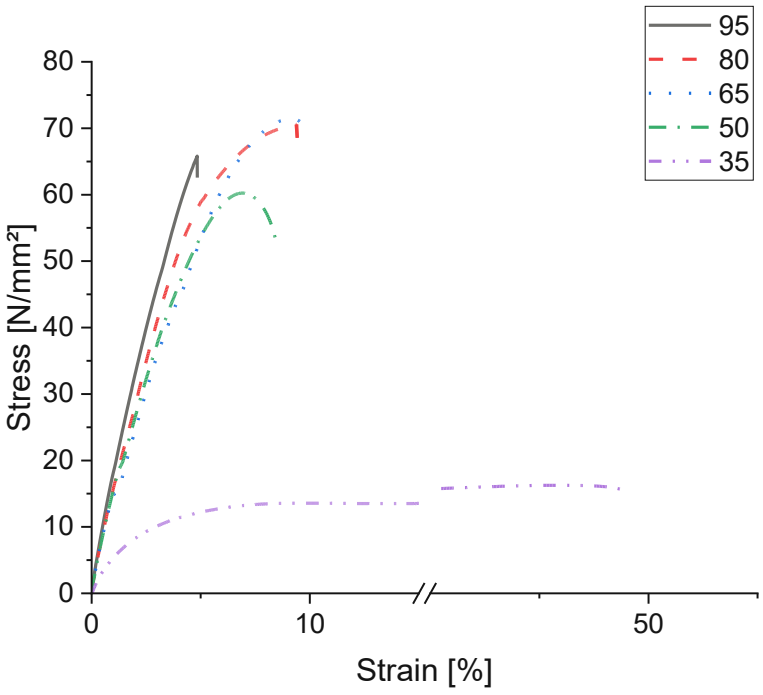

Figure 25: Stress-strain curves obtained by the tensile tests of the formulation with Et-C, 35 (purple), 50 (green), 65 (blue), 80 (red), 95 (black) mol% Di-C and 5 mol% PL-DBN. The tensile strength increases with the addition of reactive diluent. However, there is a drastic change in behaviour if the reactive diluent is the main component of the formulation, e.g. using 35 mol% Di-C (purple).

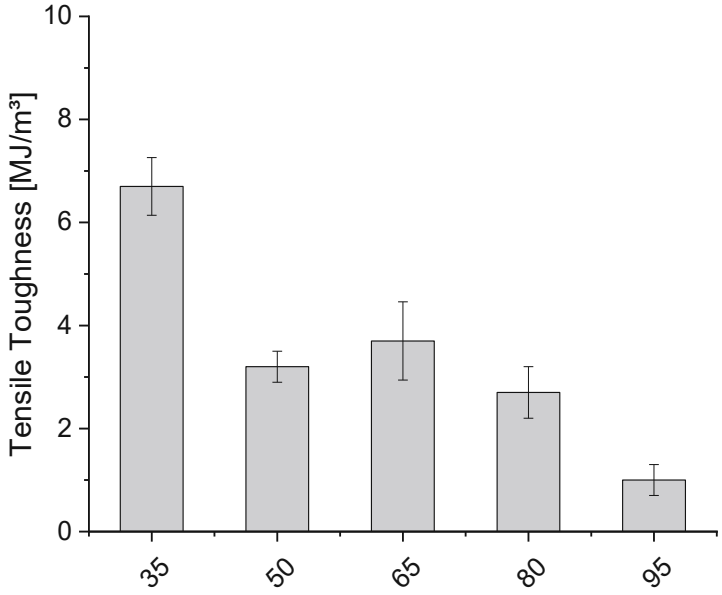

Figure 26: Tensile toughness of the obtained materials (Et-C, x mol% Di-C and 5 mol% PL-DBN). The tensile toughness increased with an increasing amount of reactive diluent.

Reactive diluent contents of up to 45 mol% increase the tensile strength and tensile toughness compared to the pure crosslinker system. Stress at break and strain at break were doubled with 15 – 30 mol% of reactive diluent, as shown in Table 7.

Table 7. Summarised results from the evaluation of the tensile tests.

Formulation	elongation at break (%)	stress at break (N mm^{-2})
35Di-C	38.5 ± 7.7	13.2 ± 2.1
50Di-C	5.6 ± 1.7	49.8 ± 10.3
65Di-C	7.5 ± 1.8	64.0 ± 10.3
80Di-C	7.3 ± 1.5	69.8 ± 2.4
95Di-C	3.1 ± 1.0	34.3 ± 15.7

Furthermore, the system shows better homogeneity due to smaller relative deviations within the measurements. A drastic change in the behaviour can be observed if the reactive diluent

is the system's main component. With 35 mol% Di-C, the elongation at break increased from under 10% to 40%. The stress at break was also lowered under 20 N mm^{-2}, which showed a quarter of the specimen's results with higher crosslinker content. The increased tensile toughness of the 35Di-C sample is due to the high elongation at break. The increasing amount of reactive diluent shifts the mechanical characteristics towards elastomeric behaviour.

3.4.6 Light Exposure Tests for Hot Lithography

Light exposure tests were performed to investigate the behaviour and printability of the cyclic carbonates. During the light exposure tests, the sample is irradiated by a laser, and the form stability of the sample is tested. Important parameters for the light exposure test, such as the need for a sensitizer, writing speed, and temperature, were based on photo-DSC and photo-rheology tests. The experiments were performed with a Caligma 2000 UV Hot Lithography device from Cubicure GmbH. The device's maximum temperature was 100 °C, and therefore, only the formulations 35Di-C and 50Di-C were tested. Higher amounts of crosslinker increased the melting point of the formulation drastically, as it was not possible to transfer the formulation onto the building platform without crystallisation. Di-C has a melting point of 104 °C, and therefore, higher contents of Di-C result in high melting points of the formulation. The writing speed was set to 1 cm s^{-1} for higher exposure times. The laser irradiated the test area within the formulation twice to ensure the highest possible conversion of the initiator. After irradiation, the formulation was left on the building platform for an additional 5 min to reach past the gel point. Unpolymerised resin was removed using a plastic pipet.

However, the polymerised test specimen showed no form-stability and could not be removed from the platform in one piece. The results were identical for both formulations. Prolonged dark-curing times after irradiation up to 10 min also showed no form-stable test specimens. Initiation and some polymerisation were observed. However, form stability could not be achieved.

Summary

Hot Lithography has proven to be of increasing interest as a stereolithographic manufacturing technique. Through high operating temperatures of up to 120 °C, Hot Lithography broadens the scope of possible monomers. Additionally, viscous and/or less reactive resins are printable due to reduced viscosity and increased reactivity at higher temperatures. This thesis aimed to investigate the applicability of cyclic carbonates (CC) as monomers for Hot Lithography.

Two different CC-based reactive diluents and one CC-based crosslinker were tested in two different ionic ring opening polymerisation modes regarding their photo-reactivity. The influence of the mode of polymerisation was examined in detail. An aliphatic and an aromatic substituent (Figure 27) were chosen to investigate their influence on reactivity and material properties.

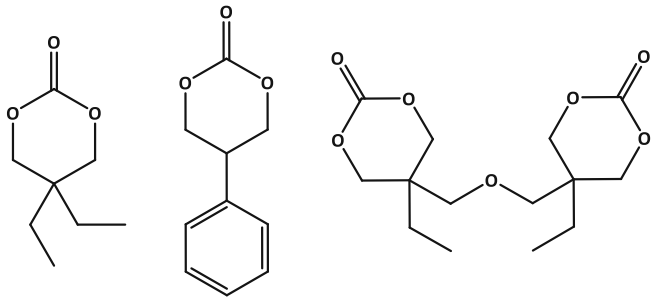

Figure 27: Investigated CCs for the applicability in Hot Lithography

Photo-DSC measurements were performed to analyse the reactivity of the monomers. Additionally, NMR- and GPC-analyses were conducted to gain information on conversion and molecular weights, respectively. Bulk curing tests were performed to investigate the bulk behaviour upon irradiation. Here, the two distinct polymerisation modes showed drastic differences. Whereas decarboxylation and generation of highly porous materials were observed in all cases under cationic ring-opening polymerisation (cROP) conditions, acceptable test specimens were obtained under anionic ring-opening polymerisation (aROP) conditions.

Ar-C has been proven as an inadequate monomer in both methods. Due to the nature of cROP for CCs, decarboxylation and formation of ether-linkages were observable under all tested

conditions. A different situation was observed under aROP conditions. Bubble formation was found to occur at higher temperatures during irradiation and in the post-curing process. This could have been caused by the sensitiser ITX, as it can be used as a photoinitiator for radical polymerisation. H-abstraction at the monomer's benzylic position might have generated a radical. Decarboxylation might have been made possible through rearrangement and therefore caused bubble formation.

Another drawback of the aROP approach was its storage stability at elevated temperatures. As proven, both monofunctional monomers and the crosslinker are prone to thermal initiation by the photobase PL-DBN. The monofunctional monomers showed differences in their reactivity. Ar-C has more than 80% conversion within 90 minutes of storage at 120 °C, whereas Et-C has 15% after 180 minutes. Di-C reacted with PL-DBN thermally to be solid after 240 min. However, there are no literature-known stabilisers for photobase generators to prevent premature polymerisation upon heating.

Nevertheless, test specimens for the analysis of (thermo-)mechanical properties of CC based materials were produced, as the future development of photobase generators might solve the stability issues. DMTA measurements were performed to determine relevant properties, such as the glass transition temperature T_g and the storage modulus G'. Furthermore, strain at break, stress at break and tensile toughness were obtained from tensile tests. The materials properties were determined with different contents of Di-C. It was proven that small additions of reactive diluent Et-C positively influence the mechanical properties without decreasing the glass transition temperature. A drastic change in the properties of the material was observed when the reactive diluent was the dominant component of the formulation. A decrease in T_g and stress at break while increasing the tensile toughness was observed. This could lead to further optimisation of the system and tunable material properties by adjusting the formulation's composition.

Light exposure tests were performed on formulation with a melting point below 100 °C. Although photo-rheology predicted a gel point after 180 s, no formstable test specimen was obtainable.

Experimental Part

1 Monomer Synthesis

1.1 Transesterification with Diethyl Carbonate

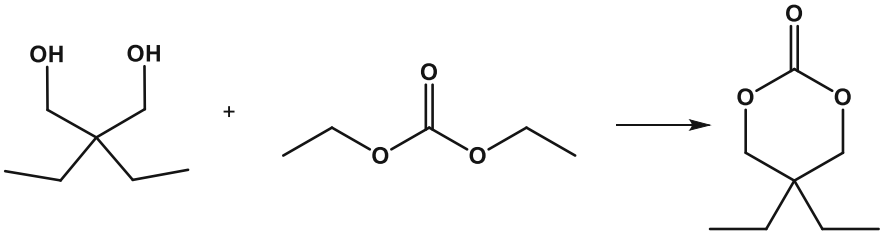

Et-C

The reaction was modified from literature.[59] 1.88 g (16 mmol, 1.4 eq) of diethyl carbonate were charged in a 10 ml round bottom flask equipped with a magnetic stirring bar. 0.1 eq of sodium hydride in paraffin were added at room temperature under a nitrogen atmosphere followed by stepwise addition of 2,2-diethylpropane-1,3-diol. The solution was stirred at room temperature for five minutes before the flask was equipped with a distillation apparatus, and the reaction mixture was heated up to 120 °C with a pre-heated oil bath. After distilling off formed ethanol, the reaction was cooled down to room temperature. Excess of diethyl carbonate was distilled off under reduced pressure at 60 °C. The temperature was then gradually raised to 220 °C. The product was distilled off at 180 - 200 °C, yielding 1.29 g (71.9%).

Yield: 71.9% of theory

Appearance: white crystals

Melting point 45.1-46.6°C (Literature: 45-46 °C[114])

^{1}H NMR (400 MHz, Chloroform-*d*): δ 4.11 (s, 4H, O-**CH$_2$**-C), 1.46 (q, *J* = 7.6 Hz, 4H, **CH$_2$**CH$_3$), 0.88 (t, *J* = 7.6 Hz, 6H, CH$_2$**CH$_3$**) ppm.

^{13}C NMR (101 MHz, CDCl$_3$) δ 148.74 (**C**=O), 75.06 (O-**C**H$_2$-C), 32.32 (CH$_2$-**C**-CH$_2$), 22.88 (C-**C**H$_2$-CH$_3$), 7.27 (-**C**H$_3$) ppm.

Melting point[115] and ^{1}H-NMR[116] were compared to the literature.

1.2 Transesterification with Diphenyl Carbonate

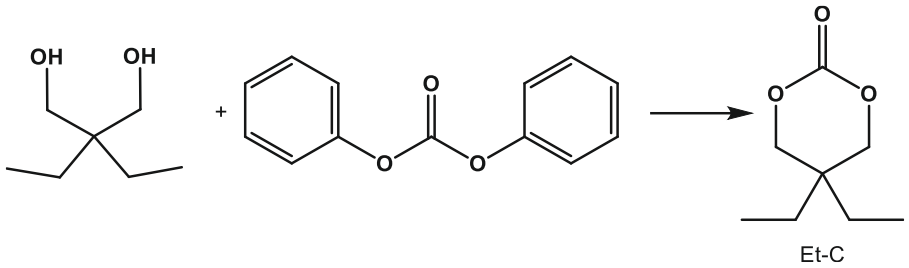

Et-C

The reaction was performed according to literature.[92] A 20 ml penicillin vial charged with a magnetic stirring bar and 24.3 g (113 mmol, 6 eq) diphenyl carbonate were heated to 140 °C. At the given temperature, 2.5 g (19 mmol, 1 eq) of 2,2-diethylpropane-1,3-diol was added. The vial was sealed and stirred for 48 h. After cooling down to room temperature the reaction solution was purified *via* column chromatography (eluent: PE:EA = 4:3). The pure product was obtained as white solids with a yield of 2.35g (78.6%).

Yield: 78.6% of theory

Appearance: white crystals

Melting point 45.2-46.1°C (Literature: 45-46 °C[114])

^{1}H NMR (400 MHz, Chloroform-*d*): δ 4.11 (s, 4H, O-**CH_2**-C), 1.46 (q, *J* = 7.6 Hz, 4H, **CH_2**CH_3), 0.88 (t, *J* = 7.6 Hz, 6H, CH_2**CH_3**) ppm.

^{13}C NMR (101 MHz, $CDCl_3$) δ 148.74 (**C**=O), 75.06 (O-**C**H_2-C), 32.32 (CH_2-**C**-CH_2), 22.88 (C-**C**H_2-CH_3), 7.27 (-**C**H_3) ppm.

Melting point[115] and ^{1}H-NMR[116] were compared to the literature.

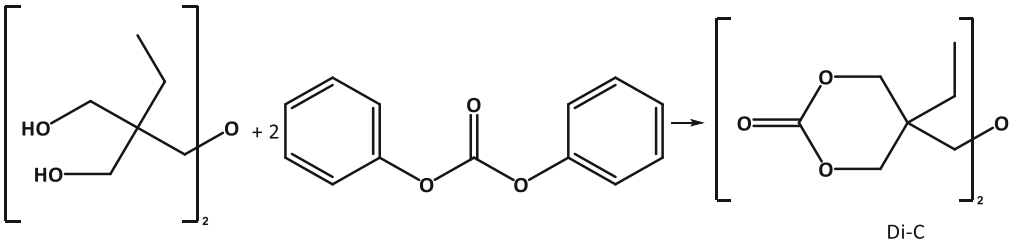

Di-C

The reaction was performed according to literature.[92] A 20 ml penicillin vial charged with a magnetic stirring bar and 15.4 g (72 mmol, 6 eq) diphenyl carbonate was heated to 140 °C. At the given temperature, 3.0 g (12 mmol, 1 eq) of di(trimethylolpropane) was added. The vial was sealed and stirred for 48 h. After cooling down to room temperature, the reaction solution was purified *via* column chromatography (eluent: PE:EA = 2:3) followed by recrystallisation from a mixed solvent of PE:EA = 1:3. The pure product was obtained as white solids with a yield of 3.05 g (84.2%).

Yield	84.2% of theory
Appearance	white crystals
Melting point	104.3-105.2 °C (104.3-105.6[92])
TLC analysis	R_f = 0.33 (petroleum ether : ethyl acetate = 1:4)
^{1}H NMR (400 MHz, $CDCl_3$)	δ 4.22 (dd, 8H), 3.49 (s, 4H), 1.49 (q, *J* = 7.6 Hz, 4H), 0.91 (t, *J* = 7.6 Hz, 6H) ppm.
^{13}C NMR (101 MHz, $CDCl_3$)	δ 148.78, 73.26, 71.30, 35.91, 24.11, 7.84 ppm.

Melting point and NMR data were in accordance with literature.[92]

1.3 Cyclisation using 1,1'-Carbonyldiimidazole

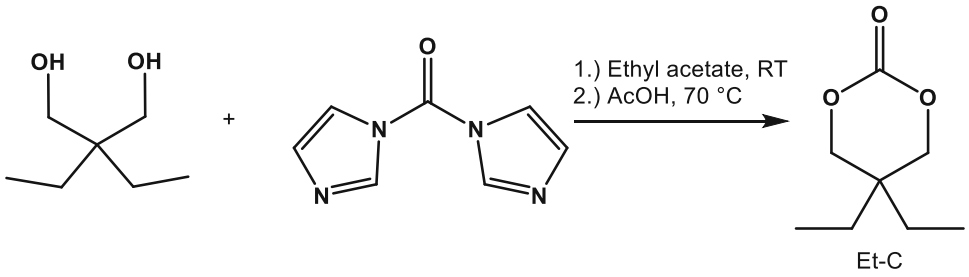

Et-C

The reaction was adopted from literature.[118] In a 250 mL round bottom flask, 8 g of 2,2-diethyl-1,3-propanediol (61 mmol, 1 eq.) were dissolved in 120 mL ethyl acetate. 14.7 g 1,1'-carbonydiimidazole (CDI) (91 mmol, 1.5 eq.) were added in two portions with 5 min of stirring at room temperature in between. After adding the second portion, the solution was stirred for 5 min at room temperature. 55 mL acetic acid (970 mmol, 16 eq.) were added slowly. Afterwards, the flask was equipped with a reflux condenser, and the solution was heated to 75 °C for 2 h. After cooling to room temperature, the solution was diluted with 200 mL ethyl acetate and washed once with 100 mL 2 N HCl. The aqueous phase was extracted twice with 75 mL ethyl acetate. The organic phases were combined and dried over Na_2SO_4. The solid compounds were filtered off, and the solvent was distilled off *in vacuo*. 200 mL of toluene were added to remove the remaining acetic acid *via* azeotropic distillation. The crude product was dissolved in 4 mL ethyl acetate and precipitated in petroleum ether. The product was filtered off, washed with petroleum ether, dried under reduced pressure, and obtained as white crystals (7.66 g, 80.0%).

Yield: 80.0 % of theory

Appearance: white crystals

Melting point 45.2-46.2°C (Literature: 45-46 °C[114])

^{1}H NMR (400 MHz, Chloroform-*d*): δ 4.11 (s, 4H, O-**CH_2**-C), 1.46 (q, *J* = 7.6 Hz, 4H, **CH_2**CH_3), 0.88 (t, *J* = 7.6 Hz, 6H, CH_2**CH_3**) ppm.

^{13}C NMR (101 MHz, $CDCl_3$) δ 148.74 (**C**=O), 75.06 (O-**C**H_2-C), 32.32 (CH_2-**C**-CH_2), 22.88 (C-**C**H_2-CH_3), 7.27 (-**C**H_3) ppm.

Melting point[115] and ^{1}H-NMR[116] were compared to the literature.

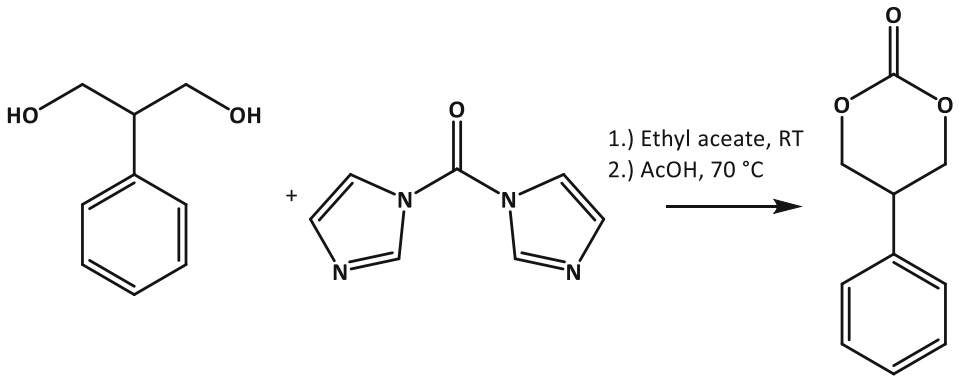

Ar-C

The reaction was adopted from literature.[91] In a 250 mL round bottom flask equipped with a magnetic stirring bar, 10 g of 2-phenyl-1,3-propanediol (67 mmol, 1 eq.) were dissolved in 130 mL ethyl acetate. 18.9 g CDI (113 mmol, 1.75 eq.) were added in two portions with 5 min in between. After adding the second portion, the solution was stirred until precipitation formed at room temperature. 61 mL (1072 mmol, 16 eq) acetic acid were added, and the flask was equipped with a reflux condenser. The reaction solution was heated to 75 °C for 2 h. After cooling, the reaction mixture was diluted with 150 mL ethyl acetate. The solution was washed once with 75 mL 2 N HCl, and the aqueous phase was re-extracted two times with 80 mL ethyl acetate. The organic phases were combined and dried over Na_2SO_4. Solid compounds were filtered off, and the solvent was distilled off *in vacuo*. The crude product was purified by column chromatography (petroleum ether : ethyl acetate = 3:1, v/v). The purified product was obtained as a colourless oil (7.84 g, 66.2%).

Yield	66.2% of theory
Appearance	colourless oil
TLC analysis	R_f = 0.33 (Petroleum ether : ethyl acetate = 3:1 v/v)

^{1}H NMR (400 MHz, Chloroform-*d*) δ 7.44 – 7.31 (m, 3H, Ph), 7.25 – 7.21 (m, 2H, Ph), 4.63 – 4.47 (m, 4H, O-**CH_2**-CH-Ar), 3.49 (hept, *J* = 10.1, 5.4 Hz, 1H, O-CH_2-**CH**-Ar) ppm.

^{13}C NMR (101 MHz, $CDCl_3$): δ 148.24 (C=O), 134.09 (CH-**C (Cq)**), 129.50 (C para Cq), 128.69 (C meta to Cq), 127.61 (C ortho to Cq), 72.18 (**C**H2), 37.64 (**C**H) ppm.

NMR data were in accordance with literature reported data.[109]

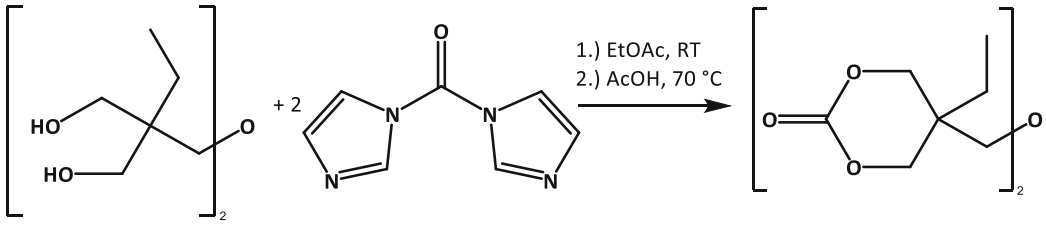

Di-C

The reaction was performed in a procedure modified from literature.[91] In a 500 mL round bottom flask, 20 g freshly ground di(trimethylolpropane) (80 mmol, 1 eq.) were suspended in ethyl acetate and stirred for 5 min. 38.9 g of CDI (240 mmol, 3 eq.) were added in small portions over 15 min. The solution was stirred at room temperature until all solids were dissolved. 73 mL (1280 mmol, 16 eq) of acetic acid were added slowly, and the flask was equipped with a reflux condenser and heated to 75 °C for 3 h. After cooling, the solution was diluted with 200 mL ethyl acetate and washed once with 150 mL 2 N HCl. The aqueous phase was washed twice with 80 mL ethyl acetate, and the combined organic phases were dried over Na_2SO_4. The solvent was removed under reduced pressure. Remaining acetic acid was removed *via* azeotropic distillation with 200 mL toluene. The crude product was dissolved in 20 mL of ethyl acetate and precipitated by adding petroleum ether. The product was filtered off, washed with petroleum ether, dried under reduced pressure and obtained as a white solid (20.8 g, 86.0%).

Yield	86.0% of theory
Appearance	white crystals
Melting point	104.3-105.8 °C (104.3-105.6[92])
TLC analysis	R_f = 0.33 (petroleum ether : ethyl acetate = 1:4)
^{1}H NMR (400 MHz, $CDCl_3$)	δ 4.22 (dd, 8H), 3.49 (s, 4H), 1.49 (q, *J* = 7.6 Hz, 4H), 0.91 (t, *J* = 7.6 Hz, 6H) ppm.
^{13}C NMR (101 MHz, $CDCl_3$)	δ 148.78, 73.26, 71.30, 35.91, 24.11, 7.84 ppm.

Melting point and NMR data were in accordance with literature.[92]

3 Anionic Ring-Opening Polymerisation

3.1 Synthesis of the Photo-Base Generator

3.1.1 Synthesis of Reduced 1,5-Diazabicyclo[4.3.0]non-5-en

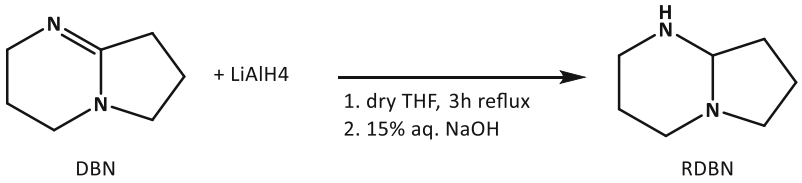

DBN RDBN

The reaction was performed according to a modified literature procedure.[112] 2.5 g of DBN (20 mmol, 1 eq.) were dissolved in dry THF (200 mL) under Ar atmosphere. 0.8g of $LiAlH_4$ (20 mmol, 1 eq.) were added in small portions under weak Ar flux. The reaction mixture was then heated to 80 °C for 3 h. After cooling to room temperature, distilled H_2O (1 mL per g $LiAlH_4$) and aqueous 15% NaOH (1 mL per g $LiAlH_4$) were added at 0 °C and stirred for 30 min. Then ethyl acetate (200 mL) was added. The solid contents were filtered off and washed with ethyl acetate. Removal of the solvent gave RDBN as a yellow liquid (2.36 g, 93.1%).

Yield	93.1% of theory
Appearance	yellow oil
^{1}H NMR (400 MHz, $CDCl_3$)	δ 3.20 – 3.07 (m, 2H), 3.04 – 2.94 (m, 1H), 2.87 – 2.77 (m, 1H), 2.71 – 2.60 (m, 1H), 2.32 – 2.19 (m, 1H), 2.18 – 2.07 (m, 1H), 2.00 – 1.88 (m, 1H), 1.83 – 1.73 (m, 1H), 1.69 – 1.58 (m, 2H), 1.53 – 1.46 (m, 1H), 1.44 – 1.32 (m, 1H), 1.14 (s, 1H) ppm.
^{13}C NMR (101 MHz, $CDCl_3$):	δ 78.83, 51.93, 51.60, 45.70, 30.18, 26.22, 19.19 ppm.

NMR data were in accordance with reported literature.[119]

3.1.2 Alkylation of Reduced 1,5-Diazabicyclo[4.3.0]non-5-en

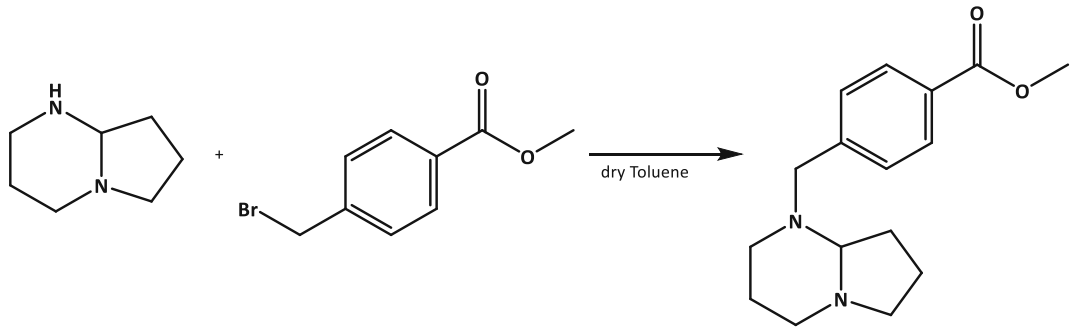

RDBN PL-DBN

The synthesis was performed according to the literature. [113]

2 g of RDBN (15 mmol, 1 eq.) were added dropwise to a solution of 3.63 g of methyl 4-(bromomethyl)-benzoate in 50 g dry toluene. The solution was stirred at room temperature for 24 h giving a viscous suspension. The suspension was filtered off, and the solvent's removal gave the product a white solid (1.97 g, 45.0% of theory).

Yield	45.0% of theory
Appearance	white solid
Melting point	112.5-114.3 °C (112.5-114.2[112]).
^{1}H NMR (400 MHz, Chloroform-*d*)	δ 7.96 (d, *J* = 8.3 Hz, 2H), 7.45 (d, *J* = 8.2 Hz, 2H), 3.94 (d, *J* = 13.8 Hz, 1H), 3.90 (s, 3H), 3.15 (d, *J* = 13.9 Hz, 1H), 3.13 – 3.02 (m, 2H), 2.85 – 2.79 (m, 1H), 2.45 (dd, 1H), 2.25 (q, *J* = 8.7 Hz, 1H), 2.15 – 2.06 (m, 1H), 2.06 – 1.96 (m, 1H), 1.93 – 1.83 (m, 3H), 1.81 – 1.61 (m, 2H), 1.54 – 1.43 (m, 1H) ppm.
^{13}C NMR (101 MHz, $CDCl_3$)	δ 167.27, 144.91, 129.68, 128.89, 84.77, 76.84, 58.41, 52.59, 52.44, 52.14, 51.24, 29.88, 24.81, 19.59 ppm.

Analysed data was compared to literature to confirm the product.[112]

Materials and Methods

Chemicals

1,1'-Carbonyldiimidazol	Abcr
1,5-Diazabicyclo(4.3.0)non-5-en	Fluka
2,2-diethylpropane-1,3-diol	Sigma Aldrich
2-phenylpropane-1,3-diol	Abcr
3-Phenylpropanol	Fluka
Acetic Acid	Merck
Chloroform -d	Eurisotop
Conc. HCl	Bussetti
Di(trimethylolpropane)	TCI
Ethyl acetate	Donau Chemie
IC 290	BASF
Lithium aluminiumhydride	Merck
Methyl-4-(bromomethyl)-benzoate	Sigma Aldrich
Petroleum ether	Donau Chemie
Pyridine	Abcr
Sodium Hydroxyde	Acros
S-Sb	Sigma Aldrich
tBuI-Al	Synthon
Tetrahydrofuran	Acros
Toluene	Donau Chemie

All chemicals were used as received without further purification, unless stated otherwise.

Methods

^{1}H- and^{13}C-NMR

NMR spectra were recorded on a BRUKER Avance DRX-400 FT-NMR spectrometer. Chemical shifts were indicated in ppm relative to tetramethylsilane (d = 0 ppm) and referenced on the used NMR-solvent. The multiplicity of the signals were stated as s = singlet, d = doublet, dd = doublet of doublets, t = triplet, q = quadruplet, hept = heptet, m = multiplet. Obtained spectra were analysed using the MestReNova software by Mestrelab Research.

Photo-DSC

Photo-DSC analyses were performed on a Netzsch DSC 204 F1 Phoenix device with an autosampler and double-core glass-fiber light guide (diameter: 3 mm). Samples were prepared by dissolving the initiators, S-Sb and PL-DBN for cROP and aROP, respectively, with the monomer and weighing 11 – 15 mg formulation in standard aluminium crucibles. The crucibles were closed with a glass lid to avoid evaporation. All measurements were performed under N_2 atmosphere with a flow of 20 mL min^{-1} at the given temperature. An Exfo OmniCure TM 2000 device with a spectral range of 320 – 500 nm from Lumen Dynamics was used as an irradiation source. The lamp was calibrated using an OmniCure R2000 radiometer. The light intensity was set to 50 mW cm^{-2} above the samples. Three samples were used from each formulation to analyse conversion and calorimetric data. The samples were irradiated twice for 300 s at the selected temperature. One measurement consisted of three segments: first, an isothermal step (240 s) to adjust the temperature of the sample, followed by two segments of irradiation (300 s). The obtained results represent the heat of polymerisation of the respective formulation as a function of time. Subtraction of the second irradiation phase was performed to remove background signals during the evaluation.

To evaluate conversion and molecular weight, two samples of the measuring series were dissolved in $CDCl_3$ and THF for NMR and GPC analysis, respectively.

0.3 wt% pyridine were added to the NMR solvent to quench the reaction. The conversion was determined using the CH_2 signals next to the carbonate unit (Ar-C: 4.55 ppm; poly(Ar-C): 4.32 ppm, Et-C: 4.12 ppm; poly(Et-C): 3.98 ppm). Using the formula::

$$NMR - conversion\ (\%) = (1 - \frac{\int Monomer - signal}{\int Monomer - signal + \int Polymer - signal}) * 100$$

The sum of the integrals of the monomer signal and the polymer signal was set to 4, for the 4 Hs next to the carbonate unit.

For the GPC analysis 0.5 mg mL^{-1} butylated 4-hydroxytoluene (BHT) was added as flow marker and transferred into GPC vials *via* syringe filters.

RT-NIR-Photorheology

Photorheology analysis was performed on an Anton Paar MCR 302 WESP device with a P-PTD 200/GL Peltier glass plate and a PP25 measuring system. The device was coupled with a Bruker Vertex 80 FTIR spectroscope, which recorded a NIR spectrum simultaneously during the rheology measurement.

An Exfo OmniCure 2000 TM was used as an irradiation source. The lamp was calibrated with an OmniCure R2000 radiometer, and the light intensities were adjusted to the stated value using an Ocean Optics device.

Formulations were prepared by dissolving the initiators and sensitiser, if necessary, in the monomer by heating and stirring. The glasse plate was heated to the selected temperature and 130 µL of formulation were placed on the plate. The stamp was lowered to a gap size of 2 mm for 1 min for formulations with a high melting point. The measuring gap size, shear rate and strain were set to 0.2 mm, 1 Hz and 1%, respectively. After 60 s the irradiation started for 900 s. Each formulation was measured three times. The values for the time until the gel point is reached (t_{gel}) were determined by the point of intersection of the storage (G') and loss (G'') modulus curves. Conversion analysis could not be conducted *via* NIR, since no clear changes in absorption could be observed.

GPC

GPC measurements were conducted on a Wasters GPC with three columns connected in series (Styragel HR 0.5, Styragel HR 3 and Styragel HR 4) and a Waters 2410 RI detector, UV Detector Module 2550 for TDA 305 and a VISCOTEK SEC-MALS 9 light scattering detector. Evaluation of the measurements was conducted using conventional calibration with polystyrene standards (375 – 177 000 Da) to determine the molecular weight of the polymers. For the measurements, the samples were dissolved in THF (0.5 mg mL^{-1} BHT as stabilizer and flow marker) and transferred into GPC vials *via* syringe filters.

STA

STA was measured on a STA 449 F1 Jupiter device from Netzsch using aluminium crucibles and N_2 as protection and purge gas. 10 – 15 mg of each sample were weighed into standard aluminium crucibles and covered with pierced lids. An empty crucible was used as reference. The prepared samples were heated with a rate of 10 K min^{-1} from 25 to 300 °C, unless stated otherwise, under N_2 atmosphere with a flow rate of 40 mL min^{-1}. Simultaneous to heating, the calorimetric information, as well as gravimetric changes were recorded. Analysis of recorded data was performed with the Netzsch Proteus thermal analysis software.

Thin-layer Chromatography (TLC)

TLC was carried out using TL-aluminium foils coated with silica gel 60 F245 from Merck.

Column Chromatography

Column chromatography was performed using a Büchi MPLC device equipped with a control unit (C-620), a fraction collector (C-660), and a UV-photometer as detector (C-635).

Melting interval

Melting intervals were measured using an automated OptiMelt device from SRS Stanford Research System.

DSC

DSC measurements were conducted on a TA Instruments DSC Q2000 V24.11 Build 124. The samples were weighed (10 – 15 mg) into aluminium crucibles and covered with a pierced lid. Two heating runs with a cooling run in between were performed with a temperature ramp of 10 °C min^{-1}. The investigated temperature ranged from -50 °C to 200 °C

TGA

Thermogravimetric analysis was performed on a TA Instrument TGA Q500 V6.7 Build 203. The samples were weighed (10 – 15 mg) into aluminium crucibles and covered with a pierced lid. The sampled were heated from 30 °C to 400 °C with a temperature ramp of 10 K min^{-1}.

Hot Lithography / Light Exposure Test

Light Exposure tests were performed on a Caligma 200 UV from Cubicure GmbH. The platform was heated to 100 °C. A 375 nm laser was used and set to an energy density of 1936 mJ cm^2 and set to a speed of 1 m s^{-1}. 1 g of each formulation was put onto the platform and exposed to light. After rastering the sample area, unreacted resin was removed with a plastic pipette.

Tensile Tests

A Zwick Z050 device with a maximum loading force of 5 N was used for tensile tests. The TestXpert II software was used to record and evaluate the data. Formulations were prepared by dissolving the initiators and sensitiser, if necessary, in the monomer by heating and stirring. The formulation was then transferred into silicone molds and irradiated in an Ivoclar Lumamat 100 at a temperature of 104 °C (400 – 580 nm) for 25 min. All test specimens were post-cured overnight at 120 °C. The test specimens were prepared according to ISO 527 test specimen 5b (a 2 x 2 x 12 mm parallel region, total length = 35 mm). The surface of the test specimens was smoothened before testing. The test specimens were fixed by two clamps and strain was applied with a constant cross-head speed of 5 mm min^{-1}.

Dynamic Mechanical Thermal Analysis (DMTA)

Formulations were prepared by dissolving the initiators and sensitiser, if necessary, in the monomer by heating and stirring. DMTA was performed on an Anton Paar MCR 301 device with a CTC 450 oven. The formulations were cured in silicone moulds (5 x 2 x 40 mm^3) in an Ivoclar Lumamat 100 at a temperature of 104 °C (400 – 580 nm) for 25 min. A post-curing step at 120 °C overnight was introduced to ensure complete conversion. The surface of all test specimens was smoothened before testing. The test specimens were measured in torsion mode with a frequency of 1 Hz and 0.1% strain. The temperature was increased from -100 to 200 C with a heating ramp of 2 °C min^{-1} and the loss factor and storage and loss modulus were recorded as a function of temperature. The glass transition temperature was defined as the temperature at the peak maximum of the loss factor (tan δ).

Literature

1. Lan, Q.; Yu, J.; Zhang, J.; He, J., Enhanced Crystallization of Bisphenol A Polycarbonate in Thin and Ultrathin Films by Supercritical Carbon Dioxide. *Macromolecules* **2011,** *44* (14), 5743-5749.
2. Bendler, J. T.; Boyles, D. A.; Edmondson, C. A.; Filipova, T.; Fontanella, J. J.; Westgate, M. A.; Wintersgill, M. C., Dielectric Properties of Bisphenol A Polycarbonate and Its Tethered Nitrile Analogue. *Macromolecules* **2013,** *46* (10), 4024-4033.
3. Artham, T.; Doble, M., Bisphenol A and metabolites released by biodegradation of polycarbonate in seawater. *Environmental Chemistry Letters* **2012,** *10* (1), 29-34.
4. de Brouwer, H.; van den Bogerd, J.; Hoover, J., Color stability of polycarbonate for optical applications. *European Polymer Journal* **2015,** *71*, 558-566.
5. Patil, A.; Patel, A.; Purohit, R., An overview of Polymeric Materials for Automotive Applications. *Materials Today: Proceedings* **2017,** *4* (2, Part A), 3807-3815.
6. Seubert, C.; Nietering, K.; Nichols, M.; Wykoff, R.; Bollin, S., An Overview of the Scratch Resistance of Automotive Coatings: Exterior Clearcoats and Polycarbonate Hardcoats. *Coatings* **2012,** *2* (4), 221-234.
7. Lu, L.; Zhu, X.; Valenzuela, R. G.; Currier, B. L.; Yaszemski, M. J., Biodegradable Polymer Scaffolds for Cartilage Tissue Engineering. *Clinical Orthopaedics and Related Research®* **2001,** *391*, S251-S270.
8. Welle, A.; Kröger, M.; Döring, M.; Niederer, K.; Pindel, E.; Chronakis, I. S., Electrospun aliphatic polycarbonates as tailored tissue scaffold materials. *Biomaterials* **2007,** *28* (13), 2211-2219.
9. Sun, J.; Birnbaum, W.; Anderski, J.; Picker, M.-T.; Mulac, D.; Langer, K.; Kuckling, D., Use of Light-Degradable Aliphatic Polycarbonate Nanoparticles As Drug Carrier for Photosensitizer. *Biomacromolecules* **2018,** *19* (12), 4677-4690.
10. Domiński, A.; Konieczny, T.; Duale, K.; Krawczyk, M.; Pastuch-Gawołek, G.; Kurcok, P., Stimuli-Responsive Aliphatic Polycarbonate Nanocarriers for Tumor-Targeted Drug Delivery. *Polymers* **2020,** *12* (12), 2890.
11. Guo, Z.; Liang, E.; Sui, J.; Ma, M.; Yang, L.; Wang, J.; Hu, J.; Sun, Y.; Fan, Y., Lapatinib-loaded acidity-triggered charge switchable polycarbonate-doxorubicin conjugate micelles for synergistic breast cancer chemotherapy. *Acta Biomaterialia* **2020,** *118*, 182-195.
12. Feng, J.; Zhuo, R.-X.; Zhang, X.-Z., Construction of functional aliphatic polycarbonates for biomedical applications. *Progress in Polymer Science* **2012,** *37* (2), 211-236.
13. Chen, Y.; Chen, G.; Niu, C.; Shang, W.; Yu, R.; Fang, C.; Ouyang, P.; Du, J., Ether-containing polycarbonate-based solid polymer electrolytes for Dendrite-Free Lithium metal batteries. *Polymer* **2021,** *223*, 123695.
14. Zhang, J.; Yang, J.; Dong, T.; Zhang, M.; Chai, J.; Dong, S.; Wu, T.; Zhou, X.; Cui, G., Aliphatic Polycarbonate-Based Solid-State Polymer Electrolytes for Advanced Lithium Batteries: Advances and Perspective. *Small* **2018,** *14* (36), 1800821.
15. Tomita, H.; Sanda, F.; Endo, T., Polyaddition behavior of bis(five- and six-membered cyclic carbonate)s with diamine. *Journal of Polymer Science Part A: Polymer Chemistry* **2001,** *39* (6), 860-867.
16. Pyo, S.-H.; Wang, P.; Hwang, H. H.; Zhu, W.; Warner, J.; Chen, S., Continuous Optical 3D Printing of Green Aliphatic Polyurethanes. *ACS Applied Materials & Interfaces* **2017,** *9* (1), 836-844.

17. Qin, Z.; Thomas, C. M.; Lee, S.; Coates, G. W., Cobalt-based complexes for the copolymerization of propylene oxide and CO2: active and selective catalysts for polycarbonate synthesis. *Angewandte Chemie* **2003,** *115* (44), 5642-5645.
18. Wu, G.-P.; Ren, W.-M.; Luo, Y.; Li, B.; Zhang, W.-Z.; Lu, X.-B., Enhanced Asymmetric Induction for the Copolymerization of CO2 and Cyclohexene Oxide with Unsymmetric Enantiopure SalenCo(III) Complexes: Synthesis of Crystalline CO2-Based Polycarbonate. *Journal of the American Chemical Society* **2012,** *134* (12), 5682-5688.
19. Wu, G.-P.; Wei, S.-H.; Lu, X.-B.; Ren, W.-M.; Darensbourg, D. J., Highly Selective Synthesis of CO2 Copolymer from Styrene Oxide. *Macromolecules* **2010,** *43* (21), 9202-9204.
20. Darensbourg, D. J.; Lewis, S. J.; Rodgers, J. L.; Yarbrough, J. C., Carbon dioxide/epoxide coupling reactions utilizing lewis base adducts of zinc halides as catalysts. Cyclic carbonate versus polycarbonate production. *Inorganic chemistry* **2003,** *42* (2), 581-589.
21. Guo, W.; Laserna, V.; Rintjema, J.; Kleij, A. W., Catalytic One-Pot Oxetane to Carbamate Conversions: Formal Synthesis of Drug Relevant Molecules. *Advanced Synthesis & Catalysis* **2016,** *358* (10), 1602-1607.
22. Yu, K. K.; Curcic, I.; Gabriel, J.; Morganstewart, H.; Tsang, S. C., Catalytic coupling of CO2 with epoxide over supported and unsupported amines. *The Journal of Physical Chemistry A* **2010,** *114* (11), 3863-3872.
23. Zhang, J.; Yang, J.; Dong, T.; Zhang, M.; Chai, J.; Dong, S.; Wu, T.; Zhou, X.; Cui, G., Aliphatic Polycarbonate-Based Solid-State Polymer Electrolytes for Advanced Lithium Batteries: Advances and Perspective. *Small* **2018,** *14* (36), e1800821.
24. Ariga, T.; Takata, T.; Endo, T., Cationic Ring-Opening Polymerization of Cyclic Carbonates with Alkyl Halides To Yield Polycarbonate without the Ether Unit by Suppression of Elimination of Carbon Dioxide. *Macromolecules* **1997,** *30* (4), 737-744.
25. Takata, T.; Sanda, F.; Ariga, T.; Nemoto, H.; Endo, T., Cyclic carbonates, novel expandable monomers on polymerization. *Macromolecular Rapid Communications* **1997,** *18* (6), 461-469.
26. Quaranta, E.; Sgherza, D.; Tartaro, G., Depolymerization of poly(bisphenol A carbonate) under mild conditions by solvent-free alcoholysis catalyzed by 1,8-diazabicyclo[5.4.0]undec-7-ene as a recyclable organocatalyst: a route to chemical recycling of waste polycarbonate. *Green Chemistry* **2017,** *19* (22), 5422-5434.
27. Guo, J.; Liu, M.; Gu, Y.; Wang, Y.; Gao, J.; Liu, F., Efficient Alcoholysis of Polycarbonate Catalyzed by Recyclable Lewis Acidic Ionic Liquids. *Industrial & Engineering Chemistry Research* **2018,** *57* (32), 10915-10921.
28. Saxon, D. J.; Gormong, E. A.; Shah, V. M.; Reineke, T. M., Rapid Synthesis of Chemically Recyclable Polycarbonates from Renewable Feedstocks. *ACS Macro Letters* **2021,** *10* (1), 98-103.
29. Iannone, F.; Casiello, M.; Monopoli, A.; Cotugno, P.; Sportelli, M. C.; Picca, R. A.; Cioffi, N.; Dell'Anna, M. M.; Nacci, A., Ionic liquids/ZnO nanoparticles as recyclable catalyst for polycarbonate depolymerization. *Journal of Molecular Catalysis A: Chemical* **2017,** *426*, 107-116.
30. Darensbourg, D. J.; Moncada, A. I.; Wei, S.-H., Aliphatic Polycarbonates Produced from the Coupling of Carbon Dioxide and Oxetanes and Their Depolymerization via Cyclic Carbonate Formation. *Macromolecules* **2011,** *44* (8), 2568-2576.
31. Li, C.; Sablong, R. J.; van Benthem, R. A. T. M.; Koning, C. E., Unique Base-Initiated Depolymerization of Limonene-Derived Polycarbonates. *ACS Macro Letters* **2017,** *6* (7), 684-688.

32. Hungenberg, K.-D., Ionic Polymerization. In *Handbook of Polymer Reaction Engineering*, 2005; pp 323-364.
33. Greenhow, E. J.; Shafi, A. A., Ionic polymerisation as a means of end-point indication in non-aqueous thermometric titrimetry. Part VIII. Solvent effects in the determination of polyfunctional carboxylic acids and phenols. *Analyst* **1976,** *101* (1203), 421-432.
34. Szwarc, M.; Van Beylen, M., *Ionic polymerization and living polymers*. Springer Science & Business Media: 2012.
35. Aoshima, S.; Kanaoka, S., A Renaissance in Living Cationic Polymerization. *Chemical Reviews* **2009,** *109* (11), 5245-5287.
36. <Handbook of Ring-Opening Polymerization.pdf>.
37. Sangermano, M.; Razza, N.; Crivello, J. V., Cationic UV-Curing: Technology and Applications. *Macromolecular Materials and Engineering* **2014,** *299* (7), 775-793.
38. Shiman, D. I.; Vasilenko, I. V.; Kostjuk, S. V., Cationic polymerization of isobutylene by complexes of alkylaluminum dichlorides with diisopropyl ether: An activating effect of water. *Journal of Polymer Science Part A: Polymer Chemistry* **2014,** *52* (16), 2386-2393.
39. Miyamoto, M.; Sawamoto, M.; Higashimura, T., Living polymerization of isobutyl vinyl ether with hydrogen iodide/iodine initiating system. *Macromolecules* **1984,** *17* (3), 265-268.
40. Endo, T.; Shibasaki, Y.; Sanda, F., Controlled ring-opening polymerization of cyclic carbonates and lactones by an activated monomer mechanism. *Journal of Polymer Science Part A: Polymer Chemistry* **2002,** *40* (13), 2190-2198.
41. Darensbourg, D. J.; Moncada, A. I.; Wilson, S. J., Ring-Opening Polymerization of Renewable Six-Membered Cyclic Carbonates. Monomer Synthesis and Catalysis. In *Green Polymerization Methods*, pp 163-200.
42. Nuyken, O.; Pask, S. D., Ring-opening polymerization—an introductory review. *Polymers* **2013,** *5* (2), 361-403.
43. Hadjichristidis, N.; Iatrou, H.; Pispas, S.; Pitsikalis, M., Anionic polymerization: High vacuum techniques. *Journal of Polymer Science Part A: Polymer Chemistry* **2000,** *38* (18), 3211-3234.
44. Wang, J.-S.; Jérôme, R.; Bayard, P.; Teyssié, P., Anionic polymerization of acrylic monomers. 21. Anionic sequential polymerization of 2-ethylhexyl acrylate and methyl methacrylate. *Macromolecules* **1994,** *27* (18), 4908-4913.
45. Baskaran, D., Strategic developments in living anionic polymerization of alkyl (meth)acrylates. *Progress in Polymer Science* **2003,** *28* (4), 521-581.
46. Fayt, R.; Forte, R.; Jacobs, C.; Jérôme, R.; Ouhadi, T.; Teyssié, P.; Varshney, S. K., New initiator system for the living anionic polymerization of tert-alkyl acrylates. *Macromolecules* **1987,** *20* (6), 1442-1444.
47. Endo, T., General Mechanisms in Ring-Opening Polymerization. In *Handbook of Ring-Opening Polymerization*, 2009; pp 53-63.
48. Delcroix, D.; Martín-Vaca, B.; Bourissou, D.; Navarro, C., Ring-Opening Polymerization of Trimethylene Carbonate Catalyzed by Methanesulfonic Acid: Activated Monomer versus Active Chain End Mechanisms. *Macromolecules* **2010,** *43* (21), 8828-8835.
49. Kricheldorf, H. R.; Jenssen, J., Polylactones. 16. Cationic Polymerization of Trimethylene Carbonate and Other Cyclic Carbonates. *Journal of Macromolecular Science: Part A - Chemistry* **1989,** *26* (4), 631-644.
50. Morikawa, H.; Sudo, A.; Nishida, H.; Endo, T., Cationic Copolymerization Behavior of Glycidyl Phenyl Ether with Seven-Membered Cyclic Carbonate. *Macromolecular Chemistry and Physics* **2005,** *206* (5), 592-599.

51. Ariga, T.; Takata, T.; Endo, T., Cationic copolymerization of cyclic carbonate and epoxide via intermediate spiro orthocarbonate. *Journal of Polymer Science Part A: Polymer Chemistry* **1994,** *32* (7), 1393-1397.
52. Kuran, W.; Listoś, T., Copolymerization of epoxides and five-membered cyclic carbonates in the presence of zinc coordination catalysts. *Die Makromolekulare Chemie* **1992,** *193* (4), 945-956.
53. Takata, T.; Endo, T., *Ionic polymerization of oxygen-containing bicyclic, spirocyclic, and related expandable monomers*. CRC Press: Boca Raton: 1992.
54. Morikawa, H.; Sudo, A.; Nishida, H.; Endo, T., Volume-expandable monomer 5,5-dimethyl-1,3-dioxolan-2-one: Its copolymerization behavior with epoxide and its applications to shrinkage-controlled epoxy-curing systems. *Journal of Applied Polymer Science* **2005,** *96* (2), 372-378.
55. Dai, Y.; Zhang, X., Recent development of functional aliphatic polycarbonates for the construction of amphiphilic polymers. *Polymer Chemistry* **2017,** *8* (48), 7429-7437.
56. Tsutsumi, C.; Yamamoto, K.; Ichimaru, A.; Nodono, M.; Nakagawa, K.; Yasuda, H., Biodegradations of block copolymers composed of l-or d, l-lactide and six-membered cyclic carbonates prepared with organolanthanide initiators. *Journal of Polymer Science Part A: Polymer Chemistry* **2003,** *41* (22), 3572-3588.
57. Yasuda, H.; Aludin, M.-S.; Kitamura, N.; Tanabe, M.; Sirahama, H., Syntheses and Physical Properties of Novel Optically Active Poly (ester− carbonate) s by Copolymerization of Substituted Trimethylene Carbonate with ε-Caprolactone and Their Biodegradation Behavior. *Macromolecules* **1999,** *32* (19), 6047-6057.
58. Ariga, T.; Takata, T.; Endo, T., Block copolymerization of cyclic carbonate and oxetanes in one-shot feeding. *Macromolecules* **1993,** *26* (25), 7106-7107.
59. Hua, G.; Olsén, P.; Franzén, J.; Odelius, K., Anionic polycondensation and equilibrium driven monomer formation of cyclic aliphatic carbonates. *RSC Advances* **2018,** *8* (68), 39022-39028.
60. Teator, A. J.; Lastovickova, D. N.; Bielawski, C. W., Switchable Polymerization Catalysts. *Chemical Reviews* **2016,** *116* (4), 1969-1992.
61. Dietliker, K.; Hüsler, R.; Birbaum, J.-L.; Ilg, S.; Villeneuve, S.; Studer, K.; Jung, T.; Benkhoff, J.; Kura, H.; Matsumoto, A., Advancements in photoinitiators—Opening up new applications for radiation curing. *Progress in organic coatings* **2007,** *58* (2-3), 146-157.
62. Dall'Argine, C.; Hochwallner, A.; Klikovits, N.; Liska, R.; Stampf, J.; Sangermano, M., Hot-Lithography SLA-3D Printing of Epoxy Resin. *Macromolecular Materials and Engineering* **2020,** *305* (10), 2000325.
63. Keitz, B. K.; Yu, C. J.; Long, J. R.; Ameloot, R., Lithographic Deposition of Patterned Metal–Organic Framework Coatings Using a Photobase Generator. *Angewandte Chemie International Edition* **2014,** *53* (22), 5561-5565.
64. Crivello, J. V., The discovery and development of onium salt cationic photoinitiators. *Journal of Polymer Science Part A: Polymer Chemistry* **1999,** *37* (23), 4241-4254.
65. Travitzky, N.; Bonet, A.; Dermeik, B.; Fey, T.; Filbert-Demut, I.; Schlier, L.; Schlordt, T.; Greil, P., Additive Manufacturing of Ceramic-Based Materials. *Advanced Engineering Materials* **2014,** *16* (6), 729-754.
66. Jongsma, L. A.; Kleverlaan, C. J., Influence of temperature on volumetric shrinkage and contraction stress of dental composites. *Dental Materials* **2015,** *31* (6), 721-725.
67. Patel, M. P.; Braden, M.; Davy, K. W. M., Polymerization shrinkage of methacrylate esters. *Biomaterials* **1987,** *8* (1), 53-56.

68. El-Bashir, S. M.; Al-Jaghwani, A. A., Perylene-doped polycarbonate coatings for acrylic active greenhouse luminescent solar concentrator dryers. *Results in Physics* **2020,** *16*, 102920.
69. Pan, K.; Li, X.; Shi, H.; Dai, M.; Yang, Z.; Chen, M.; Wei, W.; Liu, X.; Zheng, Y., Preparation of photo-crosslinked aliphatic polycarbonate coatings with predictable degradation behavior on magnesium-alloy stents by electrophoretic deposition. *Chemical Engineering Journal* **2022,** *427*, 131596.
70. Weems, A. C.; Arno, M. C.; Yu, W.; Huckstepp, R. T. R.; Dove, A. P., 4D polycarbonates via stereolithography as scaffolds for soft tissue repair. *Nature Communications* **2021,** *12* (1), 3771.
71. Ligon, S. C.; Liska, R.; Stampfl, J.; Gurr, M.; Mülhaupt, R., Polymers for 3D Printing and Customized Additive Manufacturing. *Chemical Reviews* **2017,** *117* (15), 10212-10290.
72. Steyrer, B.; Busetti, B.; Harakály, G.; Liska, R.; Stampfl, J., Hot Lithography vs. room temperature DLP 3D-printing of a dimethacrylate. *Additive Manufacturing* **2018,** *21*, 209-214.
73. Cumpston, B. H.; Ananthavel, S. P.; Barlow, S.; Dyer, D. L.; Ehrlich, J. E.; Erskine, L. L.; Heikal, A. A.; Kuebler, S. M.; Lee, I. Y. S.; McCord-Maughon, D.; Qin, J.; Röckel, H.; Rumi, M.; Wu, X.-L.; Marder, S. R.; Perry, J. W., Two-photon polymerization initiators for three-dimensional optical data storage and microfabrication. *Nature* **1999,** *398* (6722), 51-54.
74. Green, W. A., *Industrial photoinitiators: a technical guide*. CRC Press: 2010.
75. Crivello, J. V.; Lam, J., Photoinitiated cationic polymerization with triarylsulfonium salts. *Journal of Polymer Science: Polymer Chemistry Edition* **1979,** *17* (4), 977-999.
76. Kutal, C.; Willson, C. G., Photoinitiated Cross-Linking and Image Formation in Thin Polymer Films Containing a Transition Metal Compound. *Journal of The Electrochemical Society* **1987,** *134* (9), 2280-2285.
77. Crivello, J., Photoinitiators for free radical cationic and anionic photopolymerization. *Surface and coatings technology* **1998,** *168*.
78. Crivello, J.; Lam, J., Dye-sensitized photoinitiated cationic polymerization. The system: Perylene–triarylsulfonium salts. *Journal of Polymer Science: Polymer Chemistry Edition* **1979,** *17* (4), 1059-1065.
79. Zivic, N.; Kuroishi, P. K.; Dumur, F.; Gigmes, D.; Dove, A. P.; Sardon, H., Recent Advances and Challenges in the Design of Organic Photoacid and Photobase Generators for Polymerizations. *Angewandte Chemie International Edition* **2019,** *58* (31), 10410-10422.
80. Salmi, H.; Allonas, X.; Ley, C.; Marechai, D.; Ak, A., Photopolymerization using photolatent amine catalysts. *Journal of Photopolymer Science and Technology* **2012,** *25* (2), 147-151.
81. Salmi, H.; Allonas, X.; Ley, C.; Defoin, A.; Ak, A., Quaternary ammonium salts of phenylglyoxylic acid as photobase generators for thiol-promoted epoxide photopolymerization. *Polymer Chemistry* **2014,** *5* (22), 6577-6583.
82. Tachi, H.; Yamamoto, T.; Shirai, M.; Tsunooka, M., Photochemical reactions of quaternary ammonium dithiocarbamates as photobase generators and their use in the photoinitiated thermal crosslinking of poly (glycidyl methacrylate). *Journal of Polymer Science Part A: Polymer Chemistry* **2001,** *39* (9), 1329-1341.
83. Zheng, Y.; Yang, Y.; Yang, H.; Han, F.; Li, Z., Thioxanthone-based amidine: An efficient nonionic photobase generator for thiol-based click polymerization under visible LED light. *Progress in Organic Coatings* **2020,** *148*, 105842.
84. Arimitsu, K.; Endo, R., Application to Photoreactive Materials of Photochemical Generation of Superbases with High Efficiency Based on Photodecarboxylation Reactions. *Chemistry of Materials* **2013,** *25* (22), 4461-4463.

85. Clark, E. A.; Alexander, M. R.; Irvine, D. J.; Roberts, C. J.; Wallace, M. J.; Sharpe, S.; Yoo, J.; Hague, R. J. M.; Tuck, C. J.; Wildman, R. D., 3D printing of tablets using inkjet with UV photoinitiation. *International Journal of Pharmaceutics* **2017,** *529* (1), 523-530.
86. Klikovits, N.; Sinawehl, L.; Knaack, P.; Koch, T.; Stampfl, J.; Gorsche, C.; Liska, R., UV-Induced Cationic Ring-Opening Polymerization of 2-Oxazolines for Hot Lithography. *ACS Macro Letters* **2020,** *9* (4), 546-551.
87. Takojima, K.; Saito, T.; Vevert, C.; Ladelta, V.; Bilalis, P.; Watanabe, J.; Hatanaka, S.; Konno, T.; Yamamoto, T.; Tajima, K.; Hadjichristidis, N.; Isono, T.; Satoh, T., Facile synthesis of poly(trimethylene carbonate) by alkali metal carboxylate-catalyzed ring-opening polymerization. *Polymer Journal* **2020,** *52* (1), 103-110.
88. Helou, M.; Miserque, O.; Brusson, J.-M.; Carpentier, J.-F.; Guillaume, S. M., Organocatalysts for the controlled "immortal" ring-opening polymerization of six-membered-ring cyclic carbonates: a metal-free, green process. *Chem. Eur. J* **2010,** *16*, 13805-13813.
89. Nederberg, F.; Lohmeijer, B. G. G.; Leibfarth, F.; Pratt, R. C.; Choi, J.; Dove, A. P.; Waymouth, R. M.; Hedrick, J. L., Organocatalytic Ring Opening Polymerization of Trimethylene Carbonate. *Biomacromolecules* **2007,** *8* (1), 153-160.
90. Li, X.; Mignard, N.; Taha, M.; Fernández-de-Alba, C.; Chen, J.; Zhang, S.; Fort, L.; Becquart, F., Synthesis of Poly(trimethylene carbonate) Oligomers by Ring-Opening Polymerization in Bulk. *Macromolecular Chemistry and Physics* **2020,** *221* (5), 1900367.
91. Tan, E. W. P.; Hedrick, J. L.; Arrechea, P. L.; Erdmann, T.; Kiyek, V.; Lottier, S.; Yang, Y. Y.; Park, N. H., Overcoming Barriers in Polycarbonate Synthesis: A Streamlined Approach for the Synthesis of Cyclic Carbonate Monomers. *Macromolecules* **2021,** *54* (4), 1767-1774.
92. Matsukizono, H.; Endo, T., Mono- and bifunctional six-membered cyclic carbonates synthesized by diphenyl carbonate toward networked polycarbonate films. *Journal of Applied Polymer Science* **2015,** *132* (19), n/a-n/a.
93. Yang, C.; Ding, X.; Ono, R. J.; Lee, H.; Hsu, L. Y.; Tong, Y. W.; Hedrick, J.; Yang, Y. Y., Brush-Like Polycarbonates Containing Dopamine, Cations, and PEG Providing a Broad-Spectrum, Antibacterial, and Antifouling Surface via One-Step Coating. *Advanced Materials* **2014,** *26* (43), 7346-7351.
94. Kim, S. Y.; Kim, H. J.; Lee, K. E.; Han, S. S.; Sohn, Y. S.; Jeong, B., Reverse Thermal Gelling PEG−PTMC Diblock Copolymer Aqueous Solution. *Macromolecules* **2007,** *40* (15), 5519-5525.
95. Park, S. H.; Choi, B. G.; Joo, M. K.; Han, D. K.; Sohn, Y. S.; Jeong, B., Temperature-Sensitive Poly(caprolactone-co-trimethylene carbonate)−Poly(ethylene glycol)−Poly(caprolactone-co-trimethylene carbonate) as in Situ Gel-Forming Biomaterial. *Macromolecules* **2008,** *41* (17), 6486-6492.
96. Bat, E.; Grijpma, D. W.; Feijen, J., Thermoreversible gelation behaviour of PTMC-PEG-PTMC triblock copolymers. *Journal of Controlled Release* **2008,** *132* (3), e37-e39.
97. Tu, J.; Cao, Z.; Jing, Y.; Fan, C.; Zhang, C.; Liao, L.; Liu, L., Halloysite nanotube nanocomposite hydrogels with tunable mechanical properties and drug release behavior. *Composites Science and Technology* **2013,** *85*, 126-130.
98. Zhang, C.; Aung, A.; Liao, L.; Varghese, S., A novel single precursor-based biodegradable hydrogel with enhanced mechanical properties. *Soft Matter* **2009,** *5* (20), 3831-3834.
99. Barker, I. A.; Dove, A. P., Triarylsulfonium hexafluorophosphate salts as photoactivated acidic catalysts for ring-opening polymerisation. *Chemical Communications* **2013,** *49* (12), 1205-1207.

100. Jiménez-Pardo, I.; van der Ven, L. G. J.; van Benthem, R. A. T. M.; Esteves, A. C. C.; de With, G., Effect of a Set of Acids and Polymerization Conditions on the Architecture of Polycarbonates Obtained via Ring Opening Polymerization. *Journal of Polymer Science Part A: Polymer Chemistry* **2017,** *55* (9), 1502-1511.
101. Bartolini, C.; Mespouille, L.; Verbruggen, I.; Willem, R.; Dubois, P., Guanidine-based polycarbonate hydrogels: from metal-free ring-opening polymerization to reversible self-assembling properties. *Soft Matter* **2011,** *7* (20), 9628-9637.
102. Hilf, J.; Scharfenberg, M.; Poon, J.; Moers, C.; Frey, H., Aliphatic Polycarbonates Based on Carbon Dioxide, Furfuryl Glycidyl Ether, and Glycidyl Methyl Ether: Reversible Functionalization and Cross-Linking. *Macromolecular Rapid Communications* **2015,** *36* (2), 174-179.
103. Thongsomboon, W.; Sherwood, M.; Arellano, N.; Nelson, A., Thermally Induced Nanoimprinting of Biodegradable Polycarbonates Using Dynamic Covalent Cross-Links. *ACS Macro Letters* **2013,** *2* (1), 19-22.
104. Nederberg, F.; Trang, V.; Pratt, R. C.; Kim, S.-H.; Colson, J.; Nelson, A.; Frank, C. W.; Hedrick, J. L.; Dubois, P.; Mespouille, L., Exploring the versatility of hydrogels derived from living organocatalytic ring-opening polymerization. *Soft Matter* **2010,** *6* (9), 2006-2012.
105. Brutman, J. P.; De Hoe, G. X.; Schneiderman, D. K.; Le, T. N.; Hillmyer, M. A., Renewable, Degradable, and Chemically Recyclable Cross-Linked Elastomers. *Industrial & Engineering Chemistry Research* **2016,** *55* (42), 11097-11106.
106. Wang, P.; Park, J. H.; Sayed, M.; Chang, T.-S.; Moran, A.; Chen, S.; Pyo, S.-H., Sustainable synthesis and characterization of a bisphenol A-free polycarbonate from a six-membered dicyclic carbonate. *Polymer Chemistry* **2018,** *9* (27), 3798-3807.
107. Al-Azemi, T. F.; Bisht, K. S., Synthesis of novel bis- and tris-(cyclic carbonate)s and their use in preparation of polymer networks. *Polymer* **2002,** *43* (8), 2161-2167.
108. Link, L. A.; Lonnecker, A. T.; Hearon, K.; Maher, C. A.; Raymond, J. E.; Wooley, K. L., Photo-cross-linked Poly(thioether-co-carbonate) Networks Derived from the Natural Product Quinic Acid. *ACS Applied Materials & Interfaces* **2014,** *6* (20), 17370-17375.
109. Reithofer, M. R.; Sum, Y. N.; Zhang, Y., Synthesis of cyclic carbonates with carbon dioxide and cesium carbonate. *Green Chemistry* **2013,** *15* (8), 2086-2090.
110. Sarel, S.; Pohoryles, L. A., The Stereochemistry and Mechanism of Reversible Polymerization of 2,2-Disubstituted 1,3-Propanediol Carbonates. *Journal of the American Chemical Society* **1958,** *80* (17), 4596-4599.
111. Cupta, M. G.; Joseph, P. J.; Kohl, P. A., Photoacid generators for catalytic decomposition of polycarbonate. *Journal of Applied Polymer Science* **2007,** *105* (5), 2655-2662.
112. Li, J.-X.; Liu, L.; Liu, A.-H., Study on synthesis and photoactivity of N-substituted diazabicyclononane derivatives with different substituents. *International Journal of Adhesion and Adhesives* **2015,** *57*, 118-124.
113. Studer, K.; Dietliker, K.; Jung, T., Photolatent amidine bases for redox curing of radically curable formulations. Google Patents: 2011.
114. Ludwig, B. J.; Piech, E. C., Some Anticonvulsant Agents Derived from 1,3-Propanediols. *Journal of the American Chemical Society* **1951,** *73* (12), 5779-5781.
115. Sarel, S.; Pohoryles, L. A.; Ben-Shoshan, R., Organic Carbonates. IV.1a,b,c Factors Affecting Formation of Homologous Cyclic Carbonates. *The Journal of Organic Chemistry* **1959,** *24* (12), 1873-1878.

116. Matsuo, J.; Aoki, K.; Sanda, F.; Endo, T., Substituent Effect on the Anionic Equilibrium Polymerization of Six-Membered Cyclic Carbonates. *Macromolecules* **1998,** *31* (14), 4432-4438.
117. Matsukizono, H.; Endo, T., Mono- and bifunctional six-membered cyclic carbonates synthesized by diphenyl carbonate toward networked polycarbonate films. *Journal of Applied Polymer Science* **2015,** *132* (19).
118. Tan, E. W. P.; Hedrick, J. L.; Arrechea, P. L.; Erdmann, T.; Kiyek, V.; Lottier, S.; Yang, Y. Y.; Park, N. H., Overcoming Barriers in Polycarbonate Synthesis: A Streamlined Approach for the Synthesis of Cyclic Carbonate Monomers. *Macromolecules* **2021**.
119. Bergmann, D. J.; Campi, E. M.; Jackson, W. R.; McCubbin, Q. J.; Patti, A. F., Rhodium-catalysed hydroformylation and carbonylation of N-alkenyl-1, 3-diaminopropanes. *Tetrahedron* **1997,** *53* (51), 17449-17460.